UNIVERSITÀ DEGLI STUDI DI PADOVA

DIPARTIMENTO DI FISICA ED ASTRONOMIA "GALILEO GALILEI"

CORSO DI LAUREA MAGISTRALE IN FISICA

Semi-Analytical Methods beyond Standard Perturbation Theory for the Large Scale Structure of the Universe

Laureando:
MICHELE PIZZARDO

Relatore:
Prof. SABINO MATARRESE
Correlatore:
Dott. MASSIMO PIETRONI

ANNO ACCADEMICO 2015/2016

Abstract

The main aim of this thesis is to investigate new methods beyond standard perturbation theory (SPT) to study the statistical properties of the Large Scale Structure (LSS) of the Universe. In particular, we will focus on the advantages that the use of the linear response function can bring to the evaluation of the matter power spectrum at scales presenting subdominant but crucial non-linear effects. In order to pursue this end, after an introductory part where we recall the importance of the studies on the LSS for contemporary Cosmology, as well as an excursus from the first analytical and observative attempts trying to understand its features until the state of the art in the field, we develop SPT in a typical field theory fashion, that is by means of generating functionals and Feynman rules, and we derive constraints between correlators arising from the galilean invariance of the dynamical system. Then, we define the linear response function as a tracker of the coupling between different cosmological modes, a genuine non-linear effect, we give a diagrammatic representation for it and we compute this object at the lowest order in SPT, comparing our result with N-body simulations. Moreover, we present two applications of the linear response function. The first consists in an improvement of the predictions of the Γ-expansion method, based on multi-point propagators, on the power spectrum at slight non-linear scales: in particular, we show that, by restoring galilean invariance, which is broken by most resummation methods, we can increase the maximum wavenumber at which the non-linear power spectrum can be trusted by 20%, and by 50% with respect to SPT. The second consists in the possibility to use the linear response function as an interpolator between different cosmologies at slight non-linear scales: in particular, it can be seen as an object able to encode the variations between the power spectrum of a reference cosmology and the one related to a small modification of a cosmological parameter with respect the reference configuration; we obtain that the modified power spectra generally differ from the corresponding simulated ones within about the 2% by changing the parameters within an enhancement or reduction of about 3σ, even if the exact values depend on the specific considered modified parameter: this procedure is particularly interesting as it provides a tool to limit the number of heavy N-body simulations in the study of the LSS of our Universe.

Contents

Introduction.

Precision cosmology relies on the ability to accurately extract cosmological parameters from measurements of observables which stem from the temperature anisotropy and polarization of the cosmic microwave background (CMB) as well as to the Large Scale Structure of the Universe (LSS). In particular, due to the recent end of the ESA Planck Mission, that has led to outstanding results by exploiting the former feature, LSS surveys have now the potential to become the leading cosmological observable in the years to come, because future generation of galaxy redshift surveys, as the expected Euclid ESA Space Mission, are going to measure the statistical properties of matter distribution to an unprecedented accuracy, providing information on fundamental questions related to the nature of dark energy (DE) and dark matter (DM) [1], beside the expansion of Universe and the absolute scale of neutrinos masses [2]. These great expectations are basically founded on the awareness that LSS contains a tremendous amount of cosmological information: indeed, at a rough guess, if we were able to extract information from all the modes going from the horizon scale, of about $\frac{1}{H} \sim 10^4\,\mathrm{Mpc}$, to the non-linear one, of about $k_{NL}^{-1} \sim 10\,\mathrm{Mpc}$, we would obtain about $\left(\frac{10^4}{10}\right)^3 \sim 10^9$ independent modes, to be compared to the $(2 \times 10^3)^2 \sim 10^6$ modes detected by the Planck Satellite.
Unfortunately, accessing all this information is much harder than in the case of the CMB, due to the short scales non-linearities, an issue that has to be faced with LSS differently than with CMB and that is relevant even for scales well larger than the hard value k_{NL}^{-1}. Indeed, the LSS feature that above all is thought to have the potential to constrain the expansion history of the Universe and the nature of its dark side, by analysing its location and amplitude, is the baryon acoustic oscillations (BAO), wiggles in the matter power spectrum generated by the coupling of baryons to radiation by Thomson scattering in the first stage of life of our Universe, set in the range of wavenumbers $k \in (0.05, 0.25)\,h\mathrm{Mpc}^{-1}$: hence, due to the higher degree of non-linearity of the underlying density fluctuations present at these scales, compared to those relevant for the CMB, accurate computations of the power spectrum in the BAO region is of course very challenging. As a consequence, while in the CMB context the tool allowing a comparison between theoretical models and observations, at the per cent level, is surely perturbation theory at linear order, if one would like to reach the same level of precision also in the study of LSS, essential in order to exploit it at the best, this requires to go beyond the above mentioned method. To be honest, the most important features of the anisotropies of the CMB and the LSS observed in the past galaxy surveys are accurately described by linear perturbation around a homogeneous Friedman-Robertson-Walker (FRW) background, thus making of (linear) perturbation theory surely a milestone approach to the study of LSS, whose success definitely relies on the large hierarchy between the Hubble and the non-linear scale, resulting in $\varepsilon = \frac{k_{NL}^{-1}}{H^{-1}} \ll 1$. However, with the advance of observations, the study of small non-linear corrections to the long wavelength dynamics is becoming more and more relevant and thus new techniques trying to handle these features are being developed: from this perspective, it was shown [3] that standard perturbation

theory has a number of drawbacks, which are attributed to its excessive sensitivity to the ultraviolet modes, in such a way that the mode-mode coupling, a non-linear effect, receives from them very large contributions making statistics divergent, oppositely to what realistic spectra are.

But what does it mean considering non-linearities on the dynamics of the Universe? That is, what are the features going under this name and their effects on observables? Of course, maybe the most important and characteristic feature of non-linear dynamics is the so called "mode-mode" coupling: when considering linear approximations, the evolution of the Universe and its properties at a specific scale is completely independent from all the others, as can be hinted thinking for example to the Jeans' theory for the gravitational collapse, while, oppositely, non-linearities introduce a coupling between different modes, meaning that the evolved properties of the Universe at a certain scale have received contributions, during their evolution, in general from all the other scales, even if in different weights. Hence, at non-linear level two short wavelength (UV) perturbations can couple to produce a long wavelength (IR) perturbation, meaning that UV perturbations can, in principle, affect the evolution of the Universe at long-distance. Clearly this is what actually revolutionizes the framework and the issue that will be mostly developed in the following. Other two aspects are related to the effects of peculiar velocities of structures: the first consists in the fact that the frequency of light of what is observed is not directly proportional to distance, as the lowest order Hubble law states, generating redshift distortions depending on non-linear density and velocity fields [4], which are correlated, determining an enhancement of the matter power spectrum on larger scales and suppressing it at smaller ones, with a transition occurring on the scales of the baryon oscillations, fortunately without introducing a "feature", the second being the large scale flow, determining a global shift of features, actually acting simply like a boost [5]. Other relevant issues are multi-streaming, galactic bias and gravitational lensing. The first deals with the assumption of perfect collisionless fluid for the matter content of the Universe, taken to be mainly cold dark matter: if for very large scales or primordial times it is a reasonable hypothesis, at smaller scales or later times it is much less so, due to the fact that presently at small scales matter is clumped in highly non-linear structures where it is impossible the absence of some kind of dynamical interference. The second relies on the fact that we don't observe dark matter aggregated in halos, but actually luminous matter or galaxies, so that, accepting to consider the latter as a good tracker of the former, we still need at least a parameter linking them, the galaxy bias [6]. Finally, gravitational lensing further complicates observations, bending light rays in function of the relativistic local geometry of the spacetime determined by the local matter distribution [7]. The global results of all the above mentioned implementations of non-linearities have the global result of smearing statistic observables as the power spectrum, for example broadening the BAO peaks with respect to the linear theory results: this makes us aware on the importance to develop consistent methods, both numerical and (semi)analytical, allowing to take into account these effects in order to improve the precision with which we can use LSS to constrain cosmological parameters. In the following we are presenting the most interesting ones.

The most established way to handle non-linearities is by means of N-body simulations: they simulate, using as input the cosmological parameters, the evolution of structures by directly considering a huge number N of matter particles in a sufficiently huge box simulating the Universe, by evaluating the forces between them, and consequently their motions, by means of a variety of computational methods allowing to reduce the number of interactions to calculate and to avoid certain small scales drawbacks. The main problem with them relies on the need of very large simulation volumes and high resolutions in order to gain the required sensitivity, with the consequence that, due to time and computational memory limitations, only wCDM cosmologies have been investigated so far. Hence, a number of valid semi-analytical

approaches are being developed, hoping to integrate N-body simulations into analytical frameworks, in such a way to reduce, rather to eliminate, the need for them. Some of these new techniques have an exquisitely perturbative nature, even if it is different from the standard theory, others are instead formulated in a non-perturbative fashion, allowing, at least in principle, a non-perturbative study of LSS, but that, if needed, can be verged on a perturbative way.
Among the first, we can mention the Renormalized Perturbation Theory as well as the Effective Field Theory (EFT), the Coarse-Grained Perturbation Theory (CGPT) and the Time-Sliced Perturbation Theory (TSPT). The former (also in time) [3, 8], using tools typical of quantum field theory, like Feynman diagrams, is able to reorganise the perturbative expansion by resumming an infinite class of diagrams at all orders in perturbation theory. Remarkably, this idea of "resummation" of cosmic perturbations, due to its validity, has been inherited by all the following successive works. EFT [9, 10], by comparing the BAO scale $k_{BAO}^{-1} \approx 150\,\mathrm{Mpc}$ with the non-linear one, states that the LSS of Universe must be well described perturbatively by means of the small parameter $\varepsilon \ll 1$. From either Newtonian energy and momentum or Einstein equation, it is defined an effective stress-energy momentum tensor $\tau_{\mu\nu}$ in powers of ε, that once made dependent only on IR modes by a smoothing on UV modes and an ensemble average on long wavelength perturbations is declared to be what couples with the smoothed Vlasov equation, obtaining as the final result a FRW Universe with small quasi-linear long wavelength perturbations evolving in the presence of an effective fluid whose properties, tracked by the coefficients of the expansion of $\tau_{\mu\nu}$, are determined by UV modes, by matching with (much lighter) N-body simulations or direct measurements. Slightly differently, CGPT [11] writes the smoothed Vlasov equation with a source arising from the smoothing process, depending on UV modes, completely determined by N-body simulations. While these methods are mainly focused to regulate the UV scales, TSPT [12] addresses to IR ones. Starting from the classical generating functional of the system $Z[J,\eta] = \int [\mathcal{D}\Theta_{\eta_0}]\mathcal{P}[\Theta_{\eta_0}, \eta_0] e^{\int d\mathbf{k}\, \Theta_\eta(\mathbf{k}) J(-\mathbf{k})}$, written for simplicity with only the velocity divergence field Θ_η, being J its current, the statistical distribution function at initial conditions $\mathcal{P}_{\eta_0}$ is evolved through the Liouville equation in $\mathcal{P}_\eta$. Then, using perturbation theory to expand it and changing the measure of Z in $[\mathcal{D}\Theta_\eta]$ one achieves a form for Z where time and space are factored, giving IR safe correlation functions.
Among the second, we can speak about the Renormalization Group (RG) and the Linear Response Function (LRF) methods. The first starts from the consideration that RG methods are particularly suited in the study of issues as LSS [13], where there is a gap between the large scale at which the theory is well known (linear) and the scale of physical importance, where non-linear corrections must be considered: equations of RG flow permit to evolve observables as correlation functions from long wavelengths to smaller ones, by introducing a wavelength filtering function, roughly similar to a Heaviside function, depending on a scale λ, in such a way to include automatically the contributions of new fluctuations arising at scales closer and closer to the relevant ones simply by considering growing values for λ; the characteristic of resummation here is witnessed by the emergence of an intrinsic UV cut-off. Finally, a few words about the LRF [14, 15]: this object actually quantifies, at fully non-linear level, the coupling between different modes, encoding how much a small modification of the initial conditions at a scale q impacts on the non-linear power spectrum at later times at a scale k. It is an extremely versatile tool, suitable both for fundamental and numerical issues, for comparisons with simulations and adaptable to perturbative evaluations: it will be widely used in the text.
The thesis aims to study the Large Scale Structure of the Universe mainly through the use of the Linear Response Function, firstly understanding the reason and how it can be successfully employed in handling non-linearities and secondly presenting two applications based on this object showing concretely the advantages that can arise by its exploitation. We conclude this Introduction, having the mere task to contextualize the theme of the work, presenting briefly

its structure by summarizing the contents of its constitutive chapters. Chapter 1 displays the origins of the study of the LSS of the Universe, from the first attempts in its comprehension till the state of the art on the field, beside the reasons of its importance in contemporary Cosmology, both from a theoretical and an experimental perspective; moreover, it is important to fix notations and formalisms at the basis of the following developments. Chapter 2 develops standard perturbation theory, initially for an Einstein-de Sitter universe and then extending the machinery to more general wCDM models: it is important, a part from an historical point of view, since it represents a cornerstone in the whole Cosmology, for the fact that it is developed in an unusual way in Cosmology, that is through methods typical of quantum field theory, as generating functionals and Feynman rules, opening the doors to some of the more recent techniques above mentioned or, for example, to consistency relations between statistic correlators, following from galilean invariance. It is important also for the progression: indeed, in Chapter 3 we introduce the Linear Response Function and the relative definition of linear kernel function, developing a diagrammatic representation for it and performing its evaluation at one loop in perturbation theory, pointing out the region of breakdown of standard perturbation theory by comparison with N-body simulations. Chapter 4 and Chapter 5 present two possible applications of the LRF: in the first we find out a fully non-perturbative way to improve the power spectrum predicted by the semi-analytical method of multipoint propagators on slight non-linear scales, where this method wrongly looses the behaviour implied by galilean invariance, while in the second LRF is used in a perturbative fashion as an interpolator of modified cosmologies with respect to a reference one, that is it is able to enclose information on slight variations of cosmological parameters with respect to a fixed configuration, allowing to derive the modified power spectra by only mean of the reference one. Finally, we end the text with the Conclusions, briefly recollecting the main ideas that have inspired the work and pointing out its results.

Chapter 1

Preliminary notions.

1.1 Elements of cosmological dynamics.

In this section we begin to provide the basic elements for the construction and the comprehension of the formalism developed in the following chapters; even if these are canonical topics, heavily discussed in a great number of classic texts and dissertations, see for instance [16, 17, 18, 19, 20], we prefer to recall them, following mainly the first two references, hoping to present a work as much self-consistent as possible. The final aim of this part is a reasoned introduction of Vlasov (or Boltzmann collisionless) equation, for the cosmological fluid, principally making use of a newtonian approach, perfectly suitable in our context, characterized by a non-relativistic fluid and by scales smaller than the horizon but bigger than the astrophysical ones. We will always fix the speed of light equal to one, $c = 1$.

1.1.1 Newtonian dynamics in cosmology.

Here we will extend elementary dynamics to an expanding universe, aiming at the development of a consistent treatment of the motion of a non-uniform cosmological fluid in a newtonian approach.

For a self-gravitating set of massive and non-relativistic point particles, with positions $\mathbf{r}_i$ (depending by the cosmic time t) and mass m_i, in a otherwise empty universe without non-gravitational forces, Newton's law for each particle is:

$$\frac{d^2\mathbf{r}_i}{dt^2} = \mathbf{g}_i(\mathbf{r}), \qquad \text{where:} \qquad \mathbf{g}_i(\mathbf{r}_i) = -G\sum_{j\neq i} m_j \frac{(\mathbf{r}_i - \mathbf{r}_j)}{|\mathbf{r}_i - \mathbf{r}_j|^3}. \tag{1.1}$$

If we consider the fluid limit, namely the limit in which the set is made up of dense and infinitely many particles, each one with infinitesimal mass $\rho d\mathbf{r}$, where the associated density $\rho(\mathbf{r})$ is evaluated in the point where the particle is placed and the infinitesimal volume $d\mathbf{r}$ is centered around it, then we can obtain the field $\mathbf{g} = \mathbf{g}(\mathbf{r}, t)$ as the irrotational solution to the Poisson equation:

$$\nabla_{\mathbf{r}} \cdot \mathbf{g}(\mathbf{r}, t) = -4\pi G\rho(\mathbf{r}, t), \qquad \text{constrained by:} \qquad \nabla_{\mathbf{r}} \times \mathbf{g}(\mathbf{r}, t) = 0, \tag{1.2}$$

where $\nabla_{r_i} = \frac{\partial}{\partial_{r_i}}$, which fairly generalises the second of (1.1) in:

$$\mathbf{g}(\mathbf{r}, t) = -G\int d\mathbf{r}'\rho(\mathbf{r}', t)\frac{(\mathbf{r} - \mathbf{r}')}{|\mathbf{r} - \mathbf{r}'|^3}. \tag{1.3}$$

In this limit, we can introduce the newtonian potential Φ, classically defined as:

$$\mathbf{g}(\mathbf{r},t) = -\frac{\partial\Phi(\mathbf{r},t)}{\partial\mathbf{r}} = -\nabla_{\mathbf{r}}\Phi(\mathbf{r},t), \tag{1.4}$$

in such a way that it obeys the Poisson equation:

$$\nabla^2_{\mathbf{r}}\phi(\mathbf{r},t) = 4\pi G\rho(\mathbf{r},t), \tag{1.5}$$

where $\nabla^2_{\mathbf{r}} = \sum_{i=1}^{3}\frac{\partial^2}{\partial {r_i}^2}$ is the Laplacian with respect to $\mathbf{r}$.
However, in hindsight the expressions for the newtonian potential and the gravity field reveal to be ill-defined, in the sense that the first can generally diverge, while the second depends on the boundary conditions at infinity, leaving a great ambiguity in the definition of the motion of the fluid particles: this issue is known as a Newton's dilemma. Indeed, consider the case when the mass density is finite and non-zero only in a finite volume: then $\mathbf{g}$ and Φ converge to a finite value everywhere, falling to zero at infinity. This is the case of a homogeneous medium with density fixed to ρ within a sphere of radius $r^\star < R$ delimiting a mass volume $V_{r^\star}$, that applying the Gauss' theorem to the first equation of (1.2) gives, at $r < r^\star$:

$$\begin{aligned}\int d\mathbf{r}'\nabla_{\mathbf{r}}\cdot\mathbf{g}(\mathbf{r}',t) = \int_{V_r} d\mathbf{r}'\nabla_{\mathbf{r}'}\cdot\mathbf{g}(\mathbf{r}',t) = \int_{\partial V_r} d\mathbf{\Sigma}_{r'}\cdot\mathbf{n}\,\mathbf{g}(\mathbf{r}',t) = 4\pi r^2\mathbf{g}(\mathbf{r},t) = \\ = -4\pi G\int d\mathbf{r}'\rho(\mathbf{r}',t) = -4\pi G\int_{V_r} d\mathbf{r}'\rho(t) = -\frac{16}{3}\pi^2 G r^3\rho(t),\end{aligned} \tag{1.6}$$

that leads to $\mathbf{g} = -\frac{4}{3}\pi G\rho\,\mathbf{r}$, valid when $r < r^\star$, while for the other values it goes to zero as the inverse of the square of the distance from the center of the sphere and analogously for Φ, with the inverse of the same distance. Clearly, if $R \to \infty$ this doesn't affect the result at all, but even at this stage if we consider a spheroid instead of a sphere containing the mass, g becomes non-radial, enforcing the importance of the shape of the matter distribution for the final results. In a more realistic situation, where the medium is homogeneous and infinite, by considering a sphere of radius $r < R$ and following the above proof, the results for g and Φ are identical to the previous case, thus until r is finite they are well-defined, but since now all the space within $R \to \infty$ is filled with matter, when $r \longrightarrow \infty$ the two quantities aren't well-defined, resulting $\Phi \to \infty$ and g highly dependent on boundary conditions at infinity, as can be hinted from the analogue of the case of spheroid configuration bounding the mass at infinity seen previously. From the spherical and spheroidal case, we can be made aware of another problem of the above formulation: g is null only at one point, while non-zero elsewhere, in apparent violation of the newtonian relativity of absolute space, that Newton tried to solve suggesting, wrongly, that this were caused by the cancellation of the forces at infinity, leading to the existence of a static solution even without non-gravitational forces acting on the system (of course as the cosmological constant).
As we know, general relativity solves these problems, mainly showing that distant matter curves the spacetime so that the coordinates $(\mathbf{r}, t)$ aren't good in cosmology and leading to declare a global spacetime geometry taking into account distant boundary conditions. However, also the newtonian approach can be made much more consistent exploiting the suggestions given from general relativity, insofar it will give, at the end, the same results of general relativity, clearly in a non-relativistic context: in the following we will see how.
At first we think to some good coordinates for cosmology. We start from the consideration that a homogeneous self-gravitating mass distribution cannot remain static without the presence of some non-gravitational forces; what's more is that observations of our Universe widely indicate that the observed mass distribution is, on average, expanding at large scales, in agreement

with the Hubble's law, whose updated parameter at present time can be found in [21]. If the expansion is perfectly uniform, all the separations scale in proportion to $a(t)$, the so called cosmic scale factor; in presence of a slight deviation from this regime, one can reasonably factor out the mean expansion to account for the dominant motions at large distances. This is done introducing the comoving coordinates $\mathbf{x}$ and the conformal time τ, beside the physical proper coordinates $\mathbf{r}$ and the cosmic time t, as:

$$\mathbf{x} = \frac{\mathbf{r}}{a(t)} \qquad \text{and} \qquad d\tau = \frac{dt}{a(t)}. \tag{1.7}$$

Hence, if the expansion is perfectly uniform the comoving coordinates stay fixed for each fluid particle at all times. Differently, for a perturbed expansion, each particle follows a comoving trajectory $\mathbf{x}(\tau)$, determining the non-uniform motion that is peculiar of it, by which it is defined the peculiar velocity $\mathbf{v}$ as:

$$\mathbf{v}(\tau) = \frac{d\mathbf{x}}{d\tau} = a(t)\frac{d}{dt}\frac{\mathbf{r}}{a(t)} = \frac{d\mathbf{r}}{dt} - H(t)\mathbf{r}, \tag{1.8}$$

where $H(t) = \frac{d\ln a}{dt} = \frac{1}{a^2}\frac{da}{d\tau}$ is the Hubble parameter. In fulfilment of the Cosmological Principle, stating the approximate homogeneity and isotropy of our Universe, consistent with the choice of a homogeneous and isotropic mean expansion, we assume that peculiar velocities has the same order of magnitude in all the directions.
Using the new coordinates, the newtonian approach allows to derive the correct non-relativistic Friedmann equations, encoding the dynamics of the cosmic fluid in a perfect isotropic and homogeneous universe. Indeed, considering a spherical symmetric mass distribution, Birkhoff's theorem ensures that the metric inside an empty spherical cavity centered at the centre of the mass distribution is the flat minkowskian one and under the condition that the mass $m = \frac{4}{3}\pi\bar{\rho}r^3$ that would stay in this empty space satisfies the relation:

$$\frac{Gm}{r} << 1, \tag{1.9}$$

then putting inside the sphere this mass, we can safely use for it newtonian mechanics. This treatment, substantially requiring to deal with euclidean space, is an excellent approximation everywhere except very near to relativistic compact objects, as black holes, and on scales comparable or larger than the cosmological horizon, characterized by the physical Hubble distance $\frac{1}{H}$. Defining $a' = \frac{da}{dt}$ and writing $r = ax_0$, the first Friedmann's equation follows from the Newton's law:

$$\frac{d^2r}{dt^2} = -\frac{Gm}{r^2} = -\frac{4\pi G}{3}\bar{\rho}r \quad \longrightarrow \quad a''x_0 = -\frac{4\pi G}{3}\bar{\rho}\,ax_0 \quad \longrightarrow \quad a'' = -\frac{4\pi G}{3}\bar{\rho}a, \tag{1.10}$$

modulo the relativistic term accounting for the barotropic pressure of the fluid that changes $\bar{\rho} \longleftrightarrow \bar{\rho} + 3p$. The second equation represents the energy conservations:

$$\begin{aligned} \frac{1}{2}\left(\frac{dr}{dt}\right)^2 - \frac{Gm}{r} = E \quad \longrightarrow \quad \frac{1}{2}(aH)^2x_0^2 - \frac{Gm}{ax_0} = E \quad \longrightarrow \quad (aH)^2 = \frac{2Gm}{ax_0^3} + \frac{2E}{x_0^2} \\ \longrightarrow \quad (aH)^2 = \frac{8\pi G}{3}a^2\bar{\rho} + \frac{2E}{x_0^2} \quad \longrightarrow \quad (aH)^2 = \frac{8\pi G}{3}a^2\bar{\rho} - K \end{aligned} \tag{1.11}$$

and is exact even at a relativistic level; we will see in a while the importance of this equation in the determination of the motion of a non-uniform medium. As we know, general relativity gives the full interpretation for the constant K, relating it with the curvature of the model: zero for a flat universe, positive and negative respectively for a closed and open one. The third constraint equation follows from the mass conservation:

$$\frac{dm}{dt} = \frac{4\pi}{3}\frac{d\bar{\rho}}{dt}r^3 + 4\pi\bar{\rho}\frac{dr}{dt}r^2 = 0 \quad \longrightarrow \quad \frac{d\bar{\rho}}{dt} = -3\frac{a'}{a}\bar{\rho}, \tag{1.12}$$

without the relativistic term that changes $\bar{\rho} \longleftrightarrow \bar{\rho} + p$.
Clearly, the above equations can be can be found in their general form, including the pieces descending from the possibility to have relativistic components filling this uniform universe, by considering the Einstein equation:

$$G_{\mu\nu} = R_{\mu\nu} - \frac{1}{2}R\, g_{\mu\nu} = 8\pi G\, T_{\mu\nu}, \tag{1.13}$$

where $R_{\mu\nu}$ and R are the Ricci tensor and scalar respectively, while $T_{\mu\nu}$ is the stress-energy tensor, once chosen for the metric $g_{\mu\nu}$ the Friedman-Robertson-Walker one:

$$g_{\mu\nu}(x) = \begin{pmatrix} 1 & 0 & 0 & 0 \\ 0 & -\frac{a^2(t)}{1-Kr^2} & 0 & 0 \\ 0 & 0 & -a^2(t) & 0 \\ 0 & 0 & 0 & -a^2(t) \end{pmatrix}, \tag{1.14}$$

where x^μ denotes the 4-coordinate $x = (t, \mathbf{x})$, with the comoving spatial coordinate expressed in spherical coordinates as $d\,x = (dr, rd\theta, r\sin\theta d\phi)$, θ and ϕ being respectively the azimuthal and polar angles, writing the 4-interval as:

$$ds^2 = g_{\mu\nu}(x)dx^\mu\, dx^\nu = dt^2 - a^2(t)\left[\frac{dr^2}{1-Kr^2} + r^2(d\theta^2 + \sin^2\theta d\phi^2)\right] \tag{1.15}$$

or, in conformal time τ, setting $d\Omega^2 = (d\theta^2 + \sin^2\theta d\phi^2)$:

$$ds^2 = a^2(\tau)\left[d\tau^2 - \left(\frac{dr^2}{1-Kr^2} + r^2 d\Omega^2\right)\right]. \tag{1.16}$$

Finally, we are ready to describe the motion of a non-uniform matter field, in newtonian cosmology, with mass density:

$$\rho(\mathbf{x}, \tau) = \bar{\rho}(\tau) + \delta\rho(\mathbf{x}, \tau), \tag{1.17}$$

where $\bar{\rho}$ is the background density related to a perfectly uniform universe governed by the Friedmann's equations, while $\delta\rho$ represents the slight non-uniform perturbation to the background, called matter density contrast[1] and defined as:

$$\delta\rho(\mathbf{x}) = \frac{\rho(\mathbf{x}) - \bar{\rho}}{\bar{\rho}}, \tag{1.18}$$

simply expressing the Newton's law (1.1) in comoving coordinates and conformal time τ. Setting $\dot{a} = \frac{da}{d\tau}$, we have:

$$a' = \frac{da}{dt} = \frac{1}{a}\frac{da}{d\tau} = \frac{\dot{a}}{a}, \tag{1.19}$$

while by using the relations:

$$\frac{d}{dt} = \frac{1}{a}\frac{d}{d\tau} \qquad \text{and} \qquad \frac{d^2}{dt^2} = \frac{d}{dt}\left(\frac{1}{a}\frac{d}{d\tau}\right) = -\frac{1}{a^2}\frac{da}{dt}\frac{d}{d\tau} + \frac{1}{a^2}\frac{d^2}{d\tau^2} = -\frac{\dot{a}}{a^3}\frac{d}{d\tau} + \frac{1}{a^2}\frac{d^2}{d\tau^2}, \tag{1.20}$$

the left hand side of equation of motion takes the form:

$$\begin{aligned} \frac{d^2\mathbf{r}}{dt^2} &= \frac{d^2}{dt^2}(a\mathbf{x}) = \frac{d}{dt}\left(\frac{da}{dt}\mathbf{x} + a\frac{d\mathbf{x}}{dt}\right) = \frac{d}{dt}\left(\frac{da}{dt}\right)\mathbf{x} + \frac{da}{dt}\frac{d\mathbf{x}}{dt} + \frac{da}{dt}\frac{d\mathbf{x}}{dt} + a\frac{d^2\mathbf{x}}{dt^2} = \\ &= \frac{1}{a}\frac{d}{d\tau}\left(\frac{\dot{a}}{a}\right)\mathbf{x} + 2\frac{\dot{a}}{a^2}\frac{d\mathbf{x}}{d\tau} + a\left(-\frac{\dot{a}}{a^3}\frac{d\mathbf{x}}{d\tau} + \frac{1}{a^2}\frac{d^2\mathbf{x}}{d\tau^2}\right) = \\ &= \frac{1}{a}\frac{d}{d\tau}\left(\frac{\dot{a}}{a}\right)\mathbf{x} + \frac{\dot{a}}{a^2}\frac{d\mathbf{x}}{d\tau} + \frac{1}{a}\frac{d^2\mathbf{x}}{d\tau^2}, \end{aligned} \tag{1.21}$$

while the left hand side, using Eq.(1.3), is:

$$g(\mathbf{r}, t) = -Ga\int d\mathbf{x}'\,(\bar{\rho}(\tau) + \delta\rho(\mathbf{x}', t))\,\frac{(\mathbf{x} - \mathbf{x}')}{|\mathbf{x} - \mathbf{x}'|^3}, \tag{1.22}$$

giving the following form for the equation of motion of the cosmic fluid:

$$\frac{d^2\mathbf{x}}{d\tau^2} + \frac{\dot{a}}{a}\frac{d\mathbf{x}}{d\tau} + \mathbf{x}\frac{d}{d\tau}\left(\frac{\dot{a}}{a}\right) = -Ga^2\int d\mathbf{x}'\,(\bar{\rho}(\tau) + \delta\rho(\mathbf{x}', t))\,\frac{(\mathbf{x} - \mathbf{x}')}{|\mathbf{x} - \mathbf{x}'|^3}. \tag{1.23}$$

We can further simplify the above equation getting rid of the homogeneous terms in the following way. The first term at the right side, containing the background (uniform) density, assuming as boundary conditions an average spherical symmetry of the universe at large distances becomes, as we have just seen by Gauss' theorem, $-\frac{4\pi G}{3}a^2\bar{\rho}\,\mathbf{x}$; on the other hand, taking the differential of the second Friedmann's equation (1.11):

$$\frac{\dot{a}}{a}\frac{d}{d\tau}\left(\frac{\dot{a}}{a}\right) = \frac{4\pi G}{3}\frac{d}{d\tau}(\bar{\rho}a^2), \tag{1.24}$$

[1]It is useful to specify that fields like the density contrast and the peculiar velocity can be regarded as three-dimensional random fields. In order to understand the meaning of this concept, we start from a probability space $(\Omega, \mathcal{F}, P)$ (it is defined by the tern $(\Omega, \mathcal{F}, P)$, where with Ω we denote the set of all the possible results of the events, whom are gathered in the set $\mathcal{F}$, and by the map P that associates to each event in $\mathcal{F}$ its probability as value in Ω) and a measurable space (S, Σ), where Σ is the defined measure for S: a stochastic process is a set of random variables (they are functions of the kind $X : \Omega \to S$ and represent a generalization of the canonical functions, having as the latter a domain made up of different or also infinite values, but differently from them each of the domain values has an associated probability P) defined on Ω and with values on S, labelled by an integer or real parameter t of a totally ordered set T (here namely the time), possibly even different for different values of t. A random field is the generalization of a stochastic process where the underlying parameter of the set is no longer one-dimensional, but it takes values as a multidimensional vector. In the present text the set of random variables is modelled as a function of three-dimensional vectors in the euclidean space $\mathbb{R}^3$ with values in $\mathbb{R}$, to which can be associated the probability distribution function: so, in this sense the contrast is a three-dimensional random field. A gaussian random field has simply a gaussian probability associated distribution function. For further information, see [22, 23, 24].

that for non-relativistic matter can be expressed using $\bar{\rho} = C\, a^{-3}$, by which we have $\frac{d}{d\tau}(\bar{\rho}a^2) = -\dot{a}\bar{\rho}a$, in the following form:

$$\frac{d}{d\tau}\left(\frac{\dot{a}}{a}\right) = -\frac{4\pi G}{3} a^2 \bar{\rho}, \tag{1.25}$$

it results that the last term at the left hand side of Eq.(1.23) cancels with the first term at the other side, leaving the equation of motion in this form:

$$\frac{d^2\mathbf{x}}{d\tau^2} + \frac{\dot{a}}{a}\frac{d\mathbf{x}}{d\tau} = -Ga^2 \int d\mathbf{x}' \delta\rho(\mathbf{x}', t) \frac{(\mathbf{x} - \mathbf{x}')}{|\mathbf{x} - \mathbf{x}'|^3} \equiv -\nabla\tilde{\Phi}, \tag{1.26}$$

where $\nabla = \frac{\partial}{\partial \mathbf{x}}$ and

$$\tilde{\Phi}(\mathbf{x}, t) = -Ga^2 \int d\mathbf{x}' \frac{\delta\rho(\mathbf{x}', t)}{|\mathbf{x} - \mathbf{x}'|} \tag{1.27}$$

is a proper quantity, sometimes called the peculiar gravitational potential. Provided the condition $\int d\mathbf{x}\, \delta\rho \to 0$ when the integral is over all the space, following by assuming homogeneity and isotropy on large scales, then the quantity $\tilde{\Phi}$ is univocally determined unambiguously, finite and well defined over all the space, and this quantity consistently solves Newton's dilemma, eliminating every ambiguity in the equation of motion for the fluid $\mathbf{x}(\tau)$. From now on, with the potential Φ we are addressing to the peculiar potential $\tilde{\Phi}$, dropping the tilde and the adjective denoting it.

1.1.2 Lagrangian and Hamiltonian formulations.

Here we present how to describe the newtonian cosmology with an approach typical of mathematical physics, both with the Lagrangian and Hamiltonian method: in fact these formulations allow to derive the equation of motion (1.26) starting from the Lagrangian and the Hamiltonian of the system respectively, the latter being particularly suited to treat the problem in the phase space.

In the first formulation, one has to consider the particle trajectories $\mathbf{x}(\tau)$, the Lagrangian $\mathcal{L}$ and the action $\mathcal{S}$ as the building blocks. Elements of mathematical physics state that for a particle moving in a potential Φ it is $\mathcal{L} = T - W = \frac{1}{2}mv^2 - m\Phi$, where T is the kinetic energy and W the gravitational potential energy, and $\mathcal{S} = \int dt\, \mathcal{L}$; similar expressions, in comoving coordinates and taking $\dot{\mathbf{x}} = \mathbf{v}$ the peculiar velocity, can be guessed for cosmology:

$$\mathcal{L}(\mathbf{x}, \dot{\mathbf{x}}, \tau) = \frac{1}{2}mav^2 - ma\Phi \qquad \text{and} \qquad \mathcal{S}(\mathbf{x}) = \int d\tau\, \mathcal{L}(\mathbf{x}, \dot{\mathbf{x}}, \tau). \tag{1.28}$$

Clearly, now we have to prove that the above Lagrangian is the right one to describe newtonian cosmic dynamics, that is to prove that it gives Eq.(1.26). In order to do this we remind the (Hamilton's) principle of least action, stating that the physical trajectory followed by a particle corresponds to the one minimizing the action, whose dynamical equation is popularly found imposing only the stationarity of the action with respect to small variations $\delta\mathbf{x}$ of the trajectories with fixed endpoints where $\delta\mathbf{x}(\tau_{1,2}) = 0$, making possible the use of integration by parts in such a way that:

$$\delta\mathcal{S} = \int_{\tau_1}^{\tau_2} d\tau \left[\frac{\partial\mathcal{L}}{\partial\mathbf{x}} \cdot \delta\mathbf{x} + \frac{\partial\mathcal{L}}{\partial\dot{\mathbf{x}}} \cdot \frac{d}{d\tau}\delta\mathbf{x}\right] = \int_{\tau_1}^{\tau_2} d\tau \left[\frac{\partial\mathcal{L}}{\partial\mathbf{x}} - \frac{d}{d\tau}\frac{\partial\mathcal{L}}{\partial\dot{\mathbf{x}}}\right] \cdot \delta\mathbf{x} = 0, \tag{1.29}$$

implying the Euler-Lagrange equation:

$$\frac{d}{d\tau}\frac{\partial\mathcal{L}}{\partial\dot{\mathbf{x}}} - \frac{\partial\mathcal{L}}{\partial\mathbf{x}} = 0, \tag{1.30}$$

that using the Lagrangian (1.28) gives:

$$\frac{d}{d\tau}\frac{\partial \mathcal{L}}{\partial \dot{\mathbf{x}}} - \frac{\partial \mathcal{L}}{\partial \mathbf{x}} = m\left(\frac{d}{d\tau}(a\mathbf{v}) + a\nabla\Phi\right) = m\left(a\dot{\mathbf{v}} + \dot{a}\mathbf{v} + a\nabla\Phi\right) = 0, \tag{1.31}$$

bringing directly to Eq.(1.26).
Once known the correct Lagrangian for the trajectories of the fluid particles, we can introduce the second formalism, whose building blocks are the single particle phase space trajectories $\{\mathbf{x}(\tau), \mathbf{p}(\tau)\}$ and the Hamiltonian of the system, with which determining two coupled first-order equations of motion for $\mathbf{x}(\tau)$ and $\mathbf{p}(\tau)$ instead of a single second-order equation for $\mathbf{x}(\tau)$: to fulfil this program we must introduce the Hamilton's equations.
First of all we define the conjugated momentum to $\mathbf{x}$ as:

$$\mathbf{p} = \frac{\partial \mathcal{L}}{\partial \dot{\mathbf{x}}} = am\mathbf{v} = am\frac{d\mathbf{x}}{d\tau}, \tag{1.32}$$

where in the second equality we use our cosmological Lagrangian in (1.28); then we eliminate $\dot{\mathbf{x}} = \frac{d\mathbf{x}}{d\tau}$ from the Lagrangian by using the above equation, that is making the substitution $\dot{\mathbf{x}} = \frac{\mathbf{p}}{am}$. At this point we introduce the Legendre transformed of the Lagrangian, known as the Hamiltonian:

$$\mathcal{H}(\mathbf{x}, \mathbf{p}, \tau) = \mathbf{p}\cdot\dot{\mathbf{x}} - \mathcal{L}(\mathbf{x}, \mathbf{p}, \tau), \tag{1.33}$$

where $\dot{\mathbf{x}}$ is expressed by means of $\mathbf{p}$, through which Hamilton's principle applied to the action $\mathcal{S} = \int_{\tau_1}^{\tau_2} d\tau(\mathbf{p}\cdot\dot{\mathbf{x}} - \mathcal{H}(\mathbf{x}, \mathbf{p}, \tau))$ considering variations of all the phase space coordinates, by means of an integration by parts for the second to last term provided that $\mathbf{p}\cdot\delta\mathbf{x} = 0$ at the endpoints, gives:

$$\delta\mathcal{S} = \int_{\tau_1}^{\tau_2} d\tau\left[\left(\frac{d\mathbf{x}}{d\tau} - \frac{\partial\mathcal{H}}{\partial\mathbf{p}}\right)\cdot\delta\mathbf{p} + \left(-\frac{d\mathbf{p}}{d\tau} - \frac{\partial\mathcal{H}}{\partial\mathbf{x}}\right)\cdot\delta\mathbf{x}\right] = 0, \tag{1.34}$$

thanks to which we straightforwardly read the Hamilton's equations:

$$\frac{d\mathbf{x}}{d\tau} = \frac{\partial\mathcal{H}}{\partial\mathbf{p}} \qquad \text{and} \qquad \frac{d\mathbf{p}}{d\tau} = -\frac{\partial\mathcal{H}}{\partial\mathbf{x}}. \tag{1.35}$$

In our case, using the Lagrangian (1.28) and the momentum (1.32), the Hamiltonian (1.33) is:

$$\mathcal{H} = \frac{p^2}{2am} + am\Phi, \tag{1.36}$$

yielding:

$$\frac{d\mathbf{x}}{d\tau} = \frac{\mathbf{p}}{am} \qquad \text{and} \qquad \frac{d\mathbf{p}}{d\tau} = -am\nabla\Phi. \tag{1.37}$$

A legitimate question is if these two equations bring the same information of the one found with the first formalism, that is if they are equivalent to Eq.(1.26); the answer is of course affirmative, because deriving with respect to the time the first of Hamilton's equation and using the second one and the expression for the conjugate momentum we recover Eq.(1.26).

1.1.3 Vlasov equation.

We conclude this section presenting a powerful and widely used method to deal with the evolution of perturbations in a non-relativistic collisionless gas, that will summarize most of the concepts presented so far, based on the evolution of the phase space distribution. The single-particle phase space density distribution $f(\mathbf{x}, \mathbf{p}, \tau)$ is defined so that $f(\mathbf{x}, \mathbf{p}, \tau)d\mathbf{x}d\mathbf{p}$ gives the

number of particles of coordinates staying in an infinitesimal neightborhood of $(\mathbf{x}, \mathbf{p})$ in an infinitesimal phase space volume element centered in them at the time τ.
In the general case of a collisional fluid, the evolution of the distribution function f is given by Boltzmann's equation:

$$\mathbb{L}[f] = \mathbb{C}[f], \tag{1.38}$$

where $\mathbb{L}$ is the Liouville's operator, acting on f in the following way:

$$\mathbb{L}[f] = \frac{df}{d\tau} = \frac{\partial f}{\partial \tau} + \frac{d\mathbf{x}}{d\tau} \cdot \frac{\partial f}{\partial \mathbf{x}} + \frac{d\mathbf{p}}{d\tau} \cdot \frac{\partial f}{\partial \mathbf{p}}, \tag{1.39}$$

while $\mathbb{C}$ is the collisional operator, accounting for the physics of collisions of the specific fluid in consideration, so in general different for each configuration. For a collisionless fluid, the latter operator is null, so f evolves according to the Liouville's theorem, expressing the conservation of particles along the phase space trajectories:

$$\mathbb{L}[f] = \frac{\partial f}{\partial \tau} + \frac{d\mathbf{x}}{d\tau} \cdot \frac{\partial f}{\partial \mathbf{x}} + \frac{d\mathbf{p}}{d\tau} \cdot \frac{\partial f}{\partial \mathbf{p}} = 0, \tag{1.40}$$

known as Boltzmann collisionless equation or also as Vlasov equation. For our cosmic system, using Hamilton's equations (1.35) and (1.37), we find:

$$\frac{\partial f}{\partial \tau} + \frac{\mathbf{p}}{am} \cdot \frac{\partial f}{\partial \mathbf{x}} - am\nabla\Phi \cdot \frac{\partial f}{\partial \mathbf{p}} = 0. \tag{1.41}$$

To conclude, a few words about the phase space density. In priciple, the exact single-particle phase space density function for a gas of infinite particles is written as a sum over Dirac's delta functions as:

$$f(\mathbf{x}, \mathbf{p}, \tau) = \sum_{i=1}^{\infty} \delta[\mathbf{x} - \mathbf{x}_i(\tau)]\delta[\mathbf{p} - \mathbf{p}_i(\tau)], \tag{1.42}$$

known as Klimontovich density, that obeys Vlasov equation (1.40), called in this context also Klimontovich equation. Clearly, the above expression for f contains all the information about the microstate of the system, involving all the fluid particles trajectories, but is very cumbersome to manage from an analytical and numerical point of view, thus one usually reduce the content of information performing an averaging, a coarse-graining of it. In particular, we make this operation averaging over a statistical ensemble of microstates corresponding to a given macrostate, that is, for example, over the set of microstates with the same phase space density once averaged over small phase space volumes containing many particles. In our case of collisionless fluid it can be showed that we can safely take the expression:

$$\langle f(\mathbf{x}, \mathbf{p}, \tau) \rangle = \Big\langle \sum_{i=1}^{\infty} \delta[\mathbf{x} - \mathbf{x}_i(\tau)]\delta[\mathbf{p} - \mathbf{p}_i(\tau)] \Big\rangle \tag{1.43}$$

as the phase space distribution f describing the fluid, that is obeying Vlasov equation.

1.2 Insights into the Large Scale Structure of the Universe.

In this section we discuss the most important characteristics of the Large Scale Structure (LSS) of the Universe, mainly featured by the non-linear behaviour of its matter content, that according to all the most reliable cosmological observations principally consists in cold (non-relativistic) dark matter (CDM in the following). Given the importance of the topic to fix the framework, also by a figurative, even pictorial, point of view, we are intending this dissertation as the place where we paint a picture of our Universe, using historical (rough) approximations to justify analytically its main features beside modern wonderful numerical results, without an extremely formal style, that would puzzle things and it would be, on the other hand, perfectly useless for the continuation. We base the presentation mainly on [17, 19], to which we address the reader for further information.

1.2.1 Observations.

1.2.1.1 Beginnings and evolution.

Questions as the spatial distribution of galaxies and the characteristics of their peculiar motions are very interesting, but of course difficult to deal with: indeed, the understanding of the features of the structures of our Universe and of the way they formed, provide actually excellent probes of the dark side of the Universe. Until the beginning of the eighties practically nothing was known at a quantitative level at this respect: at the time the knowledge on galaxies distribution was completely bi-dimensional, so that it seemed correct the assumption of the simplistic hypothesis of a uniform distribution of the single galaxies in the whole Universe, with their own revolution motion around the center of mass of the cluster they belonged. Things changed with the arrival of redshift surveys, surveys of a section of the sky aiming to measure the redshift of astronomical objects, such as galaxies, galaxy clusters or quasars. Using Hubble's law, the redshift can be used to estimate the distance of an object from Earth and by combining the redshift with angular position data, a redshift survey maps the three-dimensional distribution of matter within a field of the sky. The first attempt to map the large-scale structure of the universe was the Harvard-Smithsonian Center for Astrophysics (CfA) Redshift Survey: it began in 1977 and released its results in 1982, classifying more than two thousands galaxies, suggesting a very different scenario than what was assumed at the time. Indeed, it was discovered the Great Wall, an impressive supercluster of galaxies, surrounded by great voids, corroborating some pioneering works highlighting the importance of non-linearities in the process of structures formation, such as the work by Zel'dovich, dating in 1970. Following surveys confirmed that superclusters and galaxy clusters are actually distributed at the surface of enormous bubbles of void, whose diameter is more than ten times thicker than their surface, with the richest clusters being set in the contact area of two bubbles and connected by filamentous structures. The number of observed objects, the detected area and the measurement precisions have constantly grown in the years: the last two surveys are the Two-degree-Field Galaxy Redshift Survey (2dFGRS)[2], conducted by the Anglo-Australian Observatory (AAO) with the $3.9\,\mathrm{m}$ Anglo-Australian Telescope between 1997 and 2002, observing two large slices of the Universe to a depth of around 2.5 billions light years ($z \approx 0.2$) in both the north and the south galactic poles, covering an area of 1500 square degrees[3] and classifying a total of 220 thousands galaxies and 12 thousands stars, and the Sloan Digital Sky Survey (SDSS)[4], using a $2.5\,\mathrm{m}$ wide-angle optical telescope at Apache Point Observatory in New Mexico, a project that began to detect the sky in 2000 and, after having concluded the first phase in 2008 (the Legacy Survey)[5] after an upgrade in 2005,

[2] The final data release and much information on this survey can be found at the official website `http://www.2dfgrs.net`.

[3] The square degree is a conventional cosmological way to measure parts of the celestial sphere, linked with steradians by the relation: $1\,\mathrm{deg}^2 = \left(\frac{\pi}{180}\right)^2 \approx \frac{1}{3283} \approx 3.046\,10^{-4}\,\mathrm{sdr}$; the total square degrees denoting a sphere are about 41253.

[4] We address to `http://www.sdss.org`.

[5] The results of this first phase can be viewed at `http://classic.sdss.org/legacy/`.

covering more than 8000 square degrees (7500 in the North and 740 in the South Galactic Cup) and classifying more than one million galaxies and 100 millions stars at the median redshift $z \sim 0.1$, has been upgraded two times, so that the SDSS IV, started in 2014, is still operative. Until now, the SDSS has created the most detailed three-dimensional maps of the Universe ever made, with deep multi-color images of one third of the sky, and spectra for more than three million astronomical objects, enlarging the mapping to the 35% of the whole sky. One of the breakthroughs of this mission is the detection of Baryon Acoustic Oscillations (BAO), through the measurement of the power spectrum, obtained a decade ago by Eisenstein et al. [25].

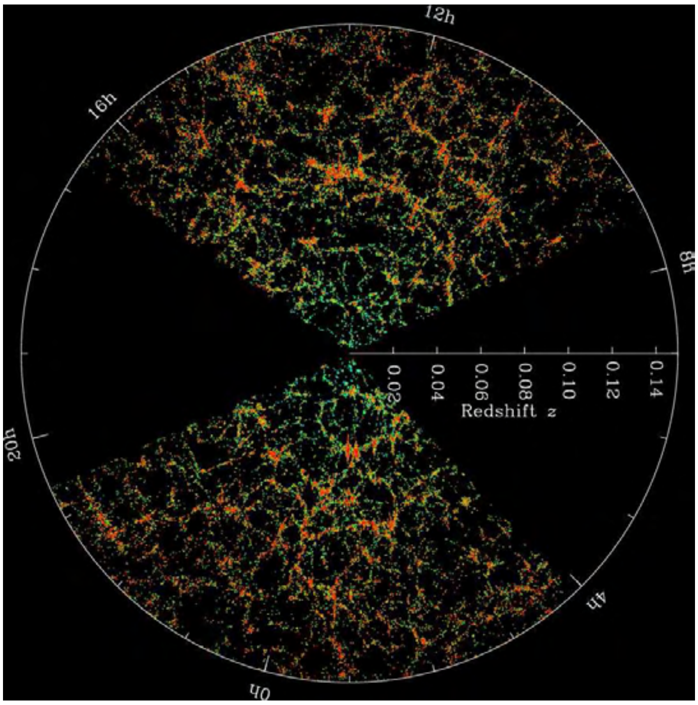

Figure 1.1: This impressive figure represents the detected Large Scale Structure of our Universe as obtained by the SDSS Legacy Survey: in particular, it is the structure in the northern equatorial slice ($2.5\,\mathrm{deg}$ thick) of the SDSS main galaxy redshift. Indeed, even if naturally the survey is three-dimensional, due to the difficulty to handle three dimensions on paper, figures usually give the right ascension coordinate (the analogue of longitude) measured in degrees (or hours as in this case) in function of the redshift, for a certain interval of the other coordinate, the declination (the analogue of latitude), measured in degrees too, determining actually a slice. The two empty sections correspond to the plane of the Milky Way, where, due to the strong luminosity, it turns out prohibitive making good observations. Figures like this straightforwardly heavily corroborate the structure of Universe described by cluster and superclusters of galaxies organized in walls and filaments surrounded by large voids; out of curiosity, the Great Wall, one of the first detected structures, is the huge supercluster that can be seen at redshift $z \approx 0.7$ extending roughly from 9 to 17 hours.

1.2.1.2 Baryon Acoustic Oscillations.

Baryon Acoustic Oscillations (BAO) are one of the most important features of the present matter distribution, consisting in wiggles in the matter power spectrum produced by the coupling between baryons and radiation by Thomson scattering in the early Universe, located in the range of wavenumbers $k \approx 0.05 - 0.3\,h\mathrm{Mpc}^{-1}$, that have the potential to constrain the expansion history and the dark content properties of Universe via redshift surveys. Following [26], at early times the Universe was hot, dense and ionized, in such a way that photons and baryons were tightly coupled, while dark matter was of course only gravitationally interacting. The presence of small perturbations both in the matter density and in the gravitational potential led to the setting of acoustic oscillation waves of the radiative (photons and baryons) fluid, due to the counteraction between the gravitational force originated by DM and the pressure arising from the fluid: indeed, at this stage temperature perturbations behave as $\delta T(k) \approx A(k)\cos(kr_s)$, where r_s is the comoving sound horizon, while $\delta_\gamma \propto (\delta T)^{\frac{1}{4}}$ and $\delta_b \propto \delta_\gamma$, where δ_γ and δ_b are the photon and baryon densities respectively [20]. In particular, considering the density perturbations having a very peaked feature centered about a small region, in each cycle of rarefaction and compression firstly pressure acted broadening the fluid distribution, then gravity tended to bring the configuration at the initial situation and so on, causing the formation of spherical acoustic waves of photons and baryons propagating out of the overdense region throughout the Universe at the velocity of sound c_s (roughly the half of the speed of light), while DM remains approximately in its centre, a part from the dragging effect due to the fluid. When Universe was about $t_{ls} = 390000$ years old, it was sufficiently cold to permit the decoupling between baryons and photons, the last then propagated by free stream, causing the freezing of the acoustic oscillations: the first compression, on the frontwave, corresponding to $k_1 r_s = \pi$, has had the time to cover the maximum possible distance from the origin of the anisotropy, the sound horizon, at the comoving length $r_s = \int_0^{t_{ls}} c_s(t')\frac{dt'}{a(t')} \approx 150\,\mathrm{Mpc}$, and thus, without photons, the driving constituent for pressure, baryons began to compress with time due to the gravitational interaction with DM, in such a way the final configuration is our original peak at the center and an "echo" in a shell roughly $150\,\mathrm{Mpc}$ in radius; the first rarefaction is placed in $k_2 r_s = 2\pi$ and so on. This happens for each single anisotropy, therefore the universe is not composed of one sound ripple, but many overlapping ripples. Since baryons constitute about the 15% of the whole matter, we expect this feature to be present still now, suppressed by a factor $\Omega_b/\Omega_m \approx 0.15$ with respect to CMB spectrum: it is exactly BAO. Indeed, many such anisotropies created the ripples in the density of space that attracted matter and eventually galaxies formed in a similar pattern. Since it was detected, this property assures the existence, at the recombination time, of both baryonic (although BAO would not have been seen) and dark (although it would have been seen with much more high peaks) matter. Moreover, it would provide a characteristic and reasonably sharp length scale (standard ruler) that can be measured at a wide range of redshifts, thereby determining purely by geometry the relation between angular diameter distance and redshift, together with the evolution of the Hubble parameter. Unfortunately, as we said the acoustic features in the matter correlations are weak (10% contrast in the power spectrum) and on large scales, meaning that one must survey very large volumes, of order $1\,h^{-3}\mathrm{Gpc}^3$, to detect the signature, so that we had to wait SDSS to confirm their existence.

1.2.1.3 Future outlooks.

To conclude, we remind that for 2020 it is programmed the launch of the Euclid satellite, presently under development, that will measure a number at the order of the billion between galaxies and other objects covering the full sky up to $z \approx 1.5$, investigating the relation between redshifts and distances and hence providing data expected to enlighten the history of the expansion of the Universe and the formation of cosmic structures, permitting to better understand dark energy and dark matter by accurately measuring the acceleration of the universe. In some respect, it will represent the natural continuation of another ESA program, the Planck Mission, whose satellite gave what is now the most precise map of the cosmic microwave background, representing the primordial Universe at the time of the last scattering. The most important feature of LSS potentially allowing to fully center this target is represented by the Baryon Acoustic Oscillations. Indeed, we know that the fist Friedman equation:

$$\frac{a''}{a} = -\frac{4\pi G}{3}\left(\bar{\rho} + 3p\right) \tag{1.44}$$

states that, if our Universe is expanding, that is if $a'' > 0$, using the equation of state $p = w\bar{\rho}$ (where $\bar{\rho} = \sum_i \bar{\rho}_i$ and $p = \sum_i p_i$), one gets the constraint: $w < -\frac{1}{3}$, meaning that we must accept that the content of the Universe has a global negative pressure, due to one (or more) constituent with this characteristic, called dark energy. The second Friedman equation (1.11) can be rewritten using the density parameter $\Omega_i = \frac{\bar{\rho}_i}{\rho_c}$ for each constituent, where the critical density $\rho_c = \frac{3H^2}{8\pi G}$, so that, for a general wCDM model with pressureless matter, radiation, curvature and dark energy, we have:

$$H^2(a) = H_0^2\left[\Omega_m a^{-3} + \Omega_r a^{-4} + \Omega_K a^{-2} + \Omega_\Lambda a^{-3(1+w)}\right], \tag{1.45}$$

all already constrained by CMB experiments, but that we want to confirm independently; naively, measuring the time-dependence of the Hubble parameter we are able to fulfil this aim. This is possible making use of the BAO: being a cosmological standard ruler, namely its (the sound horizon) physical length $\Delta\chi$ can be measured as a function of cosmic time, then, once measured the subtended angle (from Earth) $\Delta\theta$, by simple use of the definition of angular diameter distance d_A:

$$d_A(z) = \frac{\Delta\chi}{\Delta\theta(z)} \propto \int_0^z \frac{dz'}{H(z')}, \tag{1.46}$$

and measuring the redshift interval Δz from us, we finally have what we were looking for:

$$\Delta z = H(z)\Delta\chi(z). \tag{1.47}$$

Hence, measuring $\Delta\theta$ and Δz subtended by the sound horizon for various redshifts, through the expansion of Universe we can infer its history, the properties of the dark side of its content and much more.

In the following sections, we will discuss the fist analytical attempts for the understanding of the structure of the Universe at large scales as well as N-body simulations, modern numerical approaches to the issue.

1.2.2 Overview of linear perturbation theory.

Here we briefly summarize the results for cosmic perturbations in the linear theory in a expanding universe, the Jeans' theory, actually developed in 1902 to understand the formation of stars and planets, but eventually considered as the cornerstone of the standard model for the origin of galaxies and large-scale structures.

A newtonian gas subjected to self-gravity and pressure is described, in comoving coordinates $\mathbf{x}$

and cosmic time t, by the system:

$$\begin{cases} \frac{\partial}{\partial t}\rho(\mathbf{x},t) + 3H(t)\rho(\mathbf{x},t) + \frac{1}{a(t)}\nabla\cdot[\rho(\mathbf{x},t)\mathbf{v}(\mathbf{x},t)] = 0 \\ \frac{\partial}{\partial t}\mathbf{v}(\mathbf{x},t) + H(t)\mathbf{v}(\mathbf{x},t) + \frac{1}{a(t)}[\mathbf{v}(\mathbf{x},t)\cdot\nabla]\mathbf{v}(\mathbf{x},t) = -\frac{1}{a(t)\rho(\mathbf{x},t)}\nabla p - \frac{1}{a(t)}\nabla\Phi \\ \nabla^2\Phi = 4\pi G a^2(t)\delta\rho(\mathbf{x},t) \end{cases}, \tag{1.48}$$

where its density has been expressed using Eq.(1.17), Φ is the peculiar gravitational potential, $\mathbf{v} = \frac{1}{a}\frac{d\mathbf{x}}{dt}$ the peculiar velocity and p is the pressure, while $\nabla^2 = \sum_{i=1}^{3}\frac{\partial^2}{\partial {x_i}^2}$ is simply the Laplacian. The system is made of three equations: from the top we have the continuity, Euler and Poisson equations.

We define $\delta\rho = \bar{\rho}\,\delta$ as the perturbation of the background non-vanishing density $\bar{\rho}$, while the peculiar velocity and potential, $\mathbf{v}$ and Φ respectively, must be thought as perturbations around the background fluid velocity and potential respectively. The same holds for the pressure p, written as $p = \bar{p} + \delta p$. Thus, we can look for a solution of the linearised version of the system by considering the Fourier transform of the perturbations with respect to space:

$$\begin{aligned} \delta(\mathbf{x},t) &= \int \frac{d\mathbf{k}}{(2\pi)^3} e^{i\mathbf{k}\cdot\mathbf{x}}\delta_{\mathbf{k}}(t) \\ \mathbf{v}(\mathbf{x},t) &= \int \frac{d\mathbf{k}}{(2\pi)^3} e^{i\mathbf{k}\cdot\mathbf{x}}\mathbf{v}_{\mathbf{k}}(t) \\ \Phi(\mathbf{x},t) &= \int \frac{d\mathbf{k}}{(2\pi)^3} e^{i\mathbf{k}\cdot\mathbf{x}}\Phi_{\mathbf{k}}(t), \end{aligned} \tag{1.49}$$

in such a way that, imposing the adiabatic constraint fixing $\delta p = \frac{\partial p}{\partial \rho}\big|_{s=const}\delta\rho = c_s^2\,\delta\rho$, being s the entropy density, we get the linearised system:

$$\begin{cases} \delta'_{\mathbf{k}} + \frac{i\mathbf{k}\cdot\mathbf{v}_{\mathbf{k}}}{a} = 0 \\ \mathbf{v}'_{\mathbf{k}} + H\mathbf{v}_{\mathbf{k}} = -\frac{i\mathbf{k}}{a}(c_s^2\delta_{\mathbf{k}} + \Phi_{\mathbf{k}}) \\ k^2\Phi_{\mathbf{k}} = -4\pi G a^2\bar{\rho}\,\delta_{\mathbf{k}} \end{cases}. \tag{1.50}$$

The orthogonal component of $\mathbf{v}$, defined by $\mathbf{k}\cdot\mathbf{v}_{\mathbf{k},\perp} = 0$, obeys $\mathbf{v}'_{\mathbf{k},\perp} + H\mathbf{v}_{\mathbf{k},\perp} = 0$, bringing to $\mathbf{v}_{\mathbf{k},\perp} \sim 1/a$, but, since it doesn't admit an evolution for $\delta_{\mathbf{k}}$, the interesting component follows from its irrotational part, defined by $\mathbf{k}\cdot\mathbf{v}_{\mathbf{k},\parallel} = k\,v_{\mathbf{k},\parallel}$, obeying the following equation, found differentiating the linearised continuity equation:

$$\delta''_{\mathbf{k}} + \frac{ik}{a}v'_{\mathbf{k},\parallel} - \frac{ik}{a}Hv_{\mathbf{k},\parallel} = 0, \tag{1.51}$$

that using the linearised Euler equation straightforwardly gives, simplifying the notation:

$$\delta''_{\mathbf{k}} + 2H\delta'_{\mathbf{k}} + \left[\frac{c_s^2\,k^2}{a^2} - 4\pi G\bar{\rho}\right]\delta_{\mathbf{k}} = 0. \tag{1.52}$$

Clearly, the linearisation causes different modes of perturbation to evolve independently from each other. Furthermore, the comoving Jeans' wavenumber, defined as:

$$k_J = a\frac{\sqrt{4\pi G\bar{\rho}}}{c_s}, \tag{1.53}$$

denotes the borderline between the gravitational dominated modes, when $k < k_J$, and the pressure dominated ones. The latter case brings the evolution of each single matter perturbation with $k > k_J$ to oscillate as a sound wave in time (modified with gravity and actually suppressed by the scale factor), being not physically interesting, while the former situation brings

to perturbations whose amplitude grows or decreases with time.
Indeed, for $k \ll k_J$ one has:

$$\delta''_{\mathbf{k}} + 2H\delta'_{\mathbf{k}} - 4\pi G\bar{\rho}\,\delta_{\mathbf{k}} \approx 0. \tag{1.54}$$

Considering the case of an Einstein-de Sitter model, describing a flat universe with mass density parameter $\Omega_m = 1$, since $a \sim t^{\frac{2}{3}}$, $H = \frac{2}{3t}$ and $\bar{\rho} = (6\pi G t^2)^{-1}$ the above equation becomes:

$$\delta''_{\mathbf{k}} + \frac{4}{3t}\delta'_{\mathbf{k}} - \frac{2}{3t^2}\delta_{\mathbf{k}} \approx 0, \tag{1.55}$$

whose solution can be found guessing a power law behaviour $\delta_{\mathbf{k}} \propto t^{\alpha}$, from which:

$$3\alpha^2 + \alpha - 2 = 0 \qquad \Rightarrow \alpha_g = \frac{2}{3} \quad \text{and} \quad \alpha_d = -1, \tag{1.56}$$

where the subscripts g, d mean respectively the growing (collapsing) and the decaying (anti-collapsing) mode, since the density contrast has the forms:

$$\delta_{\mathbf{k},g} \propto t^{\frac{2}{3}} \quad \text{and} \quad \delta_{\mathbf{k},d} \propto t^{-1}, \tag{1.57}$$

that, used in the linearised Euler and Poisson equations, give:

$$v_{\mathbf{k},g} \propto t^{\frac{1}{3}} \quad \text{and} \quad v_{\mathbf{k},d} \propto t^{-\frac{4}{3}} \tag{1.58}$$

for the peculiar velocity, while for the potential we have:

$$\Phi_{\mathbf{k},g} = const \quad \text{and} \quad t^{-\frac{5}{3}}. \tag{1.59}$$

We summarize here below the behaviour of the growing mode:

$$\begin{cases} \delta_{\mathbf{k},g}(t) \propto t^{\frac{2}{3}} \propto a(t) \\ v_{\mathbf{k},g}(t) \propto t^{\frac{1}{3}} \\ \Phi_{\mathbf{k},g}(t) = const \end{cases} . \tag{1.60}$$

1.2.3 Non-linear dynamics of self-gravitating collisionless particles.

1.2.3.1 Analytic appoximated treatments.

As seen in the previous section, the dynamic of a self-gravitating fluid constituted by collisionless particles, or dust, is governed by Vlasov equation (1.40), that specified for a cosmic fluid using the Hamiltonian (1.36) gives the equation (1.41). The collisionless characteristic brings to the absence of any pressure and solving this equation up to the first two moments, a method that will be exposed in the next chapter, we reach the same equations in (1.48), with $p = 0$. In order to get these equations, we must also assume that the velocity dispersion σ_{ij}, arising in the second moment, is zero at all times: this happens provided that it is zero at initial time (true in a large range of scales for CDM) and that the system remains in the single-stream regime, namely one flow for each position, true before the formation of caustics. The dynamics of such a system is thus given by:

$$\begin{cases} \frac{\partial}{\partial t}\rho(\mathbf{x},t) + 3H(t)\rho(\mathbf{x},t) + \frac{1}{a(t)}\nabla\cdot[\rho(\mathbf{x},t)\mathbf{v}(\mathbf{x},t)] = 0 \\ \frac{\partial}{\partial t}\mathbf{v}(\mathbf{x},t) + H(t)\mathbf{v}(\mathbf{x},t) + \frac{1}{a(t)}[\mathbf{v}(\mathbf{x},t)\cdot\nabla]\mathbf{v}(\mathbf{x},t) = -\frac{1}{a(t)}\nabla\Phi \\ \nabla^2\Phi = 4\pi G a^2(t)\delta\rho(\mathbf{x},t) \end{cases} . \tag{1.61}$$

Before considering some numerical results, we present approximated analytical methods to understand the main features of structure formation.
In this sense, the Zel'dovich Approximation [27] gives an appropriate treatment of the non-linear dynamics of self-gravitating dust, showing that the collapse undergoes preferentially along one axis, determining that the preferential shape of collapsed structures is the oblate ellipsoid, known in slang as "pancake". We start introducing the new time variable $a(t) = a_\star\left(\frac{t}{t_\star}\right)^{\frac{2}{3}}$, consistently with an Einstein-de Sitter model, through which we change:

$$\begin{aligned} \rho &\longrightarrow \eta = \frac{\rho}{\bar{\rho}} = 1+\delta \\ \mathbf{v} &\longrightarrow \mathbf{u} = \frac{d\mathbf{x}}{da} = \frac{\mathbf{v}}{a\,\dot{a}} \\ \Phi &\longrightarrow \Psi = \frac{3t_\star^2}{2a_\star^3}\Phi, \end{aligned} \tag{1.62}$$

where the time dependence is expressed via a. With these quantities, the above system takes the form:

$$\begin{cases} \frac{D\eta}{Da} + \eta\,\nabla\cdot\mathbf{u} = 0 \\ \frac{D\mathbf{u}}{Da} + \frac{3}{2\,a}\mathbf{u} = -\frac{3}{2\,a}\nabla\Psi \\ \nabla^2\Psi = \frac{\delta}{a} \end{cases}, \tag{1.63}$$

where we compact the notation using the convective derivative $\frac{D}{Da} = \frac{\partial}{\partial a} + \mathbf{u}\cdot\nabla$. Now, recalling the results (1.60) for the growing mode of linear theory and the definitions above, it is clear that $\mathbf{u} \approx const$, in the way it results, at linear level and up to higher order terms:

$$\frac{\partial\mathbf{u}}{\partial a} = 0 \quad \text{and thus also} \quad \frac{D\mathbf{u}}{Da} = 0; \tag{1.64}$$

the latter, inserted in the Euler equation, implies that the linear solution is:

$$\mathbf{u}(\mathbf{x}, a) = -\nabla\Psi(\mathbf{x}, a). \tag{1.65}$$

Zel'dovich's ansatz consists in the assumption that even beyond the linear theory the second equation in (1.64) holds. A justification can be seen by the fact that, at linear theory, going to the Fourier space one has:

$$\Psi_{\mathbf{k}} \sim \frac{\delta_{\mathbf{k}}}{k^2} \quad \text{and} \quad u_{\mathbf{k}} \sim k\Psi_{\mathbf{k}} \sim \frac{\delta_{\mathbf{k}}}{k}, \tag{1.66}$$

stating that the above quantities stay on the linear level at smaller scales than the density fluctuation, then when we are considering a suitable range of density contrast where the dynamics is non-linear, we can continue to think that the behaviours of the peculiar velocity and of the gravitational potential are substantially linear. Hence, we are left with the new dynamical system:

$$\begin{cases} \frac{D\eta}{Da} + \eta\,\nabla\cdot\mathbf{u} = 0 \\ \frac{D\mathbf{u}}{Da} = 0 \end{cases}, \tag{1.67}$$

that highlights the fact that the Poisson equation has bees completely decoupled from the others and will be only used to fix the initial conditions. Since these equations describe the motion of dust particles moving only under the effect of their inertia, preserving their mass, the solution to the second (Euler) equation is:

$$\mathbf{u}(\mathbf{x}, a) = \mathbf{u}_0(\mathbf{q}), \tag{1.68}$$

where $\mathbf{u}_0(\mathbf{q})$ is the initial velocity (at a_0, where in this paragraph the subscript zero means initial, not present, time) in the Lagrangian position $\mathbf{q}$ of the particle, that is a particular infinitesimal fluid element, which is in the Eulerian position $\mathbf{x}$ at time a; as a note, we stress that the Lagrangian description characterizes the physical properties of a single given fluid element in time, denoted by the Lagrangian coordinate $\mathbf{q}$, while the Eulerian description characterizes the same properties, but a given comoving coordinate $\mathbf{x}$, focussing on the flowing of fluid elements at this position. Further integrating the latter equation to find the particle's trajectory, we have:

$$\mathbf{x}(\mathbf{q}, a) = \mathbf{q} + (a - a_0)\mathbf{u}_0(\mathbf{q}), \tag{1.69}$$

that is a straight line, and using for initial conditions the linear theory, which is by definition valid at initial times, we know that:

$$\mathbf{u}_0(\mathbf{q}) = -\nabla_{\mathbf{q}}\Psi_0(\mathbf{q}), \tag{1.70}$$

bringing naturally, setting for simplicity $a_0 = 0$, to:

$$\mathbf{x}(\mathbf{q}, a) = \mathbf{q} - a\nabla_{\mathbf{q}}\Psi_0(\mathbf{q}). \tag{1.71}$$

Passing to the first (continuity) equation of (1.67), we see that a formal solution can be immediately obtained by integrating along the trajectory:

$$\eta(\mathbf{x}, a) = \eta_0(\mathbf{q})e^{-\int_{a_0}^{a} da'\, \nabla\cdot\mathbf{u}[\mathbf{x}(\mathbf{q},a'),a']}, \tag{1.72}$$

but a handier form can be found realizing that the mass conservation of the individual fluid elements requires:

$$\eta(\mathbf{x}, \eta)d\mathbf{x} = \eta_0(\mathbf{q})d\mathbf{q}, \tag{1.73}$$

therefore we can write, using the Jacobian determinant:

$$\eta(\mathbf{x}(\mathbf{q}, a), a) = (1 + \delta_0(\mathbf{q}))\left|\frac{\partial\mathbf{q}}{\partial\mathbf{x}}\right|. \tag{1.74}$$

From Poisson equation we find that at initial conditions, since the potential is approximatively constant and $a \to a_0 = 0$, then $\delta_0 \to 0$, leading to:

$$\eta(\mathbf{x}(\mathbf{q}, a), a) = \left|\frac{\partial\mathbf{x}}{\partial\mathbf{q}}\right|^{-1}. \tag{1.75}$$

Using the solution of Euler equation in (1.71), we simply find that:

$$\frac{\partial x^i}{\partial q^j} = \delta^i_j - a\frac{\partial^2\Psi_0(\mathbf{q})}{\partial q_i\partial q_j}, \tag{1.76}$$

where clearly $i, j \in \{1, 2, 3\}$ and the second term at the right hand side is the deformation tensor. The analysis of this quantity is very enlightening: indeed, it can be locally diagonalized along the three principal axes Q_1, Q_2, Q_3 with eigenvalues $\lambda_1(\mathbf{q}), \lambda_2(\mathbf{q}), \lambda_3(\mathbf{q})$ and if the gravitational potential $\Psi_0(\mathbf{q})$ is a gaussian random field, consistently with inflation and data [21], it has been shown that there is the 8% of probability that all the three eigenvalues are positive, another 8% that they are all negative, a 42% that two of them are positive and one negative and a final 42% that one of them is positive and two negative, indicating a probability of the 92% that at least one eigenvalue is positive, meaning that the 92% of the initial volume is provided at least by one positive eigenvalue of the deformation tensor. Taking the determinant of the deformation tensor, whose of components are those in (1.76), using the eigenvalues, we have:

$$\eta(\mathbf{x}(\mathbf{q},a),a) = \frac{1}{(1-a\,\lambda_1(\mathbf{q}))(1-a\,\lambda_2(\mathbf{q}))(1-a\,\lambda_3(\mathbf{q}))}, \tag{1.77}$$

by which we see that, denoting with λ the largest of the positive eigenvalues (if there is at least one), indicatively at the time $a_{sc} = \lambda^{-1}(\mathbf{q})$, the density becomes locally infinite. This event is known as shell-crossing, or orbit-crossing or also caustic, and occurs when two or more particles coming from different Lagrangian positions $\mathbf{q}_\alpha$ arrive to the same Eulerian position $\mathbf{x}$ at a certain time a, causing the Jacobian to be ill-defined, diverging, due to the lost invertibility of the map $\mathbf{q}_\alpha \longleftrightarrow \mathbf{x}$ for each single particle.
These singularities, the pancakes, proceed via a quasi-one-dimensional gravitational collapse, and mark the breaking of the validity of the Zel'dovich Approximation: of course, the approximation would imply that particles continue their motion along their straight trajectories, thing that is absolutely unphysical, because the gravitational interaction between neightboring particles surely modifies their motion and thus pancakes will actually be stabilized by gravity. This means that these configurations, characterized by the aggregated presence of matter, whose density contrast is clearly very high, but actually non-infinite, will become the preferential sites for galaxies formation, that is for structure formation.
Of course, one can actually think to improve analytically the behaviour near the sites of shell-crossing, accounting for the gravitational interaction among near particles: a first attempt in this direction was done proposing the Adhesion Approximation [28], trying to overcome the limitations of the Zel'dovich Approximation at the shell-crossing adding a fictitious adhesion term in the Euler equation, in the following way:

$$\begin{cases} \frac{D\eta}{Da} + \eta\,\nabla\cdot\mathbf{u} = 0 \\ \frac{D\mathbf{u}}{Da} = \nu\nabla^2\mathbf{u} \end{cases}, \tag{1.78}$$

differing from the Zel'dovich's treatment for the kinematic viscosity term at the right hand side of the second equation, where ν is the kinematic viscosity coefficient, with dimension of the square of a length on time. This kinematic term is intended to have a large effect close to the shell-crossing sites, while to be negligible out of them.
The modified Euler equation is known as three-dimensional Burgers' equation and it is solved starting from the assumption that the velocity field is irrotational, in such a way that it can be written as the gradient of its velocity potential Υ:

$$\mathbf{u}(\mathbf{x},a) = \nabla\Upsilon(\mathbf{x},a), \tag{1.79}$$

which, noticing that $\frac{1}{2}\partial_i(\partial_j\Upsilon\partial^j\Upsilon) = u^j\partial_j u_i = (\mathbf{u}\cdot\nabla)\mathbf{u}$, using the definition of convective derivative and taking the gradient of Burgers' equation, leads to the Bernoulli equation:

$$\frac{\partial\Upsilon}{\partial a} + \frac{1}{2}(\nabla\Upsilon)^2 = \nu\nabla^2\Upsilon, \tag{1.80}$$

that can be solved analytically by means of the non-linear Hopf-Cole transformation $\Upsilon = -2\nu\ln\mathcal{U}$, where $\mathcal{U}$ is called "expotential". Indeed, making the transformation and the derivatives, we get the Fokker-Planck equation:

$$\frac{\partial\mathcal{U}}{\partial a} = \nu\,\nabla^2\mathcal{U}, \tag{1.81}$$

a parabolic linear differential equation needing both the initial and the boundary conditions in order to be solved. We start considering the classic separated variables trial solution $\mathcal{U} = f(a)\, g(\mathbf{x})$, that inserted in the Fokker-Planck gives:

$$f(a) = e^{Ea} \quad \text{and} \quad E\, g(\mathbf{x}) = \nu\, \nabla^2 g(\mathbf{x}), \tag{1.82}$$

the second giving in Fourier space the relation $E_k g_{\mathbf{k}} = -\nu k^2 g_{\mathbf{k}}$, and henceforth, enforced by the superposition principle, we write the general solution as:

$$\mathcal{U}(\mathbf{x}, a) = \int_{\mathbb{R}^3} \frac{d\mathbf{k}}{(2\pi)^3}\, e^{-\nu k^2 a}\, g_{\mathbf{k}} e^{i\mathbf{k}\cdot\mathbf{x}}, \tag{1.83}$$

with generic Fourier coefficients to be fixed by initial and boundaries conditions. We continue looking for the so called "kernel" of the solution, that is the one with free boundary conditions, or the probability that a particle has position $\mathbf{x}$ at time a given that at $a = 0$ it was in $\mathbf{q}$, corresponding to a Dirac's delta function at $a = 0$:

$$\lim_{a\to 0} \mathcal{K}(\mathbf{x}, a|\mathbf{q}, 0) = \delta(\mathbf{x} - \mathbf{q}), \tag{1.84}$$

occurring choosing straightforwardly $g_{\mathbf{k}} = e^{-i\mathbf{k}\cdot\mathbf{q}}$, in such a way that the kernel results in a gaussian function with centre in $\mathbf{q}$ and dispersion $2\nu a$, increasing with time:

$$\mathcal{K}(\mathbf{x}, a|\mathbf{q}, 0) = \int_{\mathbb{R}^3} \frac{d\mathbf{k}}{(2\pi)^3}\, e^{-\nu k^2 a} e^{i\mathbf{k}\cdot(\mathbf{x}-\mathbf{q})} = \frac{1}{(4\pi\nu a)^{3/2}} e^{-\frac{(\mathbf{x}-\mathbf{q})^2}{4\nu a}}. \tag{1.85}$$

To fulfil the initial condition fixing the velocity $\mathcal{U}_0(\mathbf{q})$ consistently with $\mathbf{u}_0(\mathbf{q})$, we use the Chapman-Kolmogorov equation:

$$\mathcal{U}(\mathbf{x}, a) = \int_{\mathbb{R}^3} d\mathbf{q}\, \mathcal{U}_0(\mathbf{q}) \mathcal{K}(\mathbf{x}, a|\mathbf{q}, 0), \tag{1.86}$$

a mere consequence of Bayes' theorem for conditional probability, stating that for two events A and B we have:

$$P(A|B) = \frac{P(A\cap B)}{P(B)} \Rightarrow P(A\cap B) = P(B)P(A|B) \Rightarrow P(A) = \int dB P(B) P(A|B), \tag{1.87}$$

reinterpreting $P(B)$ and $P(A|B)$ respectively with $\mathcal{U}_0$ and $\mathcal{K}$.
By exponentiation of the definition of $\mathcal{U}$ in terms of Υ, recalling that $\mathbf{u}$ is the gradient of Υ and using the initial condition (1.70), we obtain soon:

$$\mathcal{U}_0(\mathbf{q}) = e^{-\frac{\Upsilon_0(\mathbf{q})}{2\nu}} = e^{\frac{\Psi_0(\mathbf{q})}{2\nu}}, \tag{1.88}$$

that inserted in Eq.(1.86) gives:

$$\mathcal{U}(\mathbf{x}, a) = \int_{\mathbb{R}^3} \frac{d\mathbf{q}}{(4\pi\nu a)^{3/2}} e^{-\frac{1}{2\nu}\left[\frac{(\mathbf{x}-\mathbf{q})^2}{2a} - \Psi_0(\mathbf{q})\right]} = \int_{\mathbb{R}^3} \frac{d\mathbf{q}}{(4\pi\nu a)^{3/2}} e^{-\frac{1}{2\nu} S(\mathbf{x},\mathbf{q},a)}. \tag{1.89}$$

Hence, the solution of the Adhesion Approximation is:

$$\begin{cases} \mathbf{u}(\mathbf{x}, a) = \nabla\cdot\Upsilon(\mathbf{x}, a) = -2\nu \frac{\nabla\mathcal{U}}{\mathcal{U}} = \frac{\int_{\mathbb{R}^3} d\mathbf{q} \frac{(\mathbf{x}-\mathbf{q})}{a}\, e^{-\frac{1}{2\nu} S(\mathbf{x},\mathbf{q},a)}}{\int_{\mathbb{R}^3} d\mathbf{q}\, e^{-\frac{1}{2\nu} S(\mathbf{x},\mathbf{q},a)}} \\ \eta(\mathbf{x}, a) = \left|\frac{\partial \mathbf{x}(\mathbf{q},a)}{\partial \mathbf{q}}\right|^{-1} \end{cases}, \tag{1.90}$$

and integrating the first equation, solution of the modified Euler equation, we have:

$$\mathbf{x}(\mathbf{q}, a) = \mathbf{q} + \int_0^a da' \, \mathbf{u}[\mathbf{x}(\mathbf{q}, a'), a'], \tag{1.91}$$

while the second equation of the system, solution of the continuity equation, formally does not change with respect to the Zel'dovich Approximation.
The coefficient ν regulates the thickness of the pancakes, which is proportional to $\nu^{\frac{1}{2}}$, making them more physical objects; in particular, we are interested in small values of ν and we can perform an explicit analytical solution for $\mathbf{u}$ considering the limit $\nu \to 0$: in fact, in this limit we can evaluate the integral appearing in the solution for $\mathbf{u}$ using the steepest-descent, or saddle-point, approximation, essentially based on the exploitation of the fact that for a sharply peaked function, as $e^{-\frac{S}{2\nu}}$ for small values of ν, the largest contribution to the integral comes from the absolute minima $\mathbf{q}_s$ of S for a given $\mathbf{x}$ and a, satisfying the condition $\nabla_{\mathbf{q}} S(\mathbf{x}, \mathbf{q}, a)\big|_{\mathbf{q}_s} = 0$.
Henceforth, expanding S to the second order around these minima, for $\mathcal{U}$ in (1.89) we have, noting that S must have the same value in all the absolute minima:

$$\mathcal{U}(\mathbf{x}, a) = \frac{1}{(4\pi\nu a)^{3/2}} \, e^{-\frac{S(\mathbf{x},\mathbf{q},a)}{2\nu}} \int d\delta\mathbf{q} \, e^{-\frac{1}{4\nu} \sum_{i,j=1}^{3} \frac{\partial^2 S}{\partial q_i \partial q_j}\Big|_{\mathbf{q}_s} \delta q^i \delta q^j} = e^{-\frac{S(\mathbf{x},\mathbf{q}_s,a)}{2\nu}} \sum_s j_s(\mathbf{x}, \mathbf{q}_s, a), \tag{1.92}$$

where gaussian integration has allowed to fix:

$$j_s(\mathbf{x}, \mathbf{q}_s, a) = \left(\det \left[\frac{\partial^2 S(\mathbf{x}, \mathbf{q}, a)}{\partial q_i \partial q_j} \bigg|_{\mathbf{q}_s} \right] \right)^{-\frac{1}{2}}. \tag{1.93}$$

At this point, looking at the first equation in (1.90), noting that:

$$\nabla_{\mathbf{x}} S(\mathbf{x}, \mathbf{q}_s, a) = \frac{\mathbf{x} - \mathbf{q}_s}{a}, \tag{1.94}$$

we reach:

$$\mathbf{u}(\mathbf{x}, a) = \sum_s \frac{\mathbf{x} - \mathbf{q}_s}{a} \, w_s(\mathbf{x}, \mathbf{q}_s, a), \tag{1.95}$$

where $w_s = j_s / \sum_s j_s$, highlighting as the velocity takes contributions from different trajectories starting from the absolute minima $\mathbf{q}_s$ of S for given position and time, making us aware that in the accretion sites the dynamics described by Zel'dovich Approximation is not realistic, pre-supposing some kind of interaction between the matter particles.

1.2.3.2 N-body simulations.

Actually, as we have seen in the first subsection, the situation is a bit more complex: the most modern direct observations by redshift sky surveys (see Fig.(1.1) for SDSS results) and mappings of various wavelength bands of electromagnetic radiation have yielded much information on the content and characteristics of our Universe's structure, that has begun to be clarified in particular starting from the late eighties. The organization of structure arguably begins at the stellar level, even if the most part of the cosmologist rarely addresses on that scale; stars are organized into galaxies, which in turn form galaxy groups, galaxy clusters, superclusters, sheets, walls and filaments, separated by immense voids and thus creating a vast foam-like structure,

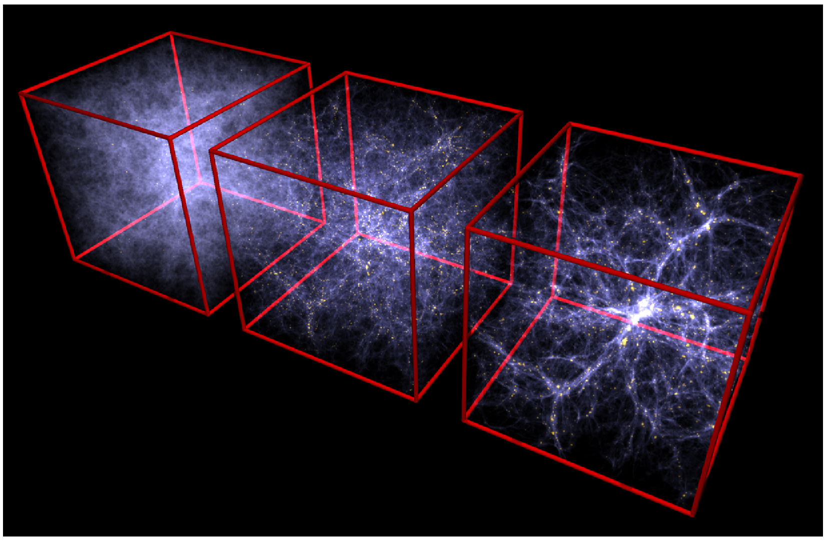

Figure 1.2: This figure shows three moments in the simulated history of structures formation in the gaseous component of the universe, in a simulation box with side of $100\,h^{-1}\mathrm{Mpc}$. From left to right it is represented the matter distribution at the three redshifts $z = 6, z = 2, z = 0$. Formed stellar material could be seen in yellow.

sometimes called the cosmic web, as showed in Fig.(1.2)[6]. The CDM model has become the leading theoretical paradigm for the formation of structure in the Universe and together with the theory of cosmic inflation, this model makes a clear prediction for the initial conditions for structure formation and predicts that structures grow hierarchically through gravitational instability. Testing this model requires that the precise measurements delivered by galaxy surveys can be compared to robust and equally precise theoretical calculations. However, the complexity of the physical behaviour of matter density fluctuations in the non-linear regime makes it impossible to study exactly the details of the Universe's structure by means of analytical methods that, although very valuable for providing us with a physical understanding of the processes involved, are completely useless to make any detailed prediction able to be tested against observations: for this task we actually need numerical simulation methods, the strongest being grouped under the name of N-body simulations.
These are based on the possibility to represent part of the expanding Universe as a box containing a large number N of point masses (representing matter particles) interacting through their mutual gravity, with chosen boundary conditions, usually taken to be periodic; this box, typically a cube, in order to provide a "fair sample" representative of our Universe as a whole, must be large at least as the scale at which the Universe is expected to become homogeneous. These codes, starting from the computation of the forces among the N particles, evaluate in a very precise way the behaviour of matter perturbations and thus they are expected to describe well the Universe's structure with its evolution. A number of different techniques, all going under the name of N-body simulations, are available at the present time, differing mainly in the way the forces on each particle are calculated; in the following we briefly describe some of the most popular N-body simulation methods.

[6]This figure, with many other ones produced by means of numerical simulations, can be found at: http://wwwmpa.mpa-garching.mpg.de/galform/data_vis/index.shtml.

Conceptually, the simplest way to compute the non-linear evolution of the cosmological fluid is to represent it as a discrete set of particles and then to compute all the pairwise gravitational interactions between them and to sum all of them to calculate directly the newtonian forces; this group of techniques is then called particle-particle, or briefly PP, computation, allowing in principle to get the resulting acceleration to update each particle velocity and position, used to recalculate the interparticles forces, proceeding in this way at all time-step. However, the pure formulation of PP simulations have an important problem: the newtonian gravitational force between two particles increases as the particles approach each other, making necessary the choice of a very small time-step in order to resolve the large velocity changes induced by this configuration, causing, jointly with a hoped large N, to the consumption of enormous amounts of time even for the most evolved and powerful computers, coupled to their inability in handling formally divergent force terms occurring when particles are arbitrarily close to each other. Wanting to use such a method, the latter problem is usually faced treating each particle as an extended body by introducing in the denominator of the definition of the newtonian gravitational force a softening length that avoids divergences, but the problem of slowness actually remains crucial: if our simulation contains N particles, the PP computation requires to evaluate $N(N-1)/2$ interactions at each time-step, determining the total computation time to scale roughly as N^2, fixing $N \approx 10^4$ as the maximum number of particles that can be possibly used, too low to give a realistic simulation of large-scale structure formation of our Universe.

The usual method to improve the N-body simulations based on direct summation methods explained above is some form of particle-mesh, or PM, scheme. The basic principle is that the system of particles is converted into a grid (the mesh) of density values, by dividing the simulation box in a given number of small cubes where we set a certain number of fluid particles; various methods for converting a system of particles into a grid of densities exist: for example, one method is that each particle simply gives its mass to its position in the mesh, another one is the Cloud-in-Cell (CIC) method, where the particles are modelled as constant density cubes, and one particle can contribute to the mass of several cells. Once the density distribution is found, the potential of each point in the mesh can be determined from the Poisson equation, that is easily solved after applying the Fourier transform, and forces are computed by means of a finite differencing scheme and applied to each particle based on what cell it is in, and where in the cell it lies. Thus it is faster to do a PM calculation than to simply add up all the interactions on a particle due to all other particles for two reasons: firstly, there are usually fewer grid points than particles, so the number of interactions to calculate is smaller (the total time of computing is reduced roughly to $N_c \ln N_c$, where N_c is the number of cells), allowing to consider a higher number of particles to simulate our Universe in a more realistic way, and secondly the grid technique permits the use of Fourier transform techniques to evaluate the potential, that can be very fast. Although the previous pros, PM is considered an obsolete method because it gives a poor force resolution on small scales, due to the finite spatial size of the mesh.

A substantial increase in spatial resolution, keeping reasonable the computational time, can be achieved using the hybrid method called particle-particle-particle mesh, aiming to improve the short range part of the PM method by using the PP method at these scales, that is solving the force by direct sum, and keeping with the pure PM method when treating larger scales, fixing the transition between the two regions by means of a comoving distance parameter r_s, usually fixed in terms of some grid units: thus, PP + PM = $\mathrm{P^3M}$.

Finally, we close with the presentation of the N-body simulations zoology spending some words on tree codes, an alternative set of procedures for enhancing the force resolution of particle codes keeping the necessary demand on computational time within a reasonable limit. This promising approach treats distant clumps of particles as single massive pseudo-particles: in particular, usually the simulation box is organized in a mesh whose single cells are divided in

eight sub-cells if they contain more than one particle and iterating the procedure if some of the sub-cells contains more than one particle, creating a tree-like structure that can be used to calculate the forces at different scales using different levels of the resulting "tree", namely treating the distant forces using the coarsely grained distribution relative to the high level of the tree, while using the finer grid for forces at short range. However, this interesting approach has a use limited to big collaborations, due to the fact that, even if the computational time is reduced with respect to P^3M methods, it requires considerable memory resources.
Nowadays, variants of PM, P^3M and tree techniques are the standard workhorses for the study of cosmological clustering and usually they are mixed together at different scales to take benefit of all their pros, discarding lots of their cons. This is the case of the Millennium Simulation[7], published in 2005 and then repeatedly updated according to the most recent constraints that have been periodically released by sky surveys, the last run being completed in 2014. When published in 2005, the Millennium Run was the largest ever simulation of the formation of structure within the ΛCDM cosmology: it used ten billion of particles to follow the dark matter distribution in a cubic region of $500h^{-1}\mathrm{Mpc}$ on a side, and has a spatial resolution of $5h^{-1}\mathrm{kpc}$. The Millennium Simulation, a project of the Virgo consortium, was carried out with a specially customised version of the GADGET2 code, using the TreePM method for evaluating gravitational forces, namely a combination of a hierarchical tree expansion and a classical Fourier transform particle-mesh method. The calculation was performed on 512 processors of an IBM computer at the Computing Centre of the Max-Planck Society in Garching (Germany) and it exploited almost all the 1 TB of physically distributed memory available, requiring about 350000 processor hours of CPU time, or 28 days of wall-clock time.
We now present a set of figures reporting some significant outputs of the Millennium Simulation, corroborating the qualitative picture given by the approximated analytical analysis presented before. In Figgs.(1.3)-(1.6), we show some slices through the matter density field at three different scales for four different redshifts, but all with a thickness of $15\,h^{-1}\mathrm{Mpc}$. In particular, for each redshift, we show three panels, each ones zooming in by a factor of four with respect to the one at its left: then, the white bars denote, for each redshift and from left to right, a scale of $500\,h^{-1}\mathrm{Mpc}$, $125\,h^{-1}\mathrm{Mpc}$ and $31.25\,h^{-1}\mathrm{Mpc}$. As we see, starting at early times with a configuration of complete isotropy and homogeneity at all scales, going on with time the matter fluid, subjected to gravitational collapse, accordingly with the "bottom-up" scheme (consequent to the choice of a non-relativistic fluid) forms the first proto-structures at very small scales, which going on with time become organised in defined structures at larger scales, ending at present time with neuronal-like large-scale structure, that however doesn't affect the isotropy and homogeneity at very large-scales.

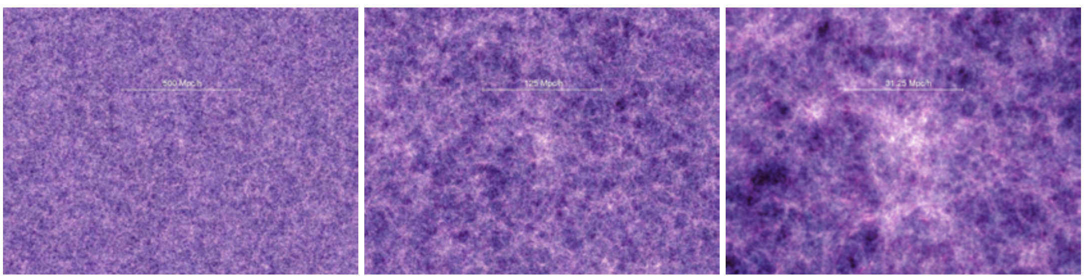

Figure 1.3: Slices of CDM density at $z = 18.3$, corresponding to and age of $0.21\,\mathrm{Gyr}$.

[7] We cite the paper [29] as a good introduction, while for further information we address the reader to `http://wwwmpa.mpa-garching.mpg.de/millennium/`, where we also found all the figures shown here.

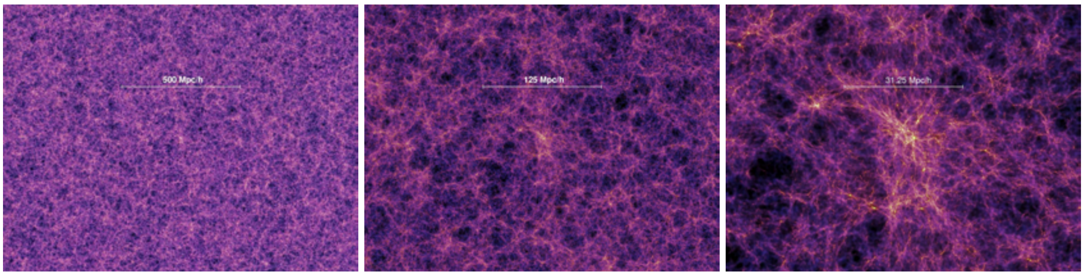

Figure 1.4: Slices of CDM density at $z = 5.7$, corresponding to and age of $1.0\,\mathrm{Gyr}$.

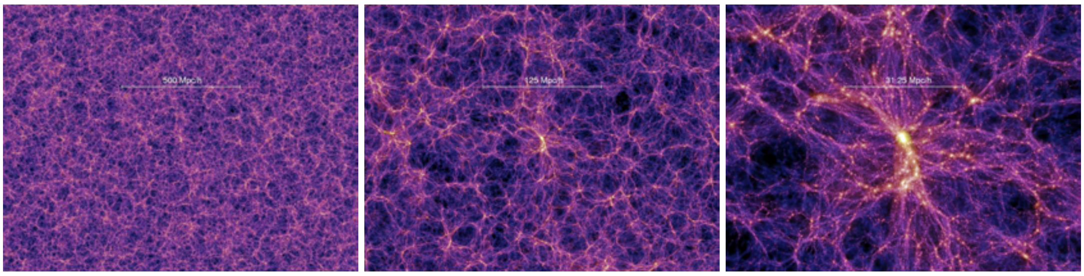

Figure 1.5: Slices of CDM density at $z = 1.4$, corresponding to and age of $4.7\,\mathrm{Gyr}$.

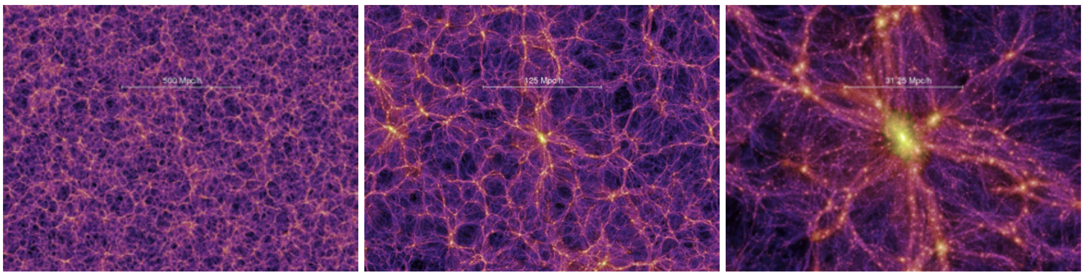

Figure 1.6: Slices of CDM density at $z = 0$, corresponding to and age of $13.6\,\mathrm{Gyr}$.

Clearly, all we can observe are galaxies, whose emitted light is due to the interactions between particles of ordinary barionic matter, a small fraction of the whole matter content of the Universe, mainly consisting in CDM: henceforth, in order to get the cosmological informations on dark matter distribution from galaxies, it is needed to understand the relation between the distributions of galaxies and that of the dark matter, known as bias problem. Nowadays it is thought that the two distributions do not coincide, but, according to the dark matter halo model, it is assumed that the former provides a good tracer for the latter, controlled by (hopefully) a few bias parameters. The simplest way to define it passes through a perturbative approach, where the density contrast of galaxies δ_g in a given position is defined as the Taylor expansion of the density contrast of dark matter δ_m at the same position, as:

$$\delta_g(\mathbf{x}) = \sum_n \frac{b_n}{n!}\delta_m(\mathbf{x}), \tag{1.96}$$

and currently truncating at the first order, in such a way that $\delta_g = b\,\delta_m$ and b is called the liner bias. Moreover, in the middle eighties cosmologists as Kaiser and Bardeen introduced the biasing mechanism [30], providing an ansatz for the structure formation that is considered correct right now: in particular, it is assumed that observed objects form in regions where the matter density contrast has a peak over a suitable threshold, namely that structures coincides with density contrast peaks or, more smoothly, that they form where the matter density field exceeds a given threshold. The ending Fig.(1.7) represents the large-scale light (galaxy) distribution in our simulated Universe and, for comparison, the corresponding dark matter distribution, at the same scale and time.

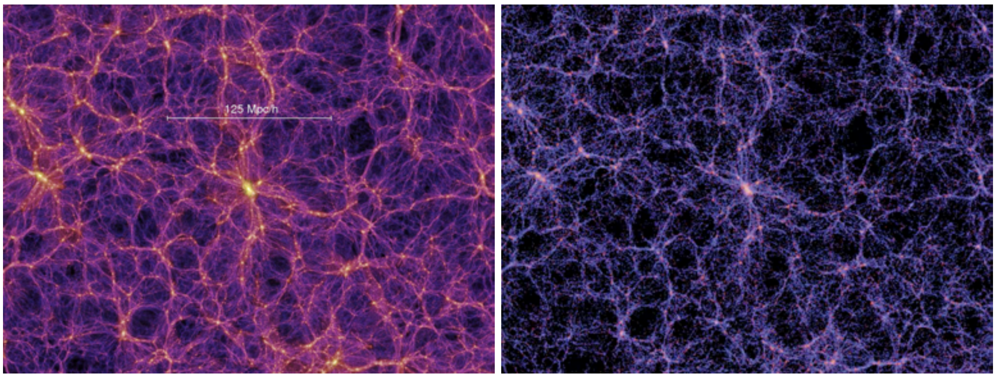

Figure 1.7: Comparison between the simulated dark matter (left) and light (galaxy) distributions at the same scale at $z = 0$.

Chapter 2

A field theory approach to cosmological dynamics.

2.1 The evolution equations for dark matter.

For the analytical purposes of the present section, we start considering an Einstein-de Sitter universe, where $\bar{\rho}$ refers to the isotropic and uniform background density of cold dark matter, taken to be the sole constituent of the whole matter filling this universe; however, throughout the work we will repeatedly consider more accurate models. We describe the distribution of a gas of CDM particles of mass m by the function $f(\mathbf{x}, \mathbf{p}, \tau)$, where, according to the eulerian description [16], $\mathbf{x}$ represents the comoving three-dimensional spatial coordinate, $\mathbf{v} = \frac{d\mathbf{x}}{d\tau}$ the peculiar velocity, $\mathbf{p} = am\frac{d\mathbf{x}}{d\tau}$ the three-dimensional moment, τ the conformal time (defined by $\frac{d\tau}{dt} = \frac{1}{a}$, being t the cosmic time) and a the time dependent scale factor. Actually, f is the probability distribution function for the DM gas, defined by the following relation:

$$\int_{\mathbb{R}^3} d^3\mathbf{p}\; f(\mathbf{x}, \mathbf{p}, \tau) \equiv \rho(\mathbf{x}, \tau) \equiv \bar{\rho}(\tau)[1 + \delta(\mathbf{x}, \tau)], \tag{2.1}$$

where $\rho(\mathbf{x}, \tau)$ is the total density of the DM gas in the coordinate $\mathbf{x}$, written in terms of the (pure Einstein-de Sitter) background density $\bar{\rho}$ and the density contrast $\delta(\mathbf{x}, \tau) = \frac{\rho(\mathbf{x},\tau)-\bar{\rho}}{\bar{\rho}}$. The evolution of f is governed by the Vlasov equation (1.41):

$$\frac{\partial f}{\partial \tau} + \frac{\mathbf{p}}{am} \cdot \nabla f - am\, \nabla\Phi \cdot \nabla_{\mathbf{p}} f = 0, \tag{2.2}$$

where the gravitational potential Φ obeys, at sub-horizon scales, the Poisson equation:

$$\nabla^2\Phi(\mathbf{x}, \tau) = \frac{3}{2}H^2(\tau)\delta(\mathbf{x}, \tau), \tag{2.3}$$

where $H(\tau) \equiv \frac{d\ln a}{d\tau} = \frac{\dot{a}}{a} = \frac{da}{dt} = aH(t)$ is the comoving Hubble parameter.
Due to the non-locality and non-linearity of the Vlasov equation, its analytic solution is not known. The canonical way to deal with this issue is to consider the moments of f. The N-th order moment of the distribution function f, is defined as:

$$\mathcal{M}_f^{(N)} = \int_{\mathbb{R}^3} d^3\mathbf{p}\; \frac{p_{i_1} p_{i_2} \cdots p_{i_N}}{a^N m^N} f(\mathbf{x}, \mathbf{p}, \tau), \tag{2.4}$$

in such a way that the 0-order moment is simply Eq.(2.1), that is the density of the gas, while the following two moments, $\mathcal{M}_f^{(1)}$ and $\mathcal{M}_f^{(2)}$ are:

$$\mathcal{M}_f^{(1)} = \int_{\mathbb{R}^3} d^3\mathbf{p}\ \frac{p_i}{am} f(\mathbf{x},\mathbf{p},\tau) = \rho(\mathbf{x},\tau) v_i(\mathbf{x},\tau) \quad \text{and} \tag{2.5}$$

$$\mathcal{M}_f^{(2)} = \int_{\mathbb{R}^3} d^3\mathbf{p}\ \frac{p_i p_j}{a^2m^2} f(\mathbf{x},\mathbf{p},\tau) = \rho(\mathbf{x},\tau) v_i(\mathbf{x},\tau) v_j(\mathbf{x},\tau) + \sigma_{ij}(\mathbf{x},\tau), \tag{2.6}$$

where v_i refers to the components of the peculiar velocity of the CDM gas, while σ is the velocity dispersion, estimating the degree of orbits crossing among the different particles of the gas. Setting this quantity to zero is equivalent to have a single valued velocity field at each particle positions: the so called single-stream approximation. According to this configuration, one keeps only the first two moments of the Vlasov equation, using the definition of moments of f and simplifying the results.
The 0-order moment gives the well known continuity equation:

$$\begin{aligned}
&\int_{\mathbb{R}^3} d^3\mathbf{p}\ \frac{\partial f}{\partial \tau} + \int_{\mathbb{R}^3} d^3\mathbf{p}\ \frac{\mathbf{p}}{am}\cdot \nabla f - \int_{\mathbb{R}^3} d^3\mathbf{p}\ am\, \nabla\Phi \cdot \nabla_{\mathbf{p}} f = \\
&\quad = \frac{\partial}{\partial \tau} \int_{\mathbb{R}^3} d^3\mathbf{p}\ f + \frac{\nabla}{am}\cdot \int_{\mathbb{R}^3} d^3\mathbf{p}\ \mathbf{p} f - am\nabla\Phi \cdot \int_{\mathbb{R}^3} d^3\mathbf{p}\ \nabla_{\mathbf{p}} f = \\
&\quad = \frac{\partial}{\partial \tau}\rho(\mathbf{x},\tau) + \nabla\cdot(\rho(\mathbf{x},\tau)\mathbf{v}(\mathbf{x},\tau)) - am\nabla\Phi \cdot \int_{\Sigma_{\mathbf{p}\infty}} d\Sigma_{\mathbf{p}}\ \hat{\mathbf{n}} f = \\
&\quad = \frac{\partial}{\partial \tau}\rho(\mathbf{x},\tau) + \nabla\cdot[\rho(\mathbf{x},\tau)\mathbf{v}(\mathbf{x},\tau)],
\end{aligned} \tag{2.7}$$

where for the third term we used the Gauss theorem, provided that $f(\mathbf{x},\mathbf{p}\to\infty,\tau) = \mathbf{0}$. Using the expression (2.1) and specifying the above result at the 0-th order, that is without the density and velocity perturbations δ and $\mathbf{v}$ as in [31], we find the constraint:

$$\frac{\partial \bar{\rho}(\tau)}{\partial \tau} = 0, \tag{2.8}$$

that inserted in the previous result gives the following form for the continuity equation:

$$\frac{\partial}{\partial \tau}\delta(\mathbf{x},\tau) + \nabla\cdot[(1+\delta(\mathbf{x},\tau))\mathbf{v}(\mathbf{x},\tau)] = 0. \tag{2.9}$$

The following moment of Vlasov equation gives indeed the Euler equation:

$$\begin{aligned}
&\frac{1}{m}\int_{\mathbb{R}^3} d^3\mathbf{p}\ p_i \frac{\partial f}{\partial \tau} + \frac{1}{m^2}\int_{\mathbb{R}^3} d^3\mathbf{p}\ \frac{p_i p_j}{a}\frac{\partial f}{\partial x_j} - \int_{\mathbb{R}^3} d^3\mathbf{p}\ a\, p_i \frac{\partial \Phi}{\partial x_j}\frac{\partial f}{\partial p_j} = \\
&\quad = \frac{\partial}{\partial \tau}(a v_i \rho) + a\frac{\partial}{\partial x_j}(\rho v_i v_j) - a\frac{\partial \Phi}{\partial x_j}\int_{\mathbb{R}^3} d^3\mathbf{p}\ a\, p_i \frac{\partial f}{\partial p_j} = \\
&= a v_i \frac{\partial \rho}{\partial \tau} + \frac{\partial a}{\partial \tau} v_i\rho + a\frac{\partial v_i}{\partial \tau}\rho + a\frac{\partial \rho}{\partial x_j} v_i v_j + a\rho v_j \frac{\partial v_i}{\partial x_j} + a\rho v_i \frac{\partial v_j}{\partial x_j} + a\frac{\partial \Phi}{\partial x_j}\int_{\mathbb{R}^3} d^3\mathbf{p}\ f\delta_{ij} = \\
&\quad = \frac{\partial a}{\partial \tau} v_i\rho + a\frac{\partial v_i}{\partial \tau}\rho + a\rho v_j \frac{\partial v_i}{\partial x_j} + a\rho\frac{\partial \Phi}{\partial x_i} = 0,
\end{aligned} \tag{2.10}$$

where for the last term we used the integration by parts with the same assumption on f of the first case, while the first term of the third line, through the continuity equation, cancels the

fourth and the sixth term of the same line.
Eventually, we are left with a closed system of equations that solves the Vlasov equation in the single stream approximation, consistently with [17, 19]:

$$\begin{cases} \frac{\partial}{\partial\tau}\delta(\mathbf{x},\tau) + \nabla\cdot[(1+\delta(\mathbf{x},\tau))\mathbf{v}(\mathbf{x},\tau)] = 0 \\ \frac{\partial}{\partial\tau}\mathbf{v}(\mathbf{x},\tau) + (\mathbf{v}(\mathbf{x},\tau)\cdot\nabla)\mathbf{v}(\mathbf{x},\tau) + H(\tau)\mathbf{v}(\mathbf{x},\tau) = -\nabla\Phi(\mathbf{x},\tau) \\ \nabla^2\phi(\mathbf{x},\tau) = \frac{3}{2}H^2(\tau)\delta(\mathbf{x},\tau) \end{cases} . \tag{2.11}$$

Now, we want to skip to the Fourier transformed of the equations in (2.11), as done in [32, 33, 34]. To do this, it is customary defining the velocity divergence $\theta(\mathbf{x},\tau) = \nabla\cdot\rho(\mathbf{x},\tau)$ and using it instead of the velocity as one of the two main fields, the other being the contrast. In this way it can be seen that the system (2.11) reduces to only two independent equations, being the Poisson equation immediately inserted in the Euler one for the velocity divergence. The Fourier transformed and anti-transformed of a field $g(\mathbf{x})$ are defined by:

$$g(\mathbf{k}) = \int_{\mathbb{R}^3} \frac{d\mathbf{x}}{(2\pi)^3}\, g(\mathbf{x})e^{i\mathbf{k}\cdot\mathbf{x}} \quad \text{and} \tag{2.12a}$$

$$g(\mathbf{x}) = \int_{\mathbb{R}^3} d\mathbf{k}\, g(\mathbf{k})e^{-i\mathbf{k}\cdot\mathbf{x}}. \tag{2.12b}$$

Here, we report the procedure only for the continuity equation, given the strong analogy with the case of the Euler one. The first step consists in expressing the fields using the form (2.12b):

$$\begin{aligned} &\frac{\partial}{\partial\tau}\int_{\mathbb{R}^3} d\mathbf{k}'\,\delta(\mathbf{k}',\tau)e^{-i\mathbf{k}'\cdot\mathbf{x}} + \int_{\mathbb{R}^3} d\mathbf{k}'\,\theta(\mathbf{k}',\tau)e^{-i\mathbf{k}'\cdot\mathbf{x}} + \\ &\quad + \Big(\nabla\int_{\mathbb{R}^3} d\mathbf{p}\,\delta(\mathbf{p},\tau)e^{-i\mathbf{p}\cdot\mathbf{x}}\Big)\cdot\int_{\mathbb{R}^3} d\mathbf{q}\,\mathbf{v}(\mathbf{q},\tau)e^{-i\mathbf{q}\cdot\mathbf{x}} + \iint_{\mathbb{R}^3} d\mathbf{p}d\mathbf{q}\,\delta(\mathbf{p},\tau)\theta(\mathbf{q},\tau)e^{-i(\mathbf{p}+\mathbf{q})\cdot\mathbf{x}} = \\ &\int_{\mathbb{R}^3} d\mathbf{k}'\Big(\frac{\partial}{\partial\tau}\delta(\mathbf{k}',\tau)+\theta(\mathbf{k}',\tau)\Big)e^{-i\mathbf{k}'\cdot\mathbf{x}} + \iint_{\mathbb{R}^3} d\mathbf{p}d\mathbf{q}\Big(\frac{\mathbf{q}\cdot\mathbf{p}}{q^2}+1\Big)\delta(\mathbf{p},\tau)\theta(\mathbf{q},\tau)e^{-i(\mathbf{p}+\mathbf{q})\cdot\mathbf{x}} = 0, \end{aligned} \tag{2.13}$$

where the first term in the sum of the last integral descends from the third term of the left hand side, once made the derivation in $\mathbf{x}$ (giving $-i\mathbf{p}$) and written $\mathbf{v} = i\frac{\mathbf{q}}{q^2}\theta$: the whole term inside the parentheses can be indicated with $\alpha(\mathbf{q},\mathbf{p}) = \frac{\mathbf{q}\cdot\mathbf{p}+q^2}{q^2}$.
Taking the Fourier transform of the equation we get:

$$\begin{aligned} &\iint_{\mathbb{R}^3} d\mathbf{x}d\mathbf{k}'\Big(\frac{\partial}{\partial\tau}\delta(\mathbf{k}',\tau)+\theta(\mathbf{k}',\tau)\Big)e^{i(\mathbf{k}-\mathbf{k}')\cdot\mathbf{x}} + \iiint_{\mathbb{R}^3} d\mathbf{x}d\mathbf{p}d\mathbf{q}\,\alpha(\mathbf{q},\mathbf{p})\delta(\mathbf{p},\tau)\theta(\mathbf{q},\tau)e^{i(\mathbf{k}-\mathbf{p}-\mathbf{q})\cdot\mathbf{x}} = \\ &\quad = \Big(\frac{\partial}{\partial\tau}\delta(\mathbf{k},\tau)+\theta(\mathbf{k},\tau)\Big) + \iint_{\mathbb{R}^3} d\mathbf{p}d\mathbf{q}\,\delta(\mathbf{k}-\mathbf{p}-\mathbf{q})\alpha(\mathbf{q},\mathbf{p})\delta(\mathbf{p},\tau)\theta(\mathbf{q},\tau) = 0. \end{aligned} \tag{2.14}$$

An analogue expression can be found for the Euler equation, using the transformed of the Poisson equation $-k^2\Phi = \frac{3}{2}H^2\delta$ and defining $\beta(\mathbf{q},\mathbf{p}) = \frac{(\mathbf{q}+\mathbf{p})^2\mathbf{q}\cdot\mathbf{p}}{2q^2p^2}$, in such a way that the system (2.11) in Fourier space is:

$$\begin{cases} \frac{\partial}{\partial\tau}\delta(\mathbf{k},\tau) + \theta(\mathbf{k},\tau) + \iint_{\mathbb{R}^3} d\mathbf{p}d\mathbf{q}\,\delta(\mathbf{k}-\mathbf{p}-\mathbf{q})\alpha(\mathbf{q},\mathbf{p})\theta(\mathbf{q},\tau)\delta(\mathbf{p},\tau) = 0 \\ \frac{\partial}{\partial\tau}\theta(\mathbf{k},\tau) + H(\tau)\theta(\mathbf{k},\tau) + \frac{3}{2}H^2(\tau)\delta(\mathbf{p},\tau) + \iint_{\mathbb{R}^3} d\mathbf{p}d\mathbf{q}\,\delta(\mathbf{k}-\mathbf{p}-\mathbf{q})\beta(\mathbf{q},\mathbf{p})\theta(\mathbf{q},\tau)\theta(\mathbf{p},\tau) = 0 \end{cases} . \tag{2.15}$$

We can note that the two functions $\alpha(\mathbf{q},\mathbf{p})$ and $\beta(\mathbf{q},\mathbf{p})$ encode all the non-linearity and non-locality of Valsov equation. Setting them to zero we recover the linear (newtonian) theory and the well-known power law solutions of the above system (the superscript "0" means linear theory):

$$\begin{aligned} \delta^{(0)}(\mathbf{k},\tau) &= \delta^{(0)}(\mathbf{k},\tau_{in})\Big(\frac{a(\tau)}{a(\tau_{in})}\Big)^m \\ -\frac{\theta^{(0)}(\mathbf{k},\tau)}{H(\tau)} &= m\delta^{(0)}(\mathbf{k},\tau), \end{aligned} \tag{2.16}$$

where τ_{in} is the initial time, while $m = 1$ and $m = -\frac{3}{2}$ correspond to the growing and the decaying modes respectively.
Now, following mainly [13], we give a more compact form of the system (2.15). To this end, we define the vertex matrix $\gamma_{abc}(\mathbf{k},\mathbf{p},\mathbf{q})$, whose only non-zero entries are:

$$\begin{aligned} \gamma_{121}(\mathbf{k},\mathbf{p},\mathbf{q}) &= \frac{1}{2}\delta(\mathbf{k}-\mathbf{p}-\mathbf{q})\alpha(\mathbf{p},\mathbf{q}), \\ \gamma_{112}(\mathbf{k},\mathbf{p},\mathbf{q}) &= \frac{1}{2}\delta(\mathbf{k}-\mathbf{p}-\mathbf{q})\alpha(\mathbf{q},\mathbf{p}), \\ \gamma_{222}(\mathbf{k},\mathbf{p},\mathbf{q}) &= \delta(\mathbf{k}-\mathbf{p}-\mathbf{q})\beta(\mathbf{p},\mathbf{q}), \end{aligned} \tag{2.17}$$

with the property of parity and the symmetry $\gamma_{abc}(\mathbf{k},\mathbf{p},\mathbf{q}) = \gamma_{acb}(\mathbf{k},\mathbf{q},\mathbf{p})$. We also introduce the Ω-matrix, that in a Einstein-de Sitter model is:

$$\Omega = \begin{pmatrix} 1 & -1 \\ -\frac{3}{2} & \frac{3}{2} \end{pmatrix} \tag{2.18}$$

and the field doublet ϕ_a ($a = 1, 2$), set as [35, 36]:

$$\begin{pmatrix} \phi_1(\mathbf{k},\eta) \\ \phi_2(\mathbf{k},\eta) \end{pmatrix} \equiv e^{-\eta} \begin{pmatrix} \delta(\mathbf{k},\eta) \\ -\frac{\theta(\mathbf{k},\eta)}{H(\eta)} \end{pmatrix}, \tag{2.19}$$

where the new time variable is taken to be $\eta = \ln\frac{a}{a_{in}}$, a_{in} being the scale factor evaluated at a primordial (linear) epoch. With this definitions it is clear that the linear growing mode corresponds to $\phi_a^{(0)} = const$. Furthermore, the system (2.15) can be expressed with the following compact equation, where one has to remind that repeated indices are summed over and repeated momenta are integrated over (while ∂_η is a shorthand for $\frac{\partial}{\partial\eta}$):

$$(\delta_{ab}\partial_\eta + \Omega_{ab})\phi_b(\mathbf{k},\eta) = e^\eta\gamma_{abc}(\mathbf{k},\mathbf{p},\mathbf{q})\phi_b(\mathbf{p},\eta)\phi_c(\mathbf{q},\eta). \tag{2.20}$$

The proof can be made by hand, for example setting $a = 1$ Eq.(2.20) gives:

$$\begin{aligned} &(\delta_{1b}\partial_\eta + \Omega_{1b})\phi_b(\mathbf{k},\eta) = e^\eta\gamma_{1bc}(\mathbf{k},\mathbf{p},\mathbf{q})\phi_b(\mathbf{p},\eta)\phi_c(\mathbf{q},\eta) \\ &\Big[(\partial_\eta+1)\delta(\mathbf{k},\eta) + \frac{\theta(\mathbf{k},\eta)}{H(\eta)}\Big]e^{-\eta} = -\frac{e^{-\eta}}{2H(\eta)}\delta(\mathbf{k}-\mathbf{p}-\mathbf{q})\Big[\alpha(\mathbf{q},\mathbf{p})\delta(\mathbf{p},\eta)\theta(\mathbf{q},\eta) + \alpha(\mathbf{p},\mathbf{q})\theta(\mathbf{p},\eta)\delta(\mathbf{q},\eta)\Big] \\ &\partial_\eta\delta(\mathbf{k},\eta) - \delta(\mathbf{k},\eta) + \delta(\mathbf{k},\eta) + \frac{\theta(\mathbf{k},\eta)}{H(\eta)} = -\frac{1}{H(\eta)}\delta(\mathbf{k}-\mathbf{p}-\mathbf{q})\alpha(\mathbf{q},\mathbf{p})\delta(\mathbf{p},\eta)\theta(\mathbf{q},\eta) \\ &\partial_\tau\delta(\mathbf{k},\eta) + \theta(\mathbf{k},\eta) + \delta(\mathbf{k}-\mathbf{p}-\mathbf{q})\alpha(\mathbf{q},\mathbf{p})\delta(\mathbf{p},\eta)\theta(\mathbf{q},\eta) = 0, \end{aligned} \tag{2.21}$$

that is exactly the continuity equation in (2.15), once re-expressing the temporal fields dependence in τ rather than in η. The two addends on the right hand side of the second equation are indeed the same after an exchange between momenta integration, while the derivation on η, being related to that on τ by $\partial_\eta = \frac{1}{H}\partial_\tau$, makes possible the simplification of the Hubble parameter.
Now, we introduce the linear retarded propagator, a very important tool for the following developments. The linearised version of Eq.(2.20) can be obtained setting the vertex γ_{abc} to zero, in such a way that labelling the corresponding linear doublet as $\phi_a^{(0)}(\mathbf{k}, \eta)$ we get:

$$(\delta_{ab}\partial_\eta + \Omega_{ab})\phi_b^{(0)}(\mathbf{k}, \eta) = 0. \tag{2.22}$$

The linear retarded propagator $g_{ab}(\eta_a, \eta_b)$ is defined as the Green's function associated to the above equation, that is:

$$(\delta_{ab}\partial_{\eta_a}+\Omega_{ab})g_{bc}(\eta_a, \eta_b) = \delta_{ac}\delta(\eta_a - \eta_b), \tag{2.23}$$

and gives the linear evolution (to η_a) of density and velocity fields from any configuration of initial conditions (at η_b), because contracting Eq.(2.23) at the right with $\phi_c^{(0)}(\mathbf{k}, \eta_b)$, we obtain:

$$(\delta_{ab}\partial_{\eta_a} + \Omega_{ab})g_{bc}(\eta_a, \eta_b)\phi_c^{(0)}(\mathbf{k}, \eta_b) = \phi_a^{(0)}(\mathbf{k}, \eta_b)\delta(\eta_a - \eta_b), \tag{2.24}$$

that, taking $\eta_a > \eta_b$ (from which the adjective retarded), reduces to Eq.(2.22) if we write:

$$\phi_a^{(0)}(\mathbf{k}, \eta_a) = g_{ab}(\eta_a, \eta_b)\phi_b^{(0)}(\mathbf{k}, \eta_b), \tag{2.25}$$

actually giving the evolved doublet of the linearised fields, justifying the name of linear propagator to g_{ab}.
It is also straightforward to see that we can obtain the linear growing mode by taking the initial doublet simply proportional to $u = \left(\begin{smallmatrix}1\\1\end{smallmatrix}\right)$, while for the decaying one $v = \left(\begin{smallmatrix}1\\-3/2\end{smallmatrix}\right)$.
Since it will be useful in the following, we conclude the present part with the derivation of the full integral solution to Eq.(2.20), that allows moreover to reach the analytical form for the linear propagator, solution of Eq.(2.23), as done in [3]. Recalling the definition (2.19) of the fields doublet, we start specifying it as:

$$\phi_a(\mathbf{k}, \eta_a) = e^{-\eta_a}\tilde{\phi}_a(\mathbf{k}, \eta_a), \tag{2.26}$$

that writes Eq.(2.20) in the following way:

$$(\delta_{ab}\partial_\eta + \tilde{\Omega}_{ab})\tilde{\phi}_b(\mathbf{k}, \eta) = \gamma_{abc}(\mathbf{k}, \mathbf{p}, \mathbf{q})\tilde{\phi}_b(\mathbf{p}, \eta)\tilde{\phi}_c(\mathbf{q}, \eta), \tag{2.27}$$

where one of the two terms of the η-derivation subtracts a δ_{ab} to the matrix Ω, hence:

$$\tilde{\Omega} = \begin{pmatrix} 0 & -1 \\ -\frac{3}{2} & \frac{1}{2} \end{pmatrix} \tag{2.28}$$

We now introduce the time Laplace transform and antitransform respectively as:

$$g(\mathbf{k}, \omega) = \int_0^\infty d\eta\, g(\mathbf{k}, \eta)e^{-\omega\eta} \quad \text{and} \tag{2.29a}$$

$$g(\mathbf{x}, \eta) = \int_{c-i\infty}^{c+i\infty} \frac{d\omega}{2\pi i}\, g(\mathbf{k}, \omega)e^{\omega\eta}, \tag{2.29b}$$

where $\omega = \alpha + i\beta$ is a complex variable, often called frequency. Applying the Laplace transform to Eq.(2.27), we get:

$$\begin{aligned}
&\int_0^\infty d\eta\,(\delta_{ab}\partial_\eta + \tilde{\Omega}_{ab})\tilde{\phi}_b(\mathbf{k},\eta)\,e^{-\omega\eta} = \gamma_{abc}(\mathbf{k},\mathbf{p},\mathbf{q})\int_0^\infty d\eta\,\tilde{\phi}_b(\mathbf{p},\eta)\tilde{\phi}_c(\mathbf{q},\eta)\,e^{-\omega\eta}\\
&\omega\,\tilde{\phi}_a(\mathbf{k},\omega) - \tilde{\phi}_b(\mathbf{k},0) + \tilde{\Omega}_{ab}\,\tilde{\phi}_b(\mathbf{k},\omega) = \gamma_{abc}(\mathbf{k},\mathbf{p},\mathbf{q})\int_{c-i\infty}^{c+i\infty}\frac{d\omega'}{2\pi i}\,\tilde{\phi}_b(\mathbf{p},\omega')\,\tilde{\phi}_c(\mathbf{q},\omega-\omega') \qquad (2.30)\\
&\sigma^{-1}_{ab}\,\tilde{\phi}_b(\mathbf{k},\omega) = \tilde{\phi}_a(\mathbf{k},0) + \gamma_{abc}(\mathbf{k},\mathbf{p},\mathbf{q})\int_{c-i\infty}^{c+i\infty}\frac{d\omega'}{2\pi i}\,\tilde{\phi}_b(\mathbf{p},\omega')\,\tilde{\phi}_c(\mathbf{q},\omega-\omega'),
\end{aligned}$$

where in the first step we make use of the convolution theorem for Laplace transforms and in the second step we set $\sigma^{-1}_{ab}(\omega) = \omega\,\delta_{ab} + \tilde{\Omega}_{ab}$, whose inverse is simply:

$$\tilde{\sigma}(\omega) = \frac{1}{(2\omega+3)(\omega-1)}\begin{pmatrix} 2\omega+1 & 2 \\ 3 & 2\omega \end{pmatrix}. \qquad (2.31)$$

Next, multiplying the result of the Laplace transform for the above matrix and then straightforwardly antitrasforming we get:

$$\begin{aligned}
\tilde{\phi}_a(\mathbf{k},\eta) =& \Big[\int_{c-i\infty}^{c+i\infty}\frac{d\omega}{2\pi i}\,\sigma_{ab}(\omega)e^{\omega\eta}\Big]\tilde{\phi}_b(\mathbf{k},0) + \\
&+\int_0^\eta d\eta'\Big[\int_{c-i\infty}^{c+i\infty}\frac{d\omega}{2\pi i}\,\sigma_{ab}(\omega)e^{\omega(\eta-\eta')}\Big]\gamma_{bcd}(\mathbf{k},\mathbf{p},\mathbf{q})\tilde{\phi}_c(\mathbf{p},\eta')\tilde{\phi}_d(\mathbf{q},\eta'),
\end{aligned} \qquad (2.32)$$

that, recovering the old notation for fields, defining the linear propagator g_{ab} as:

$$g_{ab}(\eta) = e^{-\eta}\int_{c-i\infty}^{c+i\infty}\frac{d\omega}{2\pi i}\,\sigma_{ab}(\omega)e^{\omega\eta} \qquad (2.33)$$

and leaving free the initial time, arising simply changing the lower integration extreme from zero to, say, η_b, the full form of ϕ_a is:

$$\phi_a(\mathbf{k},\eta_a) = g_{ab}(\eta_a-\eta_b)\phi_b(\mathbf{k},\eta_b) + \int_{\eta_b}^{\eta_a} d\eta' g_{ab}(\eta_a-\eta')\,e^{\eta'}\gamma_{bcd}(\mathbf{k},\mathbf{p},\mathbf{q})\phi_c(\mathbf{p},\eta')\phi_d(\mathbf{q},\eta'), \quad (2.34)$$

meaning that the complete solution is the linear evolution of the initial fields, given by g_{ab}, plus a genuine non-linear correction term.
Of course we have to prove the equivalence between this definition of linear propagator with the the solution of Eq.(2.23): this naturally is possible and for this reason we have maintained the same notation. In order to obtain the proof, we need to calculate explicitly the integral in the definition (2.33): to this aim, we only need a bit of complex analysis, see [37]. Taking $\eta = \eta_a - \eta_b$, if $\eta < 0$ then $g_{ab} = 0$ for definition of Laplace antitrasformed, while if $\eta > 0$ we can define an integration path closing a semicircle at the left of the line $c = \mathrm{Re}\,\omega^\star$, according to the Jordan's theorem and choosing the line in such a way it contains the two singularities of the integrand $\omega_{1,2} = -\frac{3}{2}, 1$, as depicted in Fig.(2.1), taking the limit of infinite ray, $R \to \infty$.
Thus, when $\eta > 0$ the result of the integration is given by:

$$g_{ab}(\eta) = \frac{e^{-\eta}}{2\pi i}\{\mathrm{Res}\,[\sigma_{ab}(\omega)e^{\omega\eta}]\big|_{\omega_1} + \mathrm{Res}\,[\sigma_{ab}(\omega)e^{\omega\eta}]\big|_{\omega_2}\}, \qquad (2.35)$$

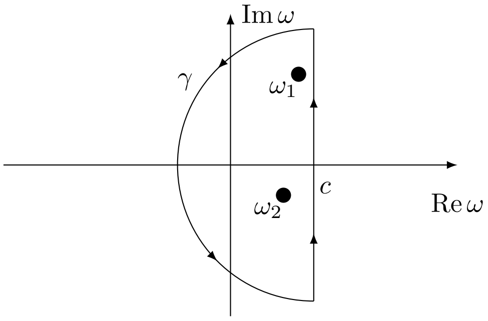

Figure 2.1: Sketch of the integration path γ for the integral in Eq.(2.33).

that can be written in a straightforward way by means of the following two matrices:

$$\begin{aligned} A &= \frac{e^{\frac{3}{2}\eta}}{2\pi i}\mathrm{Res}\left[\sigma_{ab}(\omega)e^{\omega\eta}\right]\Big|_{\omega_1=-\frac{3}{2}} = \frac{1}{5}\begin{pmatrix} 2 & -2 \\ -3 & 3 \end{pmatrix}, \\ B &= \frac{e^{-\eta}}{2\pi i}\mathrm{Res}\left[\sigma_{ab}(\omega)e^{\omega\eta}\right]\Big|_{\omega_2=1} = \frac{1}{5}\begin{pmatrix} 3 & 2 \\ 3 & 2 \end{pmatrix}. \end{aligned} \tag{2.36}$$

Indeed, using the above matrices, restoring the notation with the explicit initial and final times and introducing the Heaviside function $\Theta(\eta_a - \eta_b)$, the result of the integral in (2.33) gives

$$g_{ab}(\eta_a, \eta_b) = \left[B + A\, e^{-\frac{5}{2}(\eta_a - \eta_b)}\right]_{ab} \Theta(\eta_a - \eta_b), \tag{2.37}$$

that is remarkably the solution of Eq.(2.23).
Before going on we discuss the extension of the above equations beyond the Einstein-de Sitter cosmology. In general cosmologies with $\Omega_m < 1$, such as the ΛCDM model itself, we can write the dynamical equation in a way that is formally identical to Eq.(2.20), by means of the linear growth factor $D^+(\tau)$, that is defined in the explicit density solution of the linearised system for a generic cosmology and neglecting initial vorticity [38]:

$$\delta(\mathbf{x}, \tau) = D^+(\tau)A(\mathbf{x}) + D^-(\tau)B(\mathbf{x}), \tag{2.38}$$

obeying to the equation (see Eq.(1.54)):

$$\ddot{D}^+(\tau) + H(\tau)\dot{D}^+(\tau) - 4\pi G\, a^2(\tau)D^+(\tau) = 0 \tag{2.39}$$

and which depends on time through the scale factor (for Einstein-de Sitter we have $D^+ = a$). Indeed, if one makes the following replacements [39]:

$$\eta \longrightarrow \ln\frac{D^+(a)}{D^+(a_{in})} \quad \text{and} \quad \phi_2(\mathbf{k}, \eta) \longrightarrow \frac{\phi_2(\mathbf{k}, \eta)}{f_+(\eta)}, \tag{2.40}$$

where $f_+ = \frac{d\ln D^+(a)}{d\ln a}$ is the growth rate, one gets formally the same dynamical equation above (2.20), but with the matrix Ω replaced by:

$$\Omega(\eta) = \begin{pmatrix} 1 & -1 \\ -\frac{3\Omega_m(\eta)}{2f_+^2(\eta} & \frac{3\Omega_m(\eta)}{2f_+^2(\eta)} \end{pmatrix}. \tag{2.41}$$

The time-dependence of Ω induces some complications [8]. Indeed, the Laplace transform that we used to find the complete solution for ϕ_a through the linear propagator is no more useful. Due to the fact that $\frac{\Omega_m}{f_+^2} \approx 1$ during most of the time evolution, the phenomenologically interesting cases of ΛCDM-type cosmologies are usually treated using the switches (2.40) and approximating the above time-dependent Ω matrix with the Einstein-de Sitter one (2.18). Since the vertex γ_{abc} mixes growing and decaying modes, this approximation is expected to work well in the linear regime and to fail when non-linearities become important: indeed, in this approximation the growing mode of matter perturbations is treated properly, but oppositely the decaying mode has the wrong time dependence and the wrong ratio between density and velocity perturbations.

2.2 Generating functionals and Feynman rules.

2.2.1 The action S and the generating functional Z.

In this section we will apply methods familiar in quantum field theory to cosmological dynamics, in order to establish generating functionals for statistical objects like the power spectrum, the bispectrum, the propagator and deriving the suitable Feynman rules for a perturbative approach to their evaluation, mainly following [13]. The first step consists in finding the action S that gives the dynamic equation (2.20) of the doublet ϕ_a, its equation of motion in a field theory language, at its extrema, where $\delta S = 0$. This requires introducing an auxiliary doublet χ_a so that, keeping the usual notation for repeated indices and momenta, the action reads:

$$\begin{aligned} S &= S_{free} + S_{int} = \\ &= \int_0^{\eta_f} d\eta \, [\chi_a(-\mathbf{k},\eta)(\delta_{ab}\partial_\eta + \Omega_{ab})\phi_b(\mathbf{k},\eta) - e^{\eta}\gamma_{abc}(\mathbf{k},\mathbf{p},\mathbf{q})\chi_a(-\mathbf{k},\eta)\phi_b(\mathbf{p},\eta)\phi_c(\mathbf{q},\eta)], \end{aligned} \tag{2.42}$$

where we can recognise a sum between a free and an interaction part, respectively the first and the second addend of the second line of the above expression. Varying the action with respect to χ_a gives Eq.(2.20), while varying on ϕ_a we find the equation of motion for χ, solved by $\chi_a = 0$. It is worth pointing out that although the auxiliary fields χ_a could appear, at a first glance, simply a tricky tool by which one writes the action, at a deeper analysis they are related to the statistics of initial conditions and, as we will see in a while, they heavily enter in the building of the Feynman rules for the theory, highlighting their physical importance.
The depicted dynamics is a classic, deterministic one, so the probability (or transition amplitude), that the initial field $\phi_a(\eta_{in} = 0)$ evolves to the final value $\phi_a(\eta_f)$ is not subjected to any uncertainty and can be expressed by means of a functional Dirac's delta:

$$P[\phi_a(\eta_f);\phi_a(0)] = \delta[\phi_a(\eta_f) - \bar{\phi}_a(\eta_f,\phi_a(0))], \tag{2.43}$$

where $\bar{\phi}_a$ is the solution to the equations of motions with initial conditions given by $\phi_a(\eta = 0)$. As in the above expression, from now on we will often omit the momentum and sometimes also the temporal dependences of the fields, for clarity. In a quantum field theory fashion, the probability arises integrating over all the possible paths for a field, weighted appropriately: we can think to our case as a quantum probability with all the weight given to the classical path $\bar{\phi}_a$:

$$P[\phi_a(\eta_f);\phi_a(0)] = \mathcal{N} \int \mathcal{D}\phi_a'' \, \delta[\phi_a(\eta) - \bar{\phi}_a(\eta,\phi_a(0))], \tag{2.44}$$

where $\mathcal{D}\phi''$ is the functional measure with the extrema fixed at $\phi_a(0)$ and $\phi_a(\eta_f)$, while $\mathcal{N}$ is a normalization factor that we fix consistently to one. Now, following [40, 41], we know functionals have the following property, inherited by functions:

$$\delta f[\phi] = \frac{\delta(\phi - \phi_0)}{|\det(f'[\phi_0])|} \qquad \text{if} \;\; \exists! \;\; \phi_0 \mid f[\phi_0] = 0, \tag{2.45}$$

and since the solution of Eq.(2.20) is clearly $\bar{\phi}_a$, the functional:

$$\mathcal{F}[\phi] = (\delta_{ab}\partial_\eta + \Omega_{ab})\phi_b(\mathbf{k}, \eta) - e^\eta \gamma_{abc}(\mathbf{k}, \mathbf{p}, \mathbf{q})\phi_b(\mathbf{p}, \eta)\phi_c(\mathbf{q}, \eta) \tag{2.46}$$

has as unique zero $\bar{\phi}_a$ and therefore from the previous property it follows that:

$$\delta[\phi_a(\eta) - \bar{\phi}_a(\eta, \phi_a(0))] = \delta\mathcal{F}[\phi_a(\eta)] \; |\det\mathcal{F}[\phi_a(\eta)]|_{\phi_a = \bar{\phi}_a}. \tag{2.47}$$

Using the integral representation of the functional delta we can rewrite the above expression, modulo the determinant, as:

$$\delta[\phi_a(\eta) - \bar{\phi}_a(\eta, \phi_a(0))] = \int \mathcal{D}\chi_a e^{i\int_0^{\eta_f} d\eta [\chi_a(\delta_{ab}\partial_\eta + \Omega_{ab})\phi_b - e^\eta \gamma_{abc}\chi_a\phi_b\phi_c]} = \int \mathcal{D}\chi_a \, e^{iS[\chi, \phi]}. \tag{2.48}$$

Hence, absorbing the determinant in the normalization factor, given that it has no functional dependence on ϕ being evaluated in a specific configuration, and setting it to one by rescaling the measure, Eq.(2.44) for the probability can be re-expressed as:

$$P[\phi_a(\eta_f); \phi_a(0)] = \iint \mathcal{D}\phi_a'' \mathcal{D}\chi_b \, e^{iS[\chi, \phi]}. \tag{2.49}$$

The partition function, or generating functional of correlation functions, Z is canonically introduced by means of the sources related to the fields and integrating over all the possible final states:

$$Z[J_a, K_b; \phi_a(0)] = \iiint \mathcal{D}\phi_a(\eta_f)\mathcal{D}\phi_a''\mathcal{D}\chi_b \, e^{i\int_0^{\eta_f} d\eta \, [\chi_a(\delta_{ab}\partial_\eta + \Omega_{ab})\phi_b - e^\eta \gamma_{abc}\chi_a\phi_b\phi_c + J_a\phi_a + K_a\chi_a]}. \tag{2.50}$$

Clearly, taking $J_a = 0 = K_a$ it results, consistently with [42]:

$$\begin{aligned} Z[0] = \iiint \mathcal{D}\phi_a(\eta_f)\mathcal{D}\phi_a''\mathcal{D}\chi_b \, e^{iS[\chi, \phi]} &= \int \mathcal{D}\phi_a(\eta_f) P[\phi_a(\eta_f); \phi_a(0)] = \\ &= \int \mathcal{D}\phi_a(\eta_f)\delta[\phi_a(\eta_f) - \bar{\phi}_a(\eta_f, \phi_a(0))] = 1. \end{aligned} \tag{2.51}$$

Finally, since we are interested in statistical systems, we average the probabilities over the initial conditions too, with a statistical weight functional for the physical fields $\phi_a(0)$:

$$Z[J_a, K_b; C_s] = \int \mathcal{D}\phi_a(0) \, W[\phi_a(0), C_s] Z[J_a, K_b; \phi_a(0)]. \tag{2.52}$$

A good initial weight functional can be expressed in terms of the initial N-points irreducible connected (see the beginning of Subsection 2.2.3) correlation functions as [43]:

$$W[\phi_a(0), \{C_s\}] = e^{-\phi_a(\mathbf{k},0)C_a(\mathbf{k}) - \phi_a(\mathbf{k_1},0)C_{ab}(\mathbf{k_1},\mathbf{k_2})\phi_b(\mathbf{k_2},0) + \phi_a(\mathbf{k_1},0)\phi_b(\mathbf{k_2},0)\phi_c(\mathbf{k_3},0)C_{abc}(\mathbf{k_1},\mathbf{k_2},\mathbf{k_3}) + \cdots}. \tag{2.53}$$

In this way, the generic disconnected N-th order correlation function $C^{(N;disc)}_{a_{1,J},a_{2,K},\ldots,a_{N,J}}$ is defined as:

$$C^{(N;disc)}_{a_{1,J},a_{2,K},\ldots,a_{N,J}}(\mathbf{k}_1,\mathbf{k}_2,\ldots,\mathbf{k}_N) = \frac{(-i)^N}{Z}\frac{\delta^N Z[J_a,K_b;C_s]}{\delta J_{a_1}(\mathbf{k}_1)\delta K_{a_2}(\mathbf{k}_2)\cdots\delta J_{a_N}(\mathbf{k}_N)}. \tag{2.54}$$

Before going on, we give a brief insight trying to explain the physical meaning of correlation functions, focussing mainly in the 2-point one with $a,b=1$, or in Fourier space the matter power spectrum. First of all, the N-points correlation function define the joint probability to observe N objects, such as galaxies, in N small volumes at given distances between each other. In principle, all of them are interesting, but there are at least two reasons making the 2-point one so important. The first relies on the growing difficulties in handing higher orders correlators, both from a theoretical and observative point of view, limiting people essentially to the use of the first three lowest orders ones, with the 2-points function (or autocorrelator) above all. The second arises from the fact that in gaussian conditions all the even orders correlators are built only with it, the odds ones being null: thus now, since our Universe roughly follow this condition, the 2-point function assumes a great importance giving, modulo small corrections, the building block for the derivation of all the other observables. The 2-point correlator [44] describes the probability of observing for example two galaxies in whatever two small volumes dV_1, dV_2 at a given distance r (or k in Fourier space), the only variable assuming homogeneity and isotropy. In particular, they define, at a given time, the"excess of probability" in observing two objects at given distance with respect to what we would observe if the distribution were fully random:

$$dP = \bar{n}^2[1 + C^{(2)}_{11}(r)]dV_1 dV_2, \tag{2.55}$$

with $\bar{n}$ the mean density of objects normalized to one. Hence, we can think to the 2-points correlation as the granularity index of the Universe, or a part of it, at a given distance: higher will be $C^{(2)}_{11}(r^\star)$, higher will be the density of objects in the Universe at the scale $r^\star$. In terms of the density contrast $\delta(\vec{x})$ we can thus define:

$$C^{(2)}_{11}(r) = \langle \delta(\mathbf{x})\delta(\mathbf{x}+\mathbf{r})\rangle . \tag{2.56}$$

The brackets of the above expression indicate the statistical ensemble average: it is theoretically obtained averaging an infinite number of values taken in a set of different universes. Since it is practically impossible, it is commonly intended as a spatial mean, assuming valid the ergodic hypothesis that states their equivalence if, as we accept, our Universe is a "fair sample" of the whole ensemble [18], namely it is sufficiently large to permit the measure on whatever scale where the value of the observable is relevant.
Closed the digression, in the following we are restricting to the gaussian initial conditions case, in which case the initial weight functional has the following form:

$$W[\phi_a(0), C_s] = e^{-\frac{1}{2}\phi_a(\mathbf{k},0)C_{ab}(k)\phi_b(-\mathbf{k},0)}, \tag{2.57}$$

where $C_{ab}(k)$ is linked to the inverse of the initial power spectrum $P^0(k)$ through:

$$C^{-1}_{ab}(k) = P^0_{ab}(k) \equiv w_a w_b P^0(k), \tag{2.58}$$

where w_a is a combination of the initial growing and decaying modes compatible with the initial conditions, describing the initial mixture between them: with gaussian initial conditions and considering only the growing mode, then $w_a = u_a$.
Considering the definitions (2.52) and (2.50) one can notice that the generating functional Z can be trivially recast by means of simple variations as:

$$Z[J_a, K_b; P^0] = e^{-i\int_0^{\eta_f} d\eta\, e^{\eta}\gamma_{abc}\left(\frac{-i\delta}{\delta K_a}\frac{-i\delta}{\delta J_b}\frac{-i\delta}{\delta J_c}\right)} Z_0[J_a, K_b; P^0], \tag{2.59}$$

where Z_0 is obtained setting to zero the interaction factor $e^{\eta}\gamma_{abc}$ in Z, that is the linear theory generating functional: indeed, clearly $\lim_{\gamma_{abc}Z\to 0} = Z_0$. The above expression is very important because it allows to find the Feynman rules for the full theory, the building blocks for whatever statistical estimator in a perturbative approach. We will now compute explicitly Z_0. Simplifying the notation for the integrals, we start from:

$$Z_0[J_a, K_b; P^0] = \int \mathcal{D}\phi_a(0)\mathcal{D}\phi_a(\eta_f)\mathcal{D}\phi_a''\mathcal{D}\chi_b\, e^{-\frac{1}{2}\phi_a(0)P^{0^{-1}}_{ab}(k)\phi_b(0)} e^{i\int_0^{\eta_f} d\eta\,[\chi_a(\delta_{ab}\partial_\eta+\Omega_{ab})\phi_b+J_a\phi_a+K_a\chi_a]} \tag{2.60}$$

and as the first step we integrate on χ_b, obtaining:

$$Z_0[J_a, K_b; P^0] = \int \mathcal{D}\phi_a\, \delta\Big[(\delta_{ab}\partial_\eta + \Omega_{ab})\phi_b(\eta) + K_a(\eta)\Big] e^{-\frac{1}{2}\phi_a(0)P^{0^{-1}}_{ab}(k)\phi_b(0)} e^{i\int_0^{\eta_f} d\eta\, J_a(\eta)\phi_a(\eta)}. \tag{2.61}$$

The integration of the Dirac's delta involves $\mathcal{D}\phi_a(\eta_f)\mathcal{D}\phi_a''$ and changes the field ϕ_a in the last exponential of the above integral with the solution $\tilde{\phi}_a$ of the classical equation of motion with source K_a:

$$(\delta_{ab}\partial_\eta + \Omega_{ab})\phi_b(\eta) = -K_a(\eta), \tag{2.62}$$

given by (see equations (2.22) and (2.23)):

$$\tilde{\phi}_a(\eta) = \phi_a^{(0)}(\eta) - \int_0^\eta d\eta'\, g_{ab}(\eta, \eta')K_b(\eta'), \tag{2.63}$$

in fact:

$$\begin{aligned}
(\delta_{ab}\partial_\eta + \Omega_{ab})\tilde{\phi}_b(\eta) &= (\delta_{ab}\partial_\eta + \Omega_{ab})\Big[\phi_b^{(0)}(\eta) - \int_0^\eta d\eta'\, g_{bc}(\eta,\eta')K_c(\eta')\Big] = \\
&= (\delta_{ab}\partial_\eta + \Omega_{ab})\phi_b^{(0)}(\eta) - \int_0^\eta d\eta'\,(\delta_{ab}\partial_\eta + \Omega_{ab})g_{bc}(\eta,\eta')K_c(\eta') = \\
&= 0 - \int_0^\eta d\eta'\, \delta_{ac}\delta(\eta-\eta')K_c(\eta') = -K_a(\eta).
\end{aligned} \tag{2.64}$$

Hence, using Eq.(2.25) we arrive to the expression:

$$\begin{aligned}
Z_0[J_a, K_b; P^0] = &\Big[\int \mathcal{D}\phi_a(0)\, e^{-\frac{1}{2}\phi_a(0)P^{0^{-1}}_{ab}(k)\phi_b(0)} e^{i\int_0^{\eta_f} d\eta\, J_a(\eta)g_{ab}(\eta,0)\phi_a^{(0)}(0)}\Big]\times \\
&\times e^{-i\int_0^{\eta_f} d\eta \int_0^\eta d\eta'\, J_a(\eta)\, g_{ab}(\eta,\eta')K_b(\eta')},
\end{aligned} \tag{2.65}$$

that can be integrated on the initial fields, because the factor at the second line does not depend on them, while the term at the first line is a classic gaussian integration with a source $\hat{J}_b = J_a(\eta)g_{ab}(\eta, 0)$. Therefore, the final result for the partition function for linear theory Z_0 is:

$$Z_0[J_a, K_b; P^0] = e^{-\int d\eta_a d\eta_b [\frac{1}{2}J_a(\mathbf{k},\eta_a)P^L_{ab}(k;\eta_a,\eta_b)J_b(-\mathbf{k},\eta_b)+iJ_a(\mathbf{k},\eta_a)\, g_{ab}(\eta_a,\eta_b)K_b(-\mathbf{k},\eta_b)]}, \tag{2.66}$$

where P^L_{ab} is the power spectrum evolved at linear level:

$$P^L_{ab}(k; \eta_a, \eta_b) = g_{ac}(\eta_a, 0)g_{bd}(\eta_b, 0)P^0_{cd}(k). \tag{2.67}$$

As a check, we compute the power spectrum from (2.54):

$$\langle\phi_a(\mathbf{k}, \eta_a)\phi_b(\mathbf{k}', \eta_b)\rangle \equiv \frac{(-i)^2}{Z}\frac{\delta^2 Z[J_a, K_b; P^0]}{\delta J_a(\mathbf{k}, \eta_a)\delta J_b(\mathbf{k}', \eta_b)}\bigg|_{J_a,K_b=0} = \delta(\mathbf{k}+\mathbf{k}')P_{ab}(k; \eta_a, \eta_b), \tag{2.68}$$

by setting Z to Z_0, verifying that we obtain (2.67).
Naturally, all the results of linear theory can be recovered from Z_0. For instance, from it we read the first two Feynman rules, that are the linear power spectrum, defined as:

$$\delta(\mathbf{k}+\mathbf{k}')P^L_{ab}(k;\eta_a,\eta_b) = \frac{(-i)^2}{Z_0}\frac{\delta^2 Z_0[J_a,K_b;P^0]}{\delta J_a(\mathbf{k},\eta_a)\delta J_b(\mathbf{k}',\eta_b)}\Big|_{J_a,K_b=0} \tag{2.69}$$

and the retarded linear propagator, that with a little rearrangement of the factor i is defined as:

$$\delta(\mathbf{k}+\mathbf{k}')g_{ab}(k;\eta_a,\eta_b) = \frac{i}{Z_0}\frac{\delta^2 Z_0[J_a,K_b;P^0]}{\delta J_a(\mathbf{k},\eta_a)\delta K_b(\mathbf{k}',\eta_b)}\Big|_{J_a,K_b=0}, \tag{2.70}$$

while all the other linear statistical evaluators are obtained by further derivations of Z_0 with respect to the sources. The reason for we consider only P^L_{ab} and g_{ab} as Feynman rules is that, at this (linear) stage, they are the only fundamental blocks belonging explicitly to Z_0, meaning that, in perturbation theory, all the other linear statistical objects are built with only these two objects, in the same fashion of quantum field theory Feynman rules. In a field theoretical language, they are the only connected functions obtained by Z_0.
Turning the interaction on, that is considering a non-vanishing vertex γ_{abc}, one obtains the form (2.59) for the generating functional Z, from which we infer the third, last Feynman rule, the trilinear vertex $-ie^{\eta}\gamma_{abc}$. Since higher orders in perturbation theory are obtained by expanding the exponential in powers of the vertex γ_{abc}, one can understand that the linear regime, characterized by $\gamma_{abc}=0$, corresponds to the tree level order of perturbation theory, not presenting any interaction.
It appears very helpful to open a brief subsection to recollect the ideas on the Feynman rules, presenting their graphical and analytical forms.

2.2.2 The Feynman rules.

Fig.(2.2) represents diagrammatically the Feynman rules related to the cosmological dynamic for a gas of dark matter described by the system (2.15), or equivalently by Eq.(2.20) or also the action (2.42), with gaussian initial conditions.
In perturbation theory, all the statistical observables, defined by all the non-zero variations of the generating function Z with respect to the sources evaluated in the zero sources configuration, are obtained using only these three building blocks. In particular, they are:

- the *linear retarded propagator* $g_{ab}(\eta_a,\eta_b)$: it arises already in the linear theory, that is at the tree level of the complete theory. The prefactor in the rule comes from its definition given in (2.70), while the arrow in the graph of its Feynman rule defines the correct time flow. Through the linear propagator, defined by Eq.(2.23), we recognize the linear evolution as a fundamental in the evolution of non-linear statistics;

- the *linearly evolved power spectrum* $P^L_{ab}(k;\eta_a,\eta_b)$: it also arises already in the linear theory. It is defined by the expression (2.69) and the arrows in its graph define the flowing of momenta, not depending by the time order at all, while the box indicates the heart of this rule, that is the linear initial power spectrum. As for the linear propagator, it confirms the importance of linear evolution even in the full statistics, the true novelty of this rule is the presence of the linear initial power spectrum. While the linear propagator is completely fixed by its definition, P^0 depends on the specific cosmological model and in the case of gaussian initial conditions it contains all the statistical information of the system;

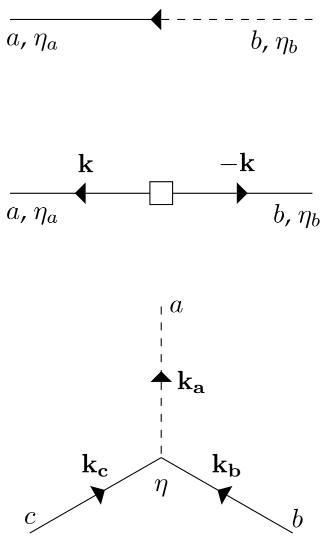

$= -i\, g_{ab}(\eta_a, \eta_b)$ (propagator)

$= P^L_{ab}(k, \eta_a, \eta_b)$ (linear power spectrum)

$= -i\, e^{\eta}\gamma_{abc}(\mathbf{k_a}, \mathbf{k_b}, \mathbf{k_c})$ (interaction vertex)

Figure 2.2: The Feynman rules for the DM gas with action (2.42).

- the *interaction vertex* $\gamma_{abc}(\mathbf{k}_a, \mathbf{b}_b, \mathbf{k}_c)$: it can be defined as the variation of the partition function (2.50) with respect to the three fields χ_a, ϕ_b and ϕ_c. The rule actually has an hidden integral on $\mathbf{k}_a$, in such a way the vertex definition (2.17) gives the relation $\mathbf{k}_a = \mathbf{k}_b + \mathbf{k}_c$ among momenta, determining a flow visualized by the arrows in its graph. Thus, the last graph in the figure, enforcing the momentum conservation delta, can be written in the following forms:

$$
\begin{aligned}
-ie^{\eta}\gamma_{121}(\mathbf{k}_a, \mathbf{k}_b, \mathbf{k}_c) &= -\frac{i}{2}e^{\eta}\int d\mathbf{k}_a \delta(\mathbf{k}_a - \mathbf{k}_b - \mathbf{k}_c)\alpha(\mathbf{k}_b, \mathbf{k}_c) = \\
&= -\frac{i}{2}e^{\eta}\int d\mathbf{k}_a \delta(\mathbf{k}_a - \mathbf{k}_b - \mathbf{k}_c)\frac{(\mathbf{k}_b + \mathbf{k}_c)\cdot\mathbf{k}_b}{k_b^2} = \\
&= -\frac{i}{2}e^{\eta}\int d\mathbf{k}_a \delta(\mathbf{k}_a - \mathbf{k}_b - \mathbf{k}_c)\,\frac{-k_c^2 + k_b^2 + k_b^2 + k_c^2 + 2\mathbf{k}_b\cdot\mathbf{k}_c}{2k_b^2} = \\
&= -ie^{\eta}\int d\mathbf{k}_a \delta(\mathbf{k}_a - \mathbf{k}_b - \mathbf{k}_c)\,\frac{-k_c^2 + k_b^2 + (\mathbf{k}_b + \mathbf{k}_c)^2}{4k_b^2} = \\
&= -ie^{\eta}\,\frac{k_a^2 + k_b^2 - k_c^2}{4k_b^2},
\end{aligned}
\tag{2.71}
$$

or analogously:

$$
-ie^{\eta}\gamma_{112}(\mathbf{k}_a, \mathbf{k}_b, \mathbf{k}_c) = -ie^{\eta}\,\frac{k_a^2 + k_c^2 - k_b^2}{4k_c^2}, \tag{2.72}
$$

or finally:

$$
\begin{aligned}
-ie^{\eta}\gamma_{222}(\mathbf{k}_a,\mathbf{k}_b,\mathbf{k}_c) &= -ie^{\eta}\int d\mathbf{k}_a\delta(\mathbf{k}_a-\mathbf{k}_b-\mathbf{k}_c)\beta(\mathbf{k}_b,\mathbf{k}_c) = \\
&= -ie^{\eta}\int d\mathbf{k}_a\delta(\mathbf{k}_a-\mathbf{k}_b-\mathbf{k}_c)\frac{(\mathbf{k}_b+\mathbf{k}_c)^2\mathbf{k}_b\cdot\mathbf{k}_c}{2k_b^2k_c^2} = \\
&= -ie^{\eta}\int d\mathbf{k}_a\delta(\mathbf{k}_a-\mathbf{k}_b-\mathbf{k}_c)\frac{(\mathbf{k}_b+\mathbf{k}_c)^2(k_b^2+k_c^2+2\mathbf{k}_b\cdot\mathbf{k}_c-k_b^2-k_c^2)}{4k_b^2k_c^2} = \\
&= -ie^{\eta}\int d\mathbf{k}_a\delta(\mathbf{k}_a-\mathbf{k}_b-\mathbf{k}_c)\frac{(\mathbf{k}_b+\mathbf{k}_c)^2((\mathbf{k}_b+\mathbf{k}_c)^2-k_b^2-k_c^2)}{4k_b^2k_c^2} = \\
&= -ie^{\eta}\,\frac{k_a^2(k_a^2-k_b^2-k_c^2)}{4k_b^2k_c^2}.
\end{aligned}
\tag{2.73}
$$

As the name says, this rule must be considered, analogously to the quantum field theory world, as a real vertex, that is with amputated legs: in other words, if the aim of the work is to build statistics, this rule cannot live without the previous ones, because glued to each of the three ends of the vertex there must be a propagator (for the a end) or either it or a power spectrum (for the b, c ones). To conclude, a bit verbosely we remind that the vertex rule encodes all the non-linearity of the theory and that the perturbative approach is obtained by power expanding the partition function (2.59) in powers of γ_{abc}: in this way, each perturbative order contribution to a n-point correlation function is given diagrammatically by all the possible combinations of the first two Feynman rules and a number $m = n+2(l-1)$ of interaction vertices, where l is the loop number, that is the perturbative order ($l = 0, 1, 2, \dots$ respectively for tree level order and one, two and following loops orders).

As we know, a diagrammatic approach to the evaluation of statistic observables is not complete without the rule for the symmetry factors to place in front of loop diagrams in order to account for their multiplicity. For this theory, the rule is the following: each loop of a given diagram contributes with a factor "2" times the number of the different kinds of internal lines with which it is built, that can be only one or two given the above Feynman rules, and the final factor of this diagram is the product of all these single loops factors related to it, obviously in a number equal to the total number of loops building up the considered diagram.
An example of the use of these Feynman rules will be exposed in the next chapter.

2.2.3 The generating functional W and the effective action Γ.

The bilinear (free) part S_{free} of the action (2.42) can be simply recast, with the use of Eq.(2.23), as:

$$S_{free} = \iint d\eta_a d\eta_b\, \chi_a(-\mathbf{k},\eta_a)g^{-1}_{ab}(\eta_a,\eta_b)\phi_b(\mathbf{k},\eta_b), \tag{2.74}$$

where g^{-1}_{ab}, using the matrix relation $A_{ef}A^{-1}_{fg} = \delta_{eg}$, is:

$$g^{-1}_{ab}(\eta_a,\eta_b) = \delta(\eta_a-\eta_b)(\delta_{ab}\partial_{\eta_b}+\Omega_{ab}); \tag{2.75}$$

so the generating functional Z in (2.59) can be written as:

$$Z[J_a,K_b;P^0] = \iint \mathcal{D}\phi_a\mathcal{D}\chi_b\, e^{-\frac{1}{2}\iint d\eta_a d\eta_b\,\chi_a P^0_{ab}\delta(\eta_a)\delta(\eta_b)\chi_b + i\int d\eta\,[\chi_a g^{-1}_{ab}\phi_b - e^{\eta}\gamma_{abc}\chi_a\phi_b\phi_c + J_a\phi_a + K_a\chi_b]}. \tag{2.76}$$

Recalling what we said about the role of the χ_a fields in the Subsection 2.2.1, we can now observe that the primordial power spectrum P^0_{ab} is directly coupled only to the χ_a-field, confirming that these fields encode the information on the statistics of the initial conditions.
From a graphical point of view, typical of Feynman diagrams, a disconnected correlator $C^{N;disc}_{a_1,\ldots,a_N}$ can be depicted as a certain series of diagrams, each of them made of lines connecting a number N of points, but in general with some contributions where not all the lines are interconnected between each others, making up disconnected graphs. However, a lot of times it is necessary limiting the correlation functions to the sole connected ones, for which each diagram of the series can be drawn "keeping the pen on the sheet". Following the usual approach of quantum field theory [42], we introduce the generating functional of connected Green functions W as:

$$W[J_a, K_b] = -i \ln Z[J_a, K_b], \tag{2.77}$$

through which we can define the classical (or more formally the expectation values of the) fields ϕ_a and χ_a in the following way:

$$\phi^{cl}_a[J_c, K_d] = \frac{\delta W[J_c, K_d]}{\delta J_a} \qquad \text{and} \qquad \chi^{cl}_a[J_c, K_d] = \frac{\delta W[J_c, K_d]}{\delta K_a}. \tag{2.78}$$

Furthermore, the full connected Green functions can be written in terms of full one-particle irreducible (1PI) Green functions. A 1PI correlation function is defined as that one whose graph, obtained by using the Feynman rules, cannot be reduced to two disconnected parts by operating a single cut in whatsoever its internal part, resulting irreducible by a single cut. Thus, we define the effective action Γ as the Legendre transform of W:

$$\Gamma[\phi^{cl}_a, \chi^{cl}_b] = W[J_a, K_b] - \int d\eta\, d\mathbf{k}[J_a(\mathbf{k},\eta)\phi^{cl}_a(\mathbf{k},\eta) + K_b(\mathbf{k},\eta)\chi^{cl}_b(\mathbf{k},\eta)], \tag{2.79}$$

whose functional derivatives with respect to the classical fields give rise to the complete set of 1PI Green functions. Note that in the above definition we explicitly indicated the integration over momenta.
Before going on, once introduced the four identities:

$$\frac{\delta\phi^{cl}_a(\mathbf{k}',\eta')}{\delta\phi^{cl}_b(\mathbf{k},\eta)} = \delta(\mathbf{k}'-\mathbf{k})\delta(\eta'-\eta)\delta_{ab}, \quad \frac{\delta\phi^{cl}_a}{\delta\chi^{cl}_b} = 0, \quad \frac{\delta\chi^{cl}_a(\mathbf{k}',\eta')}{\delta\chi^{cl}_b(\mathbf{k},\eta)} = \delta(\mathbf{k}'-\mathbf{k})\delta(\eta'-\eta)\delta_{ab}, \quad \frac{\delta\chi^{cl}_a}{\delta\phi^{cl}_b} = 0, \tag{2.80}$$

it appears important to introduce the following fundamental relation:

$$\begin{aligned}
\frac{\delta\Gamma[\phi^{cl}_a, \chi^{cl}_b]}{\delta\phi^{cl}_a(\mathbf{k},\eta)} &= \int d\eta' d\mathbf{k}' \left[\frac{\delta W[J_c, K_d]}{\delta J_b(\mathbf{k}',\eta')}\frac{\delta J_b(\mathbf{k}',\eta')}{\delta\phi^{cl}_a(\mathbf{k},\eta)} + \frac{\delta W[J_c, K_d]}{\delta K_b(\mathbf{k}',\eta')}\frac{\delta K_b(\mathbf{k}',\eta')}{\delta\chi^{cl}_a(\mathbf{k},\eta)}\right] + \\
&- \int d\eta' d\mathbf{k}' \left[J_b(\mathbf{k}',\eta')\delta(\mathbf{k}'-\mathbf{k})\delta(\eta'-\eta)\delta_{ab} + \frac{\delta J_b(\mathbf{k}',\eta')}{\delta\phi^{cl}_a(\mathbf{k},\eta)}\phi^{cl}_b(\mathbf{k}',\eta') + \frac{\delta K_b(\mathbf{k}',\eta')}{\delta\phi^{cl}_a(\mathbf{k},\eta)}\chi^{cl}_b(\mathbf{k}',\eta')\right] = \\
&= \int d\eta' d\mathbf{k}' \left[\phi^{cl}_b(\mathbf{k}',\eta')\frac{\delta J_b(\mathbf{k}',\eta')}{\delta\phi^{cl}_a(\mathbf{k},\eta)} + \chi^{cl}_b(\mathbf{k}',\eta')\frac{\delta K_b(\mathbf{k}',\eta')}{\delta\phi^{cl}_a(\mathbf{k},\eta)}\right] - J_a(\mathbf{k},\eta) + \\
&- \int d\eta' d\mathbf{k}' \left[\frac{\delta J_b(\mathbf{k}',\eta')}{\delta\phi^{cl}_a(\mathbf{k},\eta)}\phi^{cl}_b(\mathbf{k}',\eta') + \frac{\delta K_b(\mathbf{k}',\eta')}{\delta\phi^{cl}_a(\mathbf{k},\eta)}\chi^{cl}_b(\mathbf{k}',\eta')\right] = -J_a(\mathbf{k},\eta),
\end{aligned} \tag{2.81}$$

meaning in words that the variation of Γ with respect to a field gives the opposite of the source associated to that field.

Formally defining a generic N-point 1PI Green function as:

$$\delta(\sum_{s=1}^{N}\mathbf{k}_s)\Gamma^{(N)}_{\phi_{a_1}\chi_{a_2}\cdots\chi_{a_N}}(\{\mathbf{k}_s\},\{\eta_s\}) \equiv \left.\frac{\delta^N\Gamma[\phi_a^{cl},\chi_b^{cl}]}{\delta\phi_{a_1}^{cl}(\mathbf{k}_1,\eta_1)\delta\chi_{a_2}^{cl}(\mathbf{k}_2,\eta_2)\cdots\chi_{a_n}^{cl}(\mathbf{k}_n,\eta_n)}\right|_{\phi_a^{cl},\chi_b^{cl}=0}, \tag{2.82}$$

in the context of the DM gas dynamics of generating functional Z expressed in (2.76) and using the definition (2.77) for the generator W and (2.79) for the effective action Γ, it can be proved that all the N-point 1PI functions with only ϕ-type legs are zero. We can understood this at a perturbative stage, always following [13], reminding that at l-loop order a generic 1PI N-point function has a fixed number m of interaction vertices, as stated in Subsection 2.2.2, and for each vertex at most one of the three fields can be free, that is external, not glued with another via a propagator or a power spectrum, in order to preserve its 1PI characteristic; what's next, is that to have a function as $\Gamma^{(N)}_{\phi_{a_1}\cdots\phi_{a_N}}$ with only ϕ-type external legs, it is mandatory that each χ-type leg of the vertices must be contracted, clearly only via the propagator, to a ϕ-leg: even by induction to higher loops, one can realize that any diagram contributing to the graph of whatever N-point 1PI function with only ϕ-type external legs contains at least one loop made up only of propagators, that vanish due to the presence of the Heaviside function, since it cannot contemporaneously be, say, $\eta_1 > \eta_2$ for one line and $\eta_2 > \eta_1$ for the other.
We are now going to analyse the four second functional derivatives of the effective action computed at vanishing sources, that are the complete set of four 2-point PI correlators we can built. Actually, one is just $\Gamma^{(2)}_{\phi_a\phi_b} = 0$, while the other three can be written by definition as:

$$\begin{cases} \Gamma^{(2)}_{\phi_a\phi_b} &= 0 \\ \Gamma^{(2)}_{\phi_a\chi_b} &= g^{-1}_{ba} - \Sigma_{\phi_a\chi_b} \\ \Gamma^{(2)}_{\chi_a\phi_b} &= g^{-1}_{ab} - \Sigma_{\chi_a\phi_b} \\ \Gamma^{(2)}_{\chi_a\chi_b} &= iP^0_{ab}(k)\delta(\eta_a)\delta(\eta_b) + i\Phi_{ab}, \end{cases} \tag{2.83}$$

where we isolated the linear (free) parts, the first terms at the right hand side of the equations, and the fully non-linear contributions. Now, from the definition of generating functional of connected correlation functions (2.77), we define the full propagators and power spectrum, that being connected 2-point Green functions are given by the second functional derivatives of W as (ignoring the time dependence):

$$\begin{cases} \left.\frac{\delta^2 W[J_a,K_b]}{\delta J_a(\mathbf{k}_1)\delta J_b(\mathbf{k}_2)}\right|_{J_a,K_b=0} \equiv i\delta(\mathbf{k}_1+\mathbf{k}_2)P_{ab}(\{\mathbf{k}_s\}) \\ \left.\frac{\delta^2 W[J_a,K_b]}{\delta J_a(\mathbf{k}_1)\delta K_b(\mathbf{k}_2)}\right|_{J_a,K_b=0} \equiv -\delta(\mathbf{k}_1+\mathbf{k}_2)G_{ab}(\{\mathbf{k}_s\}) \\ \left.\frac{\delta^2 W[J_a,K_b]}{\delta K_a(\mathbf{k}_1)\delta J_b(\mathbf{k}_2)}\right|_{J_a,K_b=0} \equiv -\delta(\mathbf{k}_1+\mathbf{k}_2)G_{ba}(\{\mathbf{k}_s\}) \\ \left.\frac{\delta^2 W[J_a,K_b]}{\delta K_a(\mathbf{k}_1)\delta K_b(\mathbf{k}_2)}\right|_{J_a,K_b=0} = 0. \end{cases} . \tag{2.84}$$

Furthermore, we consider given the definitions of the quantities $W^{(2)}_{\phi\phi}, W^{(2)}_{\phi\chi}, W^{(2)}_{\chi\phi}, W^{(2)}_{\chi\chi}$, in perfect analogy to their Γ-counterparts in the definition (2.82). Now, making use of the definitions in (2.80) and the result (2.81), one can prove that the four derivatives written in (2.84) form the opposite of the inverse matrix made up with the four quantities in (2.83). [1] Hence, starting from

[1]Actually, here we must think a general functional $F[\varphi]$ to be the inverse of $G[\varphi]$ in a functional sense, that is if it results [45]:

$$F[\varphi(\mathbf{x})]G[\varphi(\mathbf{y})] = \delta(\mathbf{x}-\mathbf{y}). \tag{2.85}$$

some straightforward identities we obtain:

$$\frac{\delta\phi_a(\mathbf{x})}{\delta\phi_a(\mathbf{y})} = \delta(\mathbf{x}-\mathbf{y}) = \frac{\delta}{\delta\phi_a(\mathbf{y})}\Big(\frac{\delta W}{\delta J_a(\mathbf{x})}\Big) = \int d\mathbf{z}\left[\frac{\delta^2 W}{\delta J_b(\mathbf{z})\delta J_a(\mathbf{x})}\frac{\delta J_b(\mathbf{z})}{\delta\phi_a(\mathbf{y})} + \frac{\delta^2 W}{\delta K_b(\mathbf{z})\delta J_a(\mathbf{x})}\frac{\delta K_b(\mathbf{z})}{\delta\phi_a(\mathbf{y})}\right] =$$
$$= -\int d\mathbf{z}\left[\frac{\delta^2 W}{\delta J_b(\mathbf{z})\delta J_a(\mathbf{x})}\frac{\delta^2\Gamma}{\delta\phi_a(\mathbf{y})\delta\phi_b(\mathbf{z})} + \frac{\delta^2 W}{\delta K_b(\mathbf{z})\delta J_a(\mathbf{x})}\frac{\delta^2\Gamma}{\delta\phi_a(\mathbf{y})\delta\chi_b(\mathbf{z})}\right] \tag{2.86}$$

and evaluating the equation at $\phi_a, \chi_b = 0$ for the derivatives of the effective action Γ and at J_a, K_b for those of the generator W, denoting this procedure with the symbol ($\hat{=}$) and thus looking at the first of (2.83), we have:

$$\delta(\mathbf{x}-\mathbf{y}) \hat{=} -\int d\mathbf{z}\,\frac{\delta^2 W}{\delta K_b(\mathbf{z})\delta J_a(\mathbf{x})}\Big|_{J_a,K_b=0}\frac{\delta^2\Gamma}{\delta\phi_a(\mathbf{y})\delta\chi_b(\mathbf{z})}\Big|_{\phi_a,\chi_b=0}, \tag{2.87}$$

obviously verified by the expression:

$$\frac{\delta^2 W}{\delta J_a(\mathbf{x})\delta K_b(\mathbf{z})}\Big|_{J_a,K_b=0} = -\left[\frac{\delta^2\Gamma}{\delta\phi_a(\mathbf{y})\delta\chi_b(\mathbf{z})}\Big|_{\phi_a,\chi_b=0}\right]^{-1}, \tag{2.88}$$

that is what we wanted to show, modulo a Fourier transform, which, using the definitions in (2.83) and (2.84), gives:

$$G_{ab}(k,\eta_a,\eta_b) = [\Gamma^{(2)}_{\phi_a\chi_b}(k,\eta_a,\eta_b)]^{-1} = [g^{-1}_{ba} - \Sigma_{\phi_a\chi_b}]^{-1}(k,\eta_a,\eta_b). \tag{2.89}$$

This expression should formally be interpreted as a Taylor expansion around the linear propagator, in the following way:

$$G_{ab}(k,\eta_a,\eta_b) = g_{ab}(\eta_a,\eta_b) + \int_0^{\eta_a} d\eta_c \int_0^{\eta_b} d\eta_d\, g_{ac}(\eta_a,\eta_c)\Sigma_{\phi_c\chi_d}(k,\eta_c,\eta_d)g_{db}(\eta_d,\eta_b)] + \ldots \tag{2.90}$$

Using analogous methods, we can also relate the power spectrum with the functions defined in (2.83) and with the full propagator, getting:

$$P_{ab}(k,\eta_a,\eta_b) = P^I_{ab}(k,\eta_a,\eta_b) + P^{II}_{ab}(k,\eta_a,\eta_b) =$$
$$= \int_0^{\eta_a} d\eta_c \int_0^{\eta_b} d\eta_d\, G_{ac}(k,\eta_a,\eta_c)G_{bd}(k,\eta_b,\eta_d)[P^0_{cd}(k)\delta(\eta_c)\delta(\eta_d) + \Phi_{ab}(k,\eta_c,\eta_d)] =$$
$$= G_{ac}(k,\eta_a,0)G_{bd}(k,\eta_b,0)P^0_{cd}(k) + \int_0^{\eta_a} d\eta_c \int_0^{\eta_b} d\eta_d\, G_{ac}(k,\eta_a,\eta_c)G_{bd}(k,\eta_b,\eta_d)\Phi_{ab}(k,\eta_c,\eta_d). \tag{2.91}$$

2.3 Galilean invariance.

We conclude the present chapter giving an insight into galilean invariance, a crucial symmetry of the dynamical system we are considering. Its importance relies on the fact that it implies powerful constraints on the structure of the fully non-linear statistics both at a perturbative and non-perturbative level: the Ward identities and consistency relations.

2.3.1 Definition and invariance of the action.

A galilean transformation in physical coordinates is defined as follows by means of a constant boost velocity $\mathbf{w}$:

$$\begin{aligned} t' &= t, \\ \mathbf{R}' &= \mathbf{R} - \mathbf{w}t, \\ \mathbf{V}' &= \mathbf{V} - \mathbf{w}. \end{aligned} \tag{2.92}$$

Since the comoving coordinate $\mathbf{x}$ and the conformal time τ are related to the physical ones by the scale factor $a(\tau)$ as:

$$\begin{aligned} \mathbf{R} &= a\,\mathbf{x}, \\ dt &= a\,d\tau \end{aligned} \tag{2.93}$$

and remembering that the peculiar velocity is $\mathbf{v} = \frac{d\mathbf{x}}{d\tau}$, the above transformation becomes:

$$\begin{aligned} &\mathbf{R}' = \mathbf{R} - \mathbf{w}t \quad \longrightarrow \quad a\mathbf{x}' = a\mathbf{x} - \mathbf{w}\int_0^\tau d\tau' a(\tau') \quad \longrightarrow \quad \mathbf{x}' = \mathbf{x} - \mathbf{w}\frac{1}{a(\tau)}\int_0^\tau d\tau' a(\tau'), \\ &\mathbf{V}' = \mathbf{V} - \mathbf{w} \quad \longrightarrow \quad \frac{d}{dt}\mathbf{R}' = \frac{d}{dt}\mathbf{R} - \mathbf{w} \quad \longrightarrow \quad \frac{1}{a}\frac{d}{d\tau}(a\mathbf{x}') = \frac{1}{a}\frac{d}{d\tau}(a\mathbf{x}) - \mathbf{w} \quad \longrightarrow \\ &\longrightarrow \quad \frac{\dot a}{a}\mathbf{x}' + \mathbf{v}' = \frac{\dot a}{a}\mathbf{x} + \mathbf{v} - \mathbf{w} \quad \longrightarrow \quad \frac{\dot a}{a}\mathbf{x} - \frac{\dot a}{a}\mathbf{w}\frac{1}{a}\int_0^\tau d\tau' a(\tau') + \mathbf{v}' = \frac{\dot a}{a}\mathbf{x} + \mathbf{v} - \mathbf{w} \longrightarrow \\ &\longrightarrow \quad \mathbf{v}' = \mathbf{v} - \mathbf{w}\left(1 - \frac{\dot a}{a}\frac{1}{a}\int_0^\tau d\tau' a(\tau')\right), \end{aligned} \tag{2.94}$$

bringing to the comoving-conformal form of the galilean tranformation:

$$\begin{aligned} \tau' &= \tau, \\ \mathbf{x}' &= \mathbf{x} - \mathbf{w}T, \\ \mathbf{v}' &= \mathbf{v} - \mathbf{w}\dot T, \end{aligned} \tag{2.95}$$

with:

$$\begin{aligned} T(\tau) &= \frac{1}{a(\tau)}\int_0^\tau d\tau' a(\tau'), \\ \dot T(\tau) &= \frac{dT}{d\tau} = \left(1 - \frac{\dot a}{a}\frac{1}{a}\int_0^\tau d\tau' a(\tau')\right) = 1 - H(\tau)T(\tau). \end{aligned} \tag{2.96}$$

The main difference with the physical form is represented by the fact that here the galilean transformation must be regarded as a boost by a time-dependent velocity $\tilde{\mathbf{w}}(\tau) = \mathbf{w}\dot T(\tau)$, see for instance [46].

Both the invariances of Eq.(2.20) and the action (2.42) physically come from the invariance of the Vlasov equation, defined by means of the total time derivative of the DM phase-space distribution function $f(\mathbf{x}, \mathbf{p}, \tau)$ as:

$$\frac{d}{d\tau}f(\mathbf{x}, \mathbf{p}, \tau) = 0, \tag{2.97}$$

that results in Eq.(2.2), with $\mathbf{p} = am\,\mathbf{v}$ the conjugated momentum to the peculiar velocity, whose galilean transformation is simply:

$$\mathbf{p}' = \mathbf{p} - am\dot T\mathbf{w}. \tag{2.98}$$

Indeed, the distribution f is a scalar under galilean transformation:

$$f'(\mathbf{x}', \mathbf{p}', \tau) = f(\mathbf{x}, \mathbf{p}, \tau), \tag{2.99}$$

thus, using the transformation laws we have:

$$\begin{aligned}\frac{d}{d\tau} f'(\mathbf{x}', \mathbf{p}', \tau) &\equiv \left(\frac{\partial}{\partial \tau} + v_i' \frac{\partial}{\partial x_i'} + \dot{p}_i' \frac{\partial}{\partial p_i'}\right) f'(\mathbf{x}', \mathbf{p}', \tau) = \left(\frac{\partial}{\partial \tau} + (v_i - w_i \dot{T}) \frac{\partial}{\partial x_i} + \right.\\ &+ \left.\left(\dot{p}_i - \frac{d}{d\tau}(am\dot{T})w_i\right)\frac{\partial}{\partial p_i} + w_i \dot{T}\frac{\partial}{\partial x_i} + \frac{d}{d\tau}(am\dot{T})\frac{\partial}{\partial p_i}\right) f(\mathbf{x}' + \mathbf{w}T, \mathbf{p}' + am\dot{T}\mathbf{w}, \tau) = \\ &= \left(\frac{\partial}{\partial \tau} + v_i \frac{\partial}{\partial x_i} + \dot{p}_i \frac{\partial}{\partial p_i}\right) f(\mathbf{x}, \mathbf{p}, \tau).\end{aligned} \tag{2.100}$$

Expanding Vlasov equation in the first three moments and considering the single-stream approximation, we retrieve Eq.(2.20) and the related action (2.42). In order to prove their galilean invariance, we need to know the transformation of the doublet (2.19) under a galilean boost. Using Fourier transform (2.12b) we have:

$$\int_{\mathbb{R}^3} d\mathbf{k}\, e^{-i\mathbf{k}\cdot\mathbf{x}} \phi_a(\mathbf{k}, \eta) = \int_{\mathbb{R}^3} d\mathbf{k}\, e^{-i\mathbf{k}\cdot(\mathbf{x}-\mathbf{w}T)} e^{-i\mathbf{k}\cdot\mathbf{w}T} \phi_a(\mathbf{k}, \eta) = \int_{\mathbb{R}^3} d\mathbf{k}\, e^{-i\mathbf{k}\cdot(\mathbf{x}-\mathbf{w}T)} \breve{\phi}_a(\mathbf{k}, \eta), \tag{2.101}$$

from which we get that the Fourier transformed of $\phi_a(\mathbf{x}-\mathbf{w}T, \tau)$ is $\breve{\phi}_a = e^{-i\mathbf{k}\cdot\mathbf{w}T}\phi_a$; furthermore, we can write the galilean transformation of the doublet as:

$$\phi_a(\mathbf{k}, \tau) \quad \longrightarrow \quad e^{-i\mathbf{k}\cdot\mathbf{w}T}\phi_a(\mathbf{k}, \tau) - i\mathbf{k}\cdot\mathbf{w}e^{-\eta}\partial_\eta T(\eta)\delta(\mathbf{k})\delta_{a2}. \tag{2.102}$$

The second piece plays a role only in the right hand side of Eq.(2.20), where, due to the presence of terms at the order of $1/k$ coming from the vertex function, it gives a non-trivial contribution, while on the other side it is not the case; hence, the galilean transformation of Eq.(2.20) is:

$$\begin{aligned}(\delta_{ab}\partial_\eta + \Omega_{ab})\left[e^{-i\mathbf{k}\cdot\mathbf{w}T(\eta)}\phi_b(\mathbf{k}, \eta)\right] &= e^\eta \iint d\mathbf{p} d\mathbf{q}\, \gamma_{abc}(\mathbf{k}, \mathbf{p}, \mathbf{q}) e^{-i(\mathbf{p}+\mathbf{q})\cdot\mathbf{w}T(\eta)} \times \\ &\times \left[\phi_b(\mathbf{p}, \eta) - i\mathbf{p}\cdot\mathbf{w}e^{-\eta}\partial_\eta T\delta(\mathbf{p})\delta_{b2}\right]\left[\phi_c(\mathbf{q}, \eta) - i\mathbf{q}\cdot\mathbf{w}e^{-\eta}\partial_\eta T\delta(\mathbf{q})\delta_{c2}\right].\end{aligned} \tag{2.103}$$

As one can see, the right hand side is made up of four terms: the last, namely the one obtained multiplying the two last terms in the brackets at the second line, obviously vanishes due to the presence of the two Dirac's deltas, while the two mixed terms sum up to precisely cancel the phase term arising deriving the exponential in the left side. Indeed, in the context of the above expression, considering the term:

$$\mathbf{p}\cdot\mathbf{w}\,\delta(\mathbf{p})\gamma_{abc}(\mathbf{k}, \mathbf{p}, \mathbf{q})\delta_{b2}\,\phi_c(\mathbf{k}, \eta), \tag{2.104}$$

we see that the Kronecker's delta forces to consider only the middle index "2" for the interaction vertex, while the momentum Dirac's delta coming from the transformation acts setting to zero the contribution coming from the momentum $\mathbf{p}$ when summed with $\mathbf{q}$ in the definitions for the functions α and β made in Section 2.1, in such a way the above expression results in:

$$\mathbf{p}\cdot\mathbf{w}\,\delta(\mathbf{p})\gamma_{abc}(\mathbf{k}, \mathbf{p}, \mathbf{q}) = \frac{1}{2}\frac{\mathbf{p}\cdot\mathbf{q}\mathbf{p}\cdot\mathbf{w}}{p^2}\delta_{b2}\delta_{ac}\delta(\mathbf{k}-\mathbf{p}-\mathbf{q})\delta(\mathbf{p}), \tag{2.105}$$

and analogously for the homologous term obtained by means of the exchange $\mathbf{p} \longleftrightarrow \mathbf{q}$. Thus, using the condition $\mathbf{k} = \mathbf{p} + \mathbf{q}$ for the exponential, we have:

$$\begin{aligned} e^{-i\mathbf{k}\cdot\mathbf{w}T(\eta)}\big[(\delta_{ab}\partial_\eta + \Omega_{ab})\phi_b(\mathbf{k},\eta) - i\mathbf{k}\cdot\mathbf{w}\partial_\eta T\phi_a(\mathbf{k},\eta)\big] = \\ = e^{-i\mathbf{k}\cdot\mathbf{w}T(\eta)}\bigg[e^\eta \iint d\mathbf{p}d\mathbf{q}\,\gamma_{abc}(\mathbf{k},\mathbf{p},\mathbf{q})\phi_b(\mathbf{p},\eta)\phi_c(\mathbf{q},\eta) + \\ - \partial_\eta T\phi_a(\mathbf{k},\eta)\int d\mathbf{p}\frac{i\mathbf{p}\cdot\mathbf{q}\mathbf{p}\cdot\mathbf{w}}{p^2}\delta(\mathbf{p})\bigg], \end{aligned} \tag{2.106}$$

that is precisely Eq.(2.20), enforcing galilean invariance, because the term at the third line cancels against the second of the first line, the phase term.
Considering the action (2.42), we recall that it was built in such a way that the variation with respect to the field χ_a gave Eq.(2.20), that are galileian invariant. Imposing that under a galilean boost this field transforms as:

$$\chi_a(\mathbf{k},\eta) \longrightarrow e^{-i\mathbf{k}\cdot\mathbf{w}T(\eta)}\chi_a(\mathbf{k},\eta), \tag{2.107}$$

one easily verifies that under the galilean transformations (2.102) and (2.107), the action remains invariant modulo a vanishing term arising in S_{free} coming from the second part of (2.102), that is eventually:

$$S \longrightarrow S + \int d\eta d\mathbf{k}\,\chi_a(-\mathbf{k},\eta)(\delta_{a2}\partial_\eta + \Omega_{a2})i\mathbf{k}\cdot\mathbf{w}e^{-\eta}\partial_\eta T\delta(\mathbf{k}). \tag{2.108}$$

2.3.2 Consistency relations.

As pointed out in [46, 47, 48], one of the most interesting consequences of the class of symmetry we have discussed is the appearing of consistency relations between correlators. Specifically, they relate $(n+1)$-correlation functions containing a soft (long, with low wavenumber) mode to the to n-point correlation functions of the short (with higher wavenumbers) modes. In the following, we focus the discussion on correlation functions involving matter density fields, but similar consistency relations may be found involving also the velocity perturbations, even in various combinations with matter density ones.
We start stating that the action (2.42) and consequently the equation of motion (2.20) are actually invariant for a generalised version of the galilean transformation defined by (2.95), that is for:

$$\begin{aligned} \tau' &= \tau, \\ \mathbf{x}' &= \mathbf{x} - \mathbf{n}(T), \\ \mathbf{v}' &= \mathbf{v} - \dot{\mathbf{n}}(T), \end{aligned} \tag{2.109}$$

where the dot denotes the differentiation with respect to the conformal time as always, while $T(\tau)$ is defined in the same way as in (2.96); the canonical galilean transformation is recovered choosing $\mathbf{n}(T) = \mathbf{w}T$. Now, we consider the generic n-point correlation function of short modes matter density contrasts $\langle\delta_{\mathbf{k}_1}\delta_{\mathbf{k}_2}\cdots\delta_{\mathbf{k}_n}\rangle$, with the points supposed to be contained in a sphere of radius R much smaller than the long wavelength mode of size about q^{-1} and centered at the origin of the coordinates. The invariance of our system with respect to the above generalised class of transformations means that if we choose $\mathbf{n}$ in such a way to generate a long wavelength mode for the velocity perturbation $\mathbf{v}_L(\tau,\mathbf{0})$:

$$\mathbf{n}(\tau) = \int_{\tau_{in}}^{\tau} d\tau'\mathbf{v}_L(\tau',\mathbf{0}), \tag{2.110}$$

then the correlator of the short wavelength modes in the background of the long wavelength mode perturbation should satisfy the relation, in real space:

$$\langle \delta(\tau_1, \mathbf{x'}_1)\delta(\tau_2, \mathbf{x'}_2)\cdots\delta(\tau_n, \mathbf{x'}_n)\rangle_{\mathbf{v}_L} = \langle \delta(\tau_1, \mathbf{x}_1)\delta(\tau_2, \mathbf{x}_2)\cdots\delta(\tau_n, \mathbf{x}_n)\rangle\,, \tag{2.111}$$

asserting nothing else that the effect of a physical long wavelength velocity perturbation onto the short modes should be indistinguishable from the long wavelength mode velocity generated by the transformation $\delta\mathbf{x} = -\mathbf{n}$; in momentum space this gives:

$$\langle \delta_{\mathbf{q}}(\tau)\delta_{\mathbf{k}_1}(\tau_1)\delta_{\mathbf{k}_2}(\tau_2)\cdots\delta_{\mathbf{k}_n}(\tau_n)\rangle_{\mathbf{q}\to\mathbf{0}} = \langle \delta_{\mathbf{q}}(\tau)\,\langle \delta_{\mathbf{k}_1}(\tau_1)\delta_{\mathbf{k}_2}(\tau_2)\cdots\delta_{\mathbf{k}_n}(\tau_n)\rangle_{\mathbf{v}_L}\rangle\,. \tag{2.112}$$

But the variation of the n-point correlator under such a transformation is given by:

$$\begin{aligned}\delta\,\langle \delta(\tau_1, \mathbf{x}_1)\delta(\tau_2, \mathbf{x}_2)\cdots\delta(\tau_n, \mathbf{x}_n)\rangle &= \int_{\mathbb{R}^3}\cdots\int_{\mathbb{R}^3} d\mathbf{k}_1\cdots d\mathbf{k}_n\,\langle \delta_{\mathbf{k}_1}(\tau_1)\delta_{\mathbf{k}_2}(\tau_2)\cdots\delta_{\mathbf{k}_n}(\tau_n)\rangle\times\\ &\times\, e^{-i(\mathbf{k}_1\cdot\mathbf{x}_1+\mathbf{k}_2\cdot\mathbf{x}_2+\cdots+\mathbf{k}_n\cdot\mathbf{x}_n)}\sum_{a=1}^{n}\delta\mathbf{x}_a\cdot(-i\mathbf{k}_a) =\\ &= \int_{\mathbb{R}^3}\cdots\int_{\mathbb{R}^3} d\mathbf{k}_1\cdots d\mathbf{k}_n\,\langle \delta_{\mathbf{k}_1}(\tau_1)\delta_{\mathbf{k}_2}(\tau_2)\cdots\delta_{\mathbf{k}_n}(\tau_n)\rangle\times\\ &\times\, e^{i(\mathbf{k}_1\cdot\mathbf{x}_1+\mathbf{k}_2\cdot\mathbf{x}_2+\cdots+\mathbf{k}_n\cdot\mathbf{x}_n)}\sum_{a=1}^{n}\mathbf{n}_a(\tau_a)\cdot(i\mathbf{k}_a),\end{aligned} \tag{2.113}$$

from which we find that (2.112) becomes:

$$\langle \delta_{\mathbf{q}}(\tau)\delta_{\mathbf{k}_1}(\tau_1)\delta_{\mathbf{k}_2}(\tau_2)\cdots\delta_{\mathbf{k}_n}(\tau_n)\rangle_{\mathbf{q}\to\mathbf{0}} = i\,\langle \delta_{\mathbf{k}_1}(\tau_1)\delta_{\mathbf{k}_2}(\tau_2)\cdots\delta_{\mathbf{k}_n}(\tau_n)\rangle\sum_{a=1}^{n}\mathbf{k}_a\cdot\langle\delta_{\mathbf{q}}(\tau)\mathbf{n}_a(\tau_a)\rangle\,. \tag{2.114}$$

Now, since for a ΛCDM model it is:

$$\begin{aligned}\mathbf{n}(\tau) &= \int_{\tau_{in}}^{\tau} d\tau'\,\mathbf{v}_{\mathbf{q}}(\tau') = i\frac{\mathbf{q}}{q^2}\int_{\tau_{in}}^{\tau} d\tau'\,H(\tau')\frac{d\ln D^+(\tau')}{d\ln a(\tau')}\delta_{\mathbf{q}}(\tau') = i\frac{\mathbf{q}}{q^2}\int_{\tau_{in}}^{\tau} d\tau'\,H(\tau')f_+(\tau')\delta_{\mathbf{q}}(\tau') =\\ &= i\frac{\mathbf{q}}{q^2}\int_{\tau_{in}}^{\tau} d\tau'\,H(\tau')a(\tau')\frac{d\ln D^+(\tau')}{da}\delta_{\mathbf{q}}(\tau') = i\frac{\mathbf{q}}{q^2}\int_{\tau_{in}}^{\tau} d\tau'\,H(\tau')\frac{1}{H(\tau')}\frac{d\ln D^+(\tau')}{d\tau'}\frac{D^+(\tau')}{D^+(\tau_{in})}\delta_{\mathbf{q}}(\tau_{in}) =\\ &= i\frac{\mathbf{q}}{q^2}\int_{\tau_{in}}^{\tau} d\tau'\,\frac{dD^+(\tau')}{d\tau'}\frac{1}{D^+(\tau_{in})}\delta_{\mathbf{q}}(\tau_{in}) = i\frac{\mathbf{q}}{q^2}\delta_{\mathbf{q}}(\tau),\end{aligned} \tag{2.115}$$

where D^+ and f_+ are the growth factor and the growth rate respectively, hence (2.114) becomes:

$$\begin{aligned}\langle \delta_{\mathbf{q}}(\tau)\delta_{\mathbf{k}_1}(\tau_1)\delta_{\mathbf{k}_2}(\tau_2)\cdots\delta_{\mathbf{k}_n}(\tau_n)\rangle'_{\mathbf{q}\to\mathbf{0}} &= -P_\delta(\tau,q)\sum_{a=1}^{n}\frac{D^+(\tau_a)}{D^+(\tau)}\frac{\mathbf{q}\cdot\mathbf{k}_a}{q^2}\,\langle \delta_{\mathbf{k}_1}(\tau_1)\delta_{\mathbf{k}_2}(\tau_2)\cdots\delta_{\mathbf{k}_n}(\tau_n)\rangle' =\\ &= -e^{\eta}P_\delta(\tau_{in},q)\sum_{a=1}^{n}e^{\eta_a}\frac{\mathbf{q}\cdot\mathbf{k}_a}{q^2}\,\langle \delta_{\mathbf{k}_1}(\tau_1)\delta_{\mathbf{k}_2}(\tau_2)\cdots\delta_{\mathbf{k}_n}(\tau_n)\rangle'\,,\end{aligned} \tag{2.116}$$

where the primes indicate that one should remove the Dirac deltas coming from the momentum conservation and P_δ means the density-density power spectrum, related to P_{11} by a factor $e^{2\eta}$ at equal times, assuming homogeneity and isotropy.

The above relation links the $(n+1)$-th order correlator with one soft momentum to the n-th order one, as anticipated. A fundamental consequence is that, if the correlators are computed at equal times, the right hand side of the above equation vanishes by momentum conservation eliminating an important divergent contribute in the IR limit ($q \ll k$); for instance, for the bispectrum we get:

$$\langle \delta_{\mathbf{q}}(\tau)\delta_{\mathbf{k}_1}(\tau_1)\delta_{\mathbf{k}_2}(\tau_2)\rangle' = -e^{\eta} P_\delta(\tau_{in}, q)\,(e^{\eta_1} - e^{\eta_2})\,\langle \delta_{\mathbf{k}_1}(\tau_1)\delta_{\mathbf{k}_2}(\tau_2)\rangle' , \tag{2.117}$$

that of course vanishes if the times of the hard modes are the same.
We conclude this section highlighting that the result in (2.116) can be obtained working in a fully field theory approach by using the Ward identities of the theory, perfectly analogous to the famous relations bringing this name in the quantum world, for instance in quantum electrodynamics and generally in Yang-Mills theories. They stem from the the generating functional, have lots of applications, and their existence and form are completely determined by it and its symmetries. In the following we simply derive them for our system according to pure galilean invariance, although we won't use them to find the relation (2.116) another time.
Let's consider an infinitesimal galilean transformation, determined by setting the parameter $\mathbf{w}$ as infinitesimally small; in this way, under such a transformation the fields ϕ_a and χ_a transform according to the infinitesimal versions of (2.102) and (2.107), found straightforwardly by Taylor development of the exponential:

$$\begin{aligned} \delta\phi_a(\mathbf{k},\eta) &= -i\mathbf{k}\cdot\mathbf{w}\left(T(\eta)\phi_a(\mathbf{k},\eta) + e^{-\eta}\partial_\eta T(\eta)\delta(\mathbf{k})\delta_{a2}\right), \\ \delta\chi_a(\mathbf{k},\eta) &= -i\mathbf{k}\cdot\mathbf{w}T(\eta)\chi_a(\mathbf{k},\eta). \end{aligned} \tag{2.118}$$

At the same way we can obtain the infinitesimal variation of the generating functional Z (2.76) for an infinitesimal galilean transformation:

$$\begin{aligned} \delta Z = \int \mathcal{D}\phi_a \mathcal{D}\chi_b\, e^{\{\cdots\}} \iint d\eta d\mathbf{k}\,(\mathbf{k}\cdot\mathbf{w})\times \\ \times \Big\{ T(\eta)\left[J_a(-\mathbf{k},\eta)\phi_a(\mathbf{k},\eta) + K_a(-\mathbf{k},\eta)\chi_a(\mathbf{k},\eta)\right] + \\ + \left[J_2(-\mathbf{k},\eta) + \chi_a(-\mathbf{k},\eta)(\delta_{a2}\partial_\eta + \Omega_{a2})\right] e^{-\eta}\partial_\eta\delta(\mathbf{k})T(\eta)\Big\}, \end{aligned} \tag{2.119}$$

where $e^{\{\cdots\}}$ stays for the terms making the integrand of Z, that is: $Z = \iint \mathcal{D}\phi_a\chi_b\, e^{\{\cdots\}}$. However, the generating functional Z is invariant for these transformations, implying $\delta Z = 0$, and therefore, using the relations between effective action and sources (Eq.(2.81) and the homologous) we get:

$$\begin{aligned} \iint d\eta d\mathbf{k}\,(\mathbf{k}\cdot\mathbf{w})\Big\{ T(\eta)\left[\frac{\delta\Gamma}{\delta\phi_a^{cl}(\eta,-\mathbf{k})}\phi_a(\mathbf{k},\eta) + \frac{\delta\Gamma}{\delta\chi_a^{cl}(-\mathbf{k},\eta)}\chi_a(\mathbf{k},\eta)\right] + \\ + \left[\frac{\delta\Gamma}{\delta\phi_2^{cl}(-\mathbf{k},\eta)} - \chi_a(-\mathbf{k},\eta)(\delta_{a2}\partial_\eta + \Omega_{a2})\right] e^{-\eta}\partial_\eta\delta(\mathbf{k})T(\eta)\Big\}, \end{aligned} \tag{2.120}$$

the Ward identity of our cosmological system. Different one-particle irreducible Green functions can be related to each other by taking functional derivatives of this expression and then setting the fields to zero; an equivalent expression, but in terms of the generator W and the sources, can be obtained from $\delta Z = 0$ using the definitions of classical fields (2.78), generating relations between connected correlators. Considering generic n-point correlators and making use of these relations obtained from the above Ward identity, allows to recover the result in (2.116).

Chapter 3

The linear response function.

3.1 Motivation and definition.

As anticipated in the Introduction, this thesis aims to study the properties of the large-scale structure of our Universe. In fact, the LSS is widely considered to possibly unveil important geometrical features and constraints on the energetic content of the Universe, henceforth a number of wide field galaxy surveys, such as the EUCLID large-scale project, is planned in the coming decade, aiming to determine these properties with an unprecedented accuracy. In order to reach this high level of accuracy, the above measurements require the use of the statistical properties of the LSS (the most important of them being power spectra, bispectra and trispectra) up to scales entering in the weakly non-linear regime, where obviously the sole linear theory cannot be used, but meanwhile these observables need to be shielded from the (strongly non-linear) details of small (galactic and below) scales typical of astrophysics [14]. Beside the experimental effort, it is clear that the achievement of such a project could not be possible if these LSS properties will not be predicted theoretically from numerical N-body simulations or analytical models for any given kind of cosmology.
In Section 2.1, in particular from the system (2.15), we were made aware that the mode couplings between different scales are unavoidable, so we can reformulate the above question predicting quantitatively how, for any cosmology, small-scale structures impact the evolution of statistical objects at larger scales, which are typically in the weakly non-linear regime. An innovative way to solve such a question deals with the use of a two-variable kernel function, defined as the linear response at a wavemode $\mathbf{k}$ with respect to an initial perturbation of the primordial linear power spectrum at a wavemode $\mathbf{q}$.
Following [15], in order to give the formal definition of the linear kernel, we consider the fully non-linear power spectrum at the final time η and at a wave mode k, $P_{ab}(\eta;\mathbf{k})$, as a functional of the primordial linear power spectrum predicted by a particular cosmological model, given at some initial time η_{in} and function of the wavemodes $\{\mathbf{q}\} \in \mathbb{R}^3$, namely written as $P^0(\eta_{in};\mathbf{q})$, in such a way we can express the full dependence of the non-linear power spectrum as $P_{ab}[P^0](\eta_{in},\eta;\mathbf{k})$. The subscripts $(a,b=1,2)$ of the evolved power spectrum are related to the two different type of fields we can use to define the power spectrum for a dark matter particle gas, the value "1" referring to the gas matter density and the value "2" for its velocity divergence, as seen in the previous chapter. The next step consists in considering a reference linear primordial power spectrum $\bar{P}^0(\eta_{in};\mathbf{q})$ and taking $P^0(\eta_{in};\mathbf{q})$ to be a slight modification, or perturbation, of it: for example, $\bar{P}^0$ could be taken as the standard cosmological model (ΛCDM) one, by means of the best fit Planck parameters, while P^0 could be obtained from it either

by slightly changing its amplitude around some scale q_0, or by slightly changing some of the cosmological parameters. In the following we will consider both cases. Then, we expand functionally the non-linear power spectrum P_{ab} around the reference one $\bar{P}^0$, obtaining:

$$P_{ab}[P^0](\eta_{in}, \eta; \mathbf{k}) = P_{ab}[\bar{P}^0](\eta_{in}, \eta; \mathbf{k}) + \\ + \sum_{n=1}^{\infty} \frac{1}{n!} \int \cdots \int d\mathbf{q}_1 \cdots d\mathbf{q}_n \left. \frac{\delta^n P_{ab}[P^0](\eta_{in}, \eta; \mathbf{k})}{\delta P^0(\mathbf{q}_1) \cdots \delta P^0(\mathbf{q}_n)} \right|_{P^0 = \bar{P}^0} \delta P^0(\mathbf{q}_1) \cdots \delta P^0(\mathbf{q}_n), \tag{3.1}$$

where $\delta P^0(\mathbf{q}) \equiv P^0(\mathbf{q}) - \bar{P}^0(\mathbf{q})$. Introducing spherical coordinates Eq.(3.1) becomes:

$$P_{ab}[P^0](\eta_{in}, \eta; \mathbf{k}) = P_{ab}[\bar{P}^0](\eta_{in}, \eta; \mathbf{k}) + \int \frac{dq}{q} K_{ab}(\mathbf{k}, q, \Omega_{\mathbf{q}}; \eta, \eta_{in}) \delta P^0(q, \Omega_{\mathbf{q}}) + \mathcal{O}[(\delta P^0(\mathbf{q}))^2], \tag{3.2}$$

from which, assuming spatial isotropy, it follows the definition of the linear response function (LRF) K_{ab}:

$$K_{ab}(k, q; \eta, \eta_{in}) \equiv q^3 \int d\Omega_{\mathbf{q}} \left. \frac{\delta^n P_{ab}[P^0](\eta_{in}, \eta; k)}{\delta P^0(q)} \right|_{P^0 = \bar{P}^0}. \tag{3.3}$$

Here, it is important to note that, despite its name, the linear response function is a fully non-linear object, fundamentally because $P_{ab}[P^0]$ is non-linear: indeed, in a perturbative approach the LRF receives contributions at all orders: take any l-loop order diagram contributing to the power spectrum, substitute one linear power spectrum with δP_{ab}, the second term of the right hand side of (3.2), and repeat the operation for each linear power spectrum.
The SPT expansion corresponds to the "singular" choice: $\bar{P}^0 = 0$ in (3.1), in which case the LRF gives exactly the linear perturbative kernel. For any non-vanishing choice, the LRF contains all orders in $\bar{P}^0$ and can be computed either in SPT or with methods beyond SPT, and it can also be measured in N-body simulations. Finally, we note that the LRF is adimensional.
Coming back to the beginning of this section, we see that this object answers the questions we made. From a practical point of view the LRF can be used to obtain the most important LSS non-linear statistical observable, the evolved power spectrum, for cosmologies with primordial power spectra slightly different from the reference one, once the non-linear evolved one generated by the latter has been computed, for example by N-body simulations; however, from a more fundamental point of view, the linear kernel is crucial when we need to quantify the coupling between different modes at a fully non-linear level, because it encodes how much a slight modification of the initial conditions at a scale with mode q impacts on the non-linear power spectrum evolved at later times at a scale with mode k.
In Fig.(3.1) we can see a linear kernel function computed by means of N-body simulations: it is evident the strong peak corresponding to $k = q$, arising trivially at linear level, meaning remarkably that the most important contribute to the evolution of structures (matter density) at a given comoving wavemode k comes, at all the precedent times, from the properties at the same scale, but of course it also depends on the other scales, presenting non-linear couplings that gradually grow with time, making progressively the peak feature less significant; furthermore, we can observe that a large contribution comes from small wavemodes, suggesting that the growth of structures is dominated by modes flowing from larger to smaller scales: indeed, the formation of structures is more effectively amplified when it is part of a larger structure than when it contains only small scales features.
Before going on, an observation concerning the initial time η_{in}. Surely, it definitely has a great impact on the above definition, fixing the reference initial power spectrum: thus, for the analytic calculations performed throughout the text, we safely consider $\eta_{in} = -\infty$, differently from the

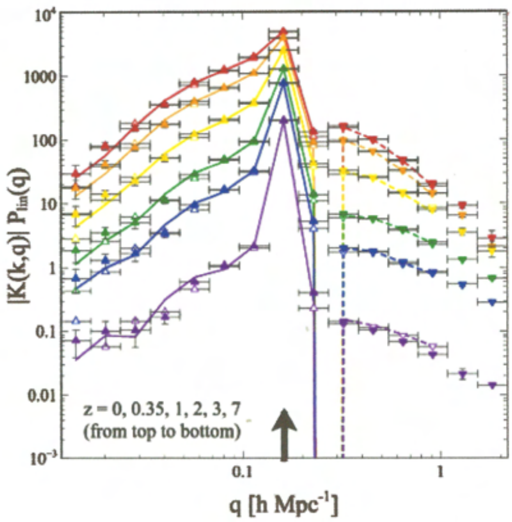

Figure 3.1: Linear response function measured by means of simulations for a flat ΛCDM universe, from [14]. The cosmological parameters used are $(\Omega_m, \Omega_b/\Omega_m, h, 10^9 A_s, n_s) = (0.279, 0.165, 0.701, 2.49, 0.96)$. In particular, we see plotted the absolute value of the kernel multiplied by the linearised version of the evolved matter power spectrum of the model for various redshifts, as a function of the primordial wavemode q for the fixed final wavemode $k = 0.161\, h\mathrm{Mpc}^{-1}$.

previous chapter, while when we will use a computational approach, this becomes a numerical issue, and we will refer to a suitable high redshift value. Furthermore, for compactness the initial time dependence of the linear kernel will be often ignored.
Finally, we make the reader aware that throughout the present chapter we are acting in accomplishment of the notation $\langle \phi_a(\mathbf{k})\phi_b(\mathbf{k}')\rangle = (2\pi)^3\delta(\mathbf{k}+\mathbf{k}')P_{ab}(k)$, not used elsewhere in this text but widely used in literature: as a consequence, the evolved power spectrum P_{ab} will present a factor $1/(2\pi)^3$.

3.2 The linear kernel in terms of 1PI functions.

Remembering the definitions of the non-linear (full) power spectrum in (2.68) and the generating functional Z in (2.76), the equal time power spectrum takes the form:

$$\langle \phi_a(\mathbf{k},\eta)\phi_b(\mathbf{k}',\eta)\rangle = \iint \mathcal{D}\phi_a \mathcal{D}\chi_b \left[e^{-\frac{1}{2}\int \frac{d\mathbf{q}}{(2\pi)^3}\chi_c(-\mathbf{q},\eta_{in})u_c P^0(\mathbf{q})u_d\chi_d(\mathbf{q},\eta_{in}) + iS[\phi_a,\chi_b]} \right] \phi_a(\mathbf{k},\eta)\phi_b(\mathbf{k}',\eta), \tag{3.4}$$

where the action, defined in (2.42), reads:

$$\begin{aligned} S[\phi_a,\chi_b] = \int_{\eta_{in}}^{\eta} d\eta' \Big[&\int \frac{d\mathbf{q}}{(2\pi)^3}\chi_c(-\mathbf{q},\eta')(\delta_{cd}\partial_{\eta'} + \Omega_{cd})\phi_d(\mathbf{q},\eta') + \\ &- e^{\eta'}\int \frac{d\mathbf{q}}{(2\pi)^3}\int \frac{d\mathbf{p}}{(2\pi)^3}\gamma_{abc}(\mathbf{q}+\mathbf{p},\mathbf{q},\mathbf{p})\chi_a(-\mathbf{q}-\mathbf{p},\eta')\phi_b(\mathbf{q},\eta')\phi_c(\mathbf{p},\eta')\Big]. \end{aligned} \tag{3.5}$$

It is worth specifying that the above definition of matter power spectrum $\langle\phi_1\phi_1\rangle$ is related to the "density-density" $\langle\delta\delta\rangle$ one (2.56) by $\langle\delta\delta\rangle = e^{2\eta}\,\langle\phi_1\phi_1\rangle$ at equal time, by consequence of (2.19). If not explicitly said, analytical results are carried on referring to the ϕ fields.
Now, if we take the functional derivative of (3.4) with respect to $P^0(\mathbf{q})$ we get:

$$
\begin{aligned}
(2\pi)^3\delta(\mathbf{k}+\mathbf{k}')\frac{\delta P_{ab}(\mathbf{k},\eta)}{\delta P^0(\mathbf{q})} =& -\frac{1}{2}\frac{1}{(2\pi)^3}\iint \mathcal{D}\phi_a\mathcal{D}\chi_b \left[e^{-\frac{1}{2}\int\frac{d\mathbf{q}}{(2\pi)^3}\,\chi_c(-\mathbf{q},\eta_{in})u_cP^0(\mathbf{q})u_d\chi_d(\mathbf{q},\eta_{in})+iS[\phi_a,\chi_b]}\right]\times\\
&\times\phi_a(\mathbf{k},\eta)\phi_b(\mathbf{k}',\eta)\chi_c(-\mathbf{q},\eta_{in})\chi_d(\mathbf{q},\eta_{in})u_cu_d =\\
=& -\frac{1}{2}\frac{1}{(2\pi)^3}\,\langle\phi_a(\mathbf{k},\eta)\phi_b(\mathbf{k}',\eta)\chi_c(-\mathbf{q},\eta_{in})\chi_d(\mathbf{q},\eta_{in})\rangle\, u_cu_d.
\end{aligned}
\tag{3.6}
$$

In order to better understand the meaning of the four point function (a trispectrum) appearing at the right hand side of the previous expression, it is worth remembering the form (2.91) for the full power spectrum, written as the sum of two connected terms, by means of 1PI functions. With these definitions and assuming spatial isotropy, the linear kernel can be written as:

$$
\begin{aligned}
K_{ab}(k,q;\eta,\eta_{in}) \equiv& \; q\int dq\,\frac{\delta^n P^I_{ab}[P^0](\eta_{in},\eta;k)}{\delta P^0(q)}\bigg|_{P^0=\bar{P}^0} + q^3\int d\Omega_{\mathbf{q}}\frac{\delta^n P^{II}_{ab}[P^0](\eta_{in},\eta;k)}{\delta P^0(q)}\bigg|_{P^0=\bar{P}^0} =\\
=& \; q\,\delta(k-q)G_{ac}(k,\eta_a,\eta_{in})G_{bd}(k,\eta_b,\eta_{in})u_cu_d +\\
&-\frac{1}{2}\frac{q^3}{(2\pi)^3}\int d\Omega_{\mathbf{q}}\,\langle\phi_a(\mathbf{k},\eta)\phi_b(-\mathbf{k},\eta)\chi_c(-\mathbf{q},\eta_{in})\chi_d(\mathbf{q},\eta_{in})\rangle_c'\,u_cu_d,
\end{aligned}
\tag{3.7}
$$

where the second line represents the disconnected contribution to the four-points function written in (3.6), while the $\langle\cdots\rangle_c'$ at the third line means the connected contribution to it, divided by $(2\pi)^3\delta(0)$, the overall momentum delta function. Incidentally, we notice that in the following the dependence $(k-q)$, appearing as the argument of the Dirac's delta, assuming homogeneity and isotropy has to be intended as difference between absolute values.
It is crucial to realise that the functional derivative with respect to the initial power spectrum P^0 doesn't act only on the explicit dependence of it in P^I_{ab} or in the piece Φ_{ab} of P^{II}_{ab}; indeed, even by the simple perturbative expansion of the non-linear propagator G_{ab} at one loop, globally drawn as its linear counterpart with a thick track, reported here below [3]:

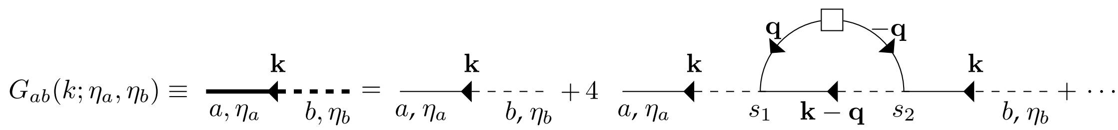

Figure 3.2: One loop expansion of the full propagator.

one can see that G_{ab} has a strong dependence on P^0, hence the functional derivative acts also on this object, present in both the two terms in which we expressed the full power spectrum. For this reason, we can understand that the connected contribution to the linear kernel, the third line of the expression (3.7), contains not only the three contributions coming from the functional derivative of P^{II}_{ab}, but also the two coming from the derivatives of the propagators present in the term P^I_{ab}.
We can now express in a diagrammatic way the linear kernel in (3.7), presented in detail in the following figure.

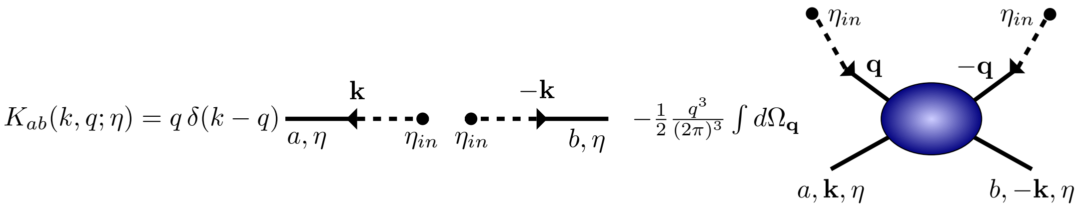

Figure 3.3: Diagrammatic expression for the linear kernel.

The diagrammatic expression reflects in a straightforward way the content of the formal expression (3.7) for the linear kernel function. The first diagram shows its disconnected term: the two propagators, that before the derivation were "glued" by the primordial power spectrum, now are detached, with the two χ_a-legs contracted (or amputated) with the growing mode doublet u_a, leaving free only the two ϕ_a-legs. A contraction is made visible in the above figure by means of a small point at the end of a χ_a-leg. The second diagram, actually the most interesting, is the connected one: it is depicted as a blob, meaning its body with all its constituents, with four legs, the two relative to χ_a being contracted, as can clearly be seen in (3.7), the ϕ_a one being free, analogously to the first term. From the Feynman rules presented in the Subsection 2.2.2, we can see that a χ_a-leg is mandatory linked to a ϕ_a one by a propagator, therefore the connected function at the third line of the expression (3.7) has the following structure:

$$\begin{aligned}&\langle\phi_a(\mathbf{k},\eta)\phi_b(-\mathbf{k},\eta)\chi_c(-\mathbf{q},\eta_{in})\chi_d(\mathbf{q},\eta_{in})\rangle_c'\,u_c u_d = \\ &\quad= \int_{\eta_{in}}^{\eta} ds \int_{\eta_{in}}^{\eta} ds'\,\tilde{T}^{\phi\phi;\phi\phi}_{ab;ef}(\mathbf{k},-\mathbf{k},\mathbf{q},-\mathbf{q};\eta,s,s')\,G_{ec}(q;s,\eta_{in})u_c\,G_{fd}(q;s',\eta_{in})u_d,\end{aligned} \tag{3.8}$$

where the four-points function $\tilde{T}^{\phi\phi,\phi\phi}_{ab;ef}(\mathbf{k},-\mathbf{k},\mathbf{q},-\mathbf{q};\eta,s,s')$ is the trispectrum to which the external legs carrying momentum $\pm\mathbf{q}$, and connected to χ_a, have been amputated, while the remaining free ends are of ϕ_a type. This expression shows the crucial importance of the non-linear propagator in encoding the relevant information about the effects of the modification of the initial power spectrum at scale q at later times.

3.3 The linear kernel at the lowest order perturbative level.

In this section, we will give the analytical expression for the kernel function at tree level and explore its behaviours in the two following important regions: the first is the infrared (IR) one, namely where the primordial wavemode $\mathbf{q}$ around which we perturb the initial conditions (that is the initial power spectrum) is much smaller than the wavemode $\mathbf{k}$ at which we want to know the impact of the perturbation at later times, thus characterized by the relation $\frac{q}{k} \to 0$, while the second is the opposite one, known as ultraviolet (UV) region, where the primordial wavemode is much bigger than the evolved one, resulting in $\frac{q}{k} \to \infty$.
In order to reach the lowest order (or tree) perturbative level expansion of the linear kernel function, it is very helpful to start from the one loop expansion of the non-linear power spectrum, given in the following figure [3].

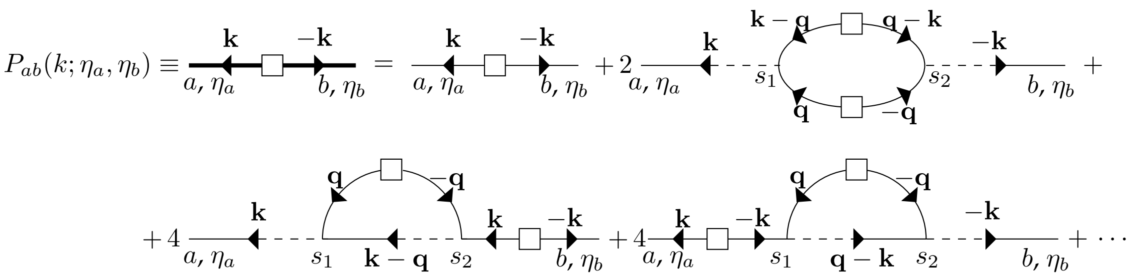

Figure 3.4: One loop expansion of the full power spectrum.

In contrast with the non perturbative expression for the kernel, reported in (3.7), the primordial power spectra that we see in the above figure bear the complete dependence on them of the full power spectrum at one loop, in the sense that there are no more hidden P^0. Hence, following the definition (3.3) and focussing only on the connected contributions, we understand that the tree level expansion for the kernel is given diagrammatically by Fig.(3.31), consisting in the tree level expansion of Fig.(3.3). In particular, Fig(3.31) can be obtained from Fig.(3.4) by opening each of the loops in correspondence of a linear power spectrum. Notice that this operation can be made in two ways for the second diagram in the diagrammatic expansion of Fig.(3.4), while there is only one possibility for both the third and the fourth ones.

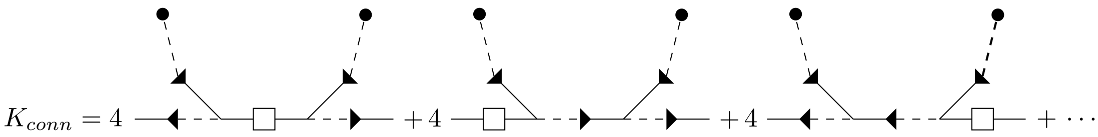

Figure 3.5: Diagrammatic constituents of the tree level linear kernel.

From the expressions (3.7) and (3.8) we can write the formal expression for the one loop kernel, simply approximating the non-linear propagator with its tree level constituent, the linear propagator g_{ab}, calculating the amputated trispectrum at tree level and using the identity $g_{ab}(\eta_a,\eta_b)u_a = u_b$ if $\eta_a > \eta_b$, coming directly from Eq.(2.25). The result is:

$$
\begin{aligned}
K^{tree}_{ab}(k,q;\eta) &= q\,\delta(k-q)\,u_a u_b + \\
&- \frac{1}{2}\frac{q^3}{(2\pi)^3}\int_{\eta_{in}}^{\eta} ds \int_{\eta_{in}}^{\eta} ds'\, \tilde{T}^{\phi\phi;\phi\phi,tree}_{ab;cd}(\mathbf{k},-\mathbf{k},\mathbf{q},-\mathbf{q};\eta,s,s')\,u_c u_d.
\end{aligned}
\tag{3.9}
$$

Fig.(3.31) represents diagrammatically the contributions to the connected part of the linear kernel, at the second line of the above expression.

In the following, we focus on the IR and UV limits of the matter linear kernel at the lowest order in perturbation theory: to this end, we will directly compute the expression of the full evolved matter power spectrum at one loop, namely evaluating the diagrams in Fig.(3.4) selecting $a = b = 1$, then by it we will derive the linear kernel using directly its definition in (3.3) and finally we will evaluate the two limits.

3.3.1 The matter power spectrum at one loop order.

In consideration of Fig.(3.4), we define P^{1-loop}_{ab} the truncation of the perturbative expansion of the non-linear evolved power spectrum up to one loop and, following the order in the figure, we express it through its constituents in the following way:

$$P_{ab}^{1-loop}(k,\eta) = P_{ab}^{(1)}(k,\eta) + P_{ab}^{(2)}(k,\eta) + P_{ab}^{(3)}(k,\eta) + P_{ab}^{(4)}(k,\eta), \tag{3.10}$$

where, for what concerns the loop terms, for the vertex s_1 we label the legs, starting from the χ_a one and going on in the clockwise sense, with $\{c, e, g\}$, and analogously for the s_2 vertex with $\{d, h, f\}$, while when we need to use the decomposition (2.67) we use the same letter at the end of the line, but with the prime. Finally, for simplicity we fix $\mathbf{p} = \mathbf{k} - \mathbf{q}$.
Clearly, remembering the expressions (2.58) and (2.67) one has $P_{ab}^{(1)}(k,\eta) = P_{ab}^{L}(k,\eta)$ as the tree level contribution, trivially the linearly evolved power spectrum, that however will not be of any importance for the kernel, giving indeed a disconnected term.
Now we address the second term, $P_{ab}^{(2)}(k,\eta)$; using the Feynman rules we get:

$$\begin{aligned}
P_{ab}^{(2)}(k,\eta) =& 2\int_{\eta_{in}}^{\eta} ds_1 \int_{\eta_{in}}^{\eta} ds_2 \int \frac{d\mathbf{q}}{(2\pi)^3}\, g_{ac}(\eta,s_1) e^{s_1}\gamma_{ceg}(\mathbf{k},\mathbf{p},\mathbf{q}) P_{ef}^{L}(p;s_1,s_2) \\
&\times e^{s_2}\gamma_{dhf}(-\mathbf{k},-\mathbf{q},-\mathbf{p}) g_{bd}(\eta,s_2) P_{gh}^{L}(q;s_1,s_2) = \\
=& 2\iint_{\eta_{in}}^{\eta} ds_1 ds_2 \int \frac{d\mathbf{q}}{(2\pi)^3}\, g_{ac}(\eta,s_1) e^{s_1}\gamma_{cge}(\mathbf{k},\mathbf{q},\mathbf{p}) P^0(p) g_{ee'}(s_1,\eta_{in}) g_{ff'}(s_2,\eta_{in}) u_{e'} u_{f'} \\
&\times e^{s_2}\gamma_{dhf}(\mathbf{k},\mathbf{q},\mathbf{p}) g_{bd}(\eta,s_2) P^0(q) g_{gg'}(s_1,\eta_{in}) g_{hh'}(s_2,\eta_{in}) u_{g'} u_{h'} = \\
=& 2\iint_{\eta_{in}}^{\eta} ds_1 ds_2 \int \frac{d\mathbf{q}}{(2\pi)^3}\, e^{s_1+s_2} g_{ac}(\eta,s_1) g_{bd}(\eta,s_2)\gamma_{cge}(\mathbf{k},\mathbf{q},\mathbf{p})\gamma_{dhf}(\mathbf{k},\mathbf{q},\mathbf{p}) \\
&\times P^0(p)P^0(q) u_e u_f u_g u_h,
\end{aligned} \tag{3.11}$$

where in the first passage we use $\gamma_{abc}(\mathbf{k},\mathbf{p},\mathbf{q}) = \gamma_{acb}(\mathbf{k},\mathbf{q},\mathbf{p})$, the parity of the vertex and the expression (2.67), while in the second mainly $g_{ab}(\eta_a,\eta_b)u_a = u_b$ if $\eta_a > \eta_b$. Now, maintaining the dependencies of the propagators and the vertices in the exact order with which they appear in the last step of (3.11), but avoiding to write them, and remembering that $u_a = \binom{1}{1}$, the non zero elements bring the matter-matter component to be:

$$\begin{aligned}
P_{11}^{(2)}(k,\eta) =& 2\iint_{\eta_{in}}^{\eta} ds_1 ds_2 \int \frac{d\mathbf{q}}{(2\pi)^3}\, e^{s_1+s_2}\Big[g_{11}g_{11}\gamma_{121}\gamma_{121} + g_{11}g_{11}\gamma_{121}\gamma_{112} + \\
&+ g_{11}g_{12}\gamma_{121}\gamma_{222} + g_{11}g_{11}\gamma_{112}\gamma_{121} + g_{11}g_{11}\gamma_{112}\gamma_{112} + g_{11}g_{12}\gamma_{112}\gamma_{222} + \\
&+ g_{12}g_{11}\gamma_{222}\gamma_{121} + g_{12}g_{11}\gamma_{222}\gamma_{112} + g_{12}g_{12}\gamma_{222}\gamma_{222}\Big] P^0(p)P^0(q),
\end{aligned} \tag{3.12}$$

that, once noticed that the second and the fourth terms are actually equal and using the explicit forms for the propagator, Eq.(2.70), and the vertex, as in Subsection 2.2.2, becomes:

$$
\begin{aligned}
P_{11}^{(2)}(k,\eta) =& 2\iint_{\eta_{in}}^{\eta} ds_1 ds_2 \int \frac{d\mathbf{q}}{(2\pi)^3}\, e^{s_1+s_2}\Bigg\{ \left(\frac{2}{5}-\frac{2}{5}e^{-\frac{5}{2}(\eta-s_1)}\right)\left(\frac{2}{5}-\frac{2}{5}e^{-\frac{5}{2}(\eta-s_2)}\right)\frac{k^4\left(k^2-p^2-q^2\right)^2}{16p^4q^4}+\\
&+\left[\left(\frac{3}{5}+\frac{2}{5}e^{-\frac{5}{2}(\eta-s_1)}\right)\left(\frac{2}{5}-\frac{2}{5}e^{-\frac{5}{2}(\eta-s_2)}\right)+\left(\frac{2}{5}-\frac{2}{5}e^{-\frac{5}{2}(\eta-s_1)}\right)\left(\frac{3}{5}+\frac{2}{5}e^{-\frac{5}{2}(\eta-s_2)}\right)\right]\times\\
&\times\frac{k^2\left(k^2-p^2-q^2\right)}{16p^2q^2}\left[\frac{\left(k^2-p^2+q^2\right)}{q^2}+\frac{\left(k^2+p^2-q^2\right)}{p^2}\right]+\\
&+\left(\frac{3}{5}+\frac{2}{5}e^{-\frac{5}{2}(\eta-s_1)}\right)\left(\frac{3}{5}+\frac{2}{5}e^{-\frac{5}{2}(\eta-s_2)}\right)\left[\frac{\left(k^2-p^2+q^2\right)\left(k^2+p^2-q^2\right)}{8p^2q^2}+\right.\\
&\left.+\frac{\left(k^2-p^2+q^2\right)^2}{16q^4}+\frac{\left(k^2+p^2-q^2\right)^2}{16p^4}\right]\Bigg\}P^0(p)P^0(q).
\end{aligned}
\tag{3.13}
$$

The above expression already takes into account that the Heaviside functions are always one here, thus the two time integrals can be solved in a straightforward way, being decoupled and completely based on the product of two integrals of the type:

$$
\int_{-\infty}^{\eta} ds\, e^{s}(a+b\,e^{-\frac{5}{2}(\eta-s)}) = e^{\eta}(a+\frac{2}{7}b),
\tag{3.14}
$$

entailing a great simplification of the form of $P_{ab}^{(2)}$, that by performing the calculations it indeed becomes:

$$
\begin{aligned}
P_{11}^{(2)}(k,\eta) = \int \frac{d\mathbf{q}}{(2\pi)^3}\Big[&\frac{k^8}{98p^4q^4}+\frac{3k^6}{98p^4q^2}+\frac{3k^6}{98p^2q^4}-\frac{11k^4}{392p^4}+\frac{29k^4}{196p^2q^2}-\frac{11k^4}{392q^4}-\frac{15k^2q^2}{196p^4}+\\
&-\frac{15k^2p^2}{196q^4}+\frac{15k^2}{196p^2}+\frac{15k^2}{196q^2}+\frac{25q^4}{392p^4}+\frac{25p^4}{392q^4}-\frac{25q^2}{98p^2}-\frac{25p^2}{98q^2}+\frac{75}{196}\Big]P^0(p)P^0(q),
\end{aligned}
\tag{3.15}
$$

which can be rewritten in the following compact form:

$$
P_{11}^{(2)}(k,\eta) = \int \frac{d\mathbf{q}}{(2\pi)^3}\,\frac{e^{2\eta}}{392p^4q^4}\left[2k^4+3k^2\left(p^2+q^2\right)-5\left(p^2-q^2\right)^2\right]^2 P^0(p)P^0(q).
\tag{3.16}
$$

The next step would be the integration on the loop momentum $\mathbf{q}$. As we know, it is customary to express it in spherical coordinates as:

$$
\int_{\mathbb{R}^3}\mathbf{q} = \int_0^{2\pi} d\phi\int_0^{\pi} d\theta\,\sin\theta\int_0^{\infty} dq\, q^2 = \int_0^{2\pi} d\phi\int_{-1}^{1} d\cos\theta\int_0^{\infty} dq\, q^2,
\tag{3.17}
$$

where, in our specific frame, ϕ is the polar angle and θ is the azimuthal angle measured between the fixed axis corresponding to the evolved momentum vector $\mathbf{k}$ and the various momenta $\mathbf{q}\in\mathbb{R}^3$, as depicted in Fig.(3.6).

In this way, calling $\cos\theta = x$ and noting that the integrand doesn't depend on ϕ, we can write:

$$
\int_{\mathbb{R}^3} d\mathbf{q} = 2\pi\int_{-1}^{1} dx\int_0^{\infty} dq\, q^2.
\tag{3.18}
$$

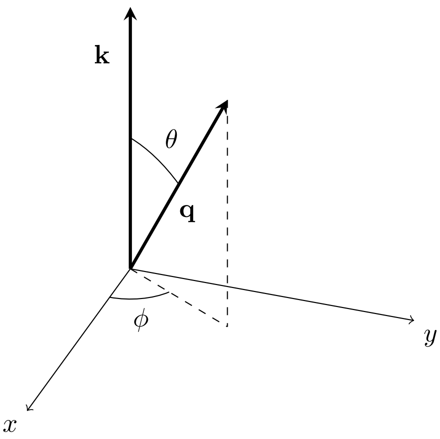

Figure 3.6: System of coordinates used in the integration.

Since the integrand of $P_{ab}^{(2)}$ involves an angular dependence in the initial power spectrum, $P^0(p)$, for now we simply express the latter as:

$$P^0(p) = P^0(|\mathbf{k} - \mathbf{q}|) = P^0\big(\sqrt{k^2 + q^2 - 2qkx}\big) = P^0\left(k\sqrt{1 + \frac{q^2}{k^2} - 2\frac{q}{k}x}\right), \tag{3.19}$$

thus, using the above expression and $p^2 = k^2 + q^2 - 2kqx$, the contribution $P_{ab}^{(2)}$ in (3.16) eventually writes, consistently with [49], as:

$$P_{11}^{(2)}(k, \eta) = \frac{k^4 e^{2\eta}}{392\pi^2} \int_{-1}^{1} dx \int_0^\infty dq \, \frac{\left(7kx + q\left(3 - 10x^2\right)\right)^2}{\left(k^2 - 2kqx + q^2\right)^2} P^0\left(k\sqrt{1 + \frac{q^2}{k^2} - 2\frac{q}{k}x}\right) P^0(q). \tag{3.20}$$

We now address to the third and fourth term in the expression (3.10) for the power spectrum, one the specular of the other, $P_{ab}^{(3)}$ and $P_{ab}^{(4)}$. Looking at their diagrams in Fig.(3.4), using the Feynman rules and maintaining the previous notation for indices, for $P_{ab}^{(3)}$ one has:

$$\begin{aligned}
P_{ab}^{(3)}(k, \eta) =& 4\int_{\eta_{in}}^{\eta} ds_1 \int_{\eta_{in}}^{\eta} ds_2 \int \frac{d\mathbf{q}}{(2\pi)^3}\, g_{ac}(\eta, s_1) e^{s_1} \gamma_{ceg}(\mathbf{k}, \mathbf{q}, \mathbf{p}) P_{ef}^L(q; s_1, s_2) \\
& \times g_{gh}(s_1, s_2) e^{s_2} \gamma_{hfd}(\mathbf{p}, -\mathbf{q}, \mathbf{k}) P_{db}^L(k, s_2, \eta) = \\
=& 4\int_{\eta_{in}}^{\eta} ds_1 \int_{\eta_{in}}^{\eta} ds_2 \int \frac{d\mathbf{q}}{(2\pi)^3}\, e^{s_1+s_2} g_{ac}(\eta, s_1) g_{gh}(s_1, s_2) \gamma_{ceg}(\mathbf{k}, \mathbf{q}, \mathbf{p}) \gamma_{hfd}(\mathbf{p}, -\mathbf{q}, \mathbf{k}) \\
& \times P^0(q) P^0(k) u_b u_d u_e u_f,
\end{aligned} \tag{3.21}$$

that for the matter component reduces, adopting the same schematic notation used in (3.12), to:

$$\begin{aligned}
P_{11}^{(3)}(k, \eta) =& 4\iint_{\eta_{in}}^{\eta} ds_1 ds_2 \int \frac{d\mathbf{q}}{(2\pi)^3}\, e^{s_1+s_2} \Big[g_{11}g_{11}\gamma_{121}\gamma_{121} + g_{11}g_{11}\gamma_{121}\gamma_{112} + \\
& + g_{11}g_{12}\gamma_{121}\gamma_{222} + g_{11}g_{21}\gamma_{112}\gamma_{121} + g_{11}g_{21}\gamma_{112}\gamma_{112} + g_{11}g_{22}\gamma_{112}\gamma_{222} + \\
& + g_{12}g_{21}\gamma_{222}\gamma_{112} + g_{12}g_{21}\gamma_{222}\gamma_{121} + g_{12}g_{22}\gamma_{222}\gamma_{222}\Big] P^0(q) P^0(k).
\end{aligned} \tag{3.22}$$

Analogously, for the last term of the one loop expansion we find:

$$
\begin{aligned}
P_{ab}^{(4)}(k,\eta) =&4\int_{\eta_{in}}^{\eta} ds_1 \int_{\eta_{in}}^{\eta} ds_2 \int \frac{d\mathbf{q}}{(2\pi)^3}\, P_{ac}^{L}(k,s_1,\eta) e^{s_1}\gamma_{gce}(-\mathbf{p},-\mathbf{k},\mathbf{q}) P_{ef}^{L}(q;s_1,s_2) g_{hg}(s_2,s_1)\\
&\times e^{s_2}\gamma_{dhf}(-\mathbf{k},-\mathbf{p},-\mathbf{q}) g_{bd}(\eta,s_2) =\\
=&4\int_{\eta_{in}}^{\eta} ds_1 \int_{\eta_{in}}^{\eta} ds_2 \int \frac{d\mathbf{q}}{(2\pi)^3}\, e^{s_1+s_2} g_{bd}(\eta,s_2) g_{hg}(s_2,s_1)\gamma_{dfh}(\mathbf{k},\mathbf{q},\mathbf{p})\gamma_{gec}(\mathbf{p},-\mathbf{q},\mathbf{k})\\
&\times P^0(q)P^0(k)u_a u_c u_e u_f,
\end{aligned}
\tag{3.23}
$$

where we make use of the parity and symmetry properties of the vertex and exchange their order. For the matter component, with the known notation, by direct calculus we reach the expected relation:

$$
P_{11}^{(3)}(k,\eta) = P_{11}^{(4)}(k,\eta). \tag{3.24}
$$

However, it is important to note that the general forms (3.21) and (3.23) are different if $a \neq b$, uniquely caused by the different indices a and b in the first propagator in the last equalities of (3.21) and (3.23).
Denoting $P_{11}^{(5)} = P_{11}^{(3)} + P_{11}^{(4)} = 2P_{11}^{(3)} = 2P_{11}^{(4)}$ and using the explicit forms for the propagators and the vertices, we get:

$$
\begin{aligned}
P_{11}^{(5)}(k,\eta) = &\frac{1}{2}\int_{\eta_{in}}^{\eta} ds_1 \int_{\eta_{in}}^{\eta} ds_2 \int \frac{d\mathbf{q}}{(2\pi)^3}\, \Theta(s_1-s_2)\, e^{s_1+s_2}\times\\
\times\Bigg\{ &\left(\frac{3}{5}+\frac{2}{5}e^{-\frac{5}{2}(\eta-s_1)}\right)\left(\frac{3}{5}+\frac{2}{5}e^{-\frac{5}{2}(s_1-s_2)}\right)\left[\frac{\left(k^2+p^2-q^2\right)}{k^2q^2}+\frac{\left(-k^2+p^2+q^2\right)}{q^4}\right]\left(k^2-p^2+q^2\right)+\\
+&\left(\frac{3}{5}+\frac{2}{5}e^{-\frac{5}{2}(\eta-s_1)}\right)\left(\frac{2}{5}-\frac{2}{5}e^{-\frac{5}{2}(s_1-s_2)}\right)\frac{p^2\left(-k^2+p^2-q^2\right)\left(k^2-p^2+q^2\right)}{k^2q^4}+\\
+&\left(\frac{3}{5}+\frac{2}{5}e^{-\frac{5}{2}(\eta-s_1)}\right)\left(\frac{3}{5}-\frac{3}{5}e^{-\frac{5}{2}(s_1-s_2)}\right)\left[\frac{\left(k^2+p^2-q^2\right)}{k^2p^2}+\frac{\left(-k^2+p^2+q^2\right)}{p^2q^2}\right]\left(k^2+p^2-q^2\right)+\\
+&\left(\frac{3}{5}+\frac{2}{5}e^{-\frac{5}{2}(\eta-s_1)}\right)\left(\frac{2}{5}+\frac{3}{5}e^{-\frac{5}{2}(s_1-s_2)}\right)\frac{\left(-k^2+p^2-q^2\right)\left(k^2+p^2-q^2\right)}{k^2q^2}+\\
+&\left(\frac{2}{5}-\frac{2}{5}e^{-\frac{5}{2}(\eta-s_1)}\right)\left(\frac{3}{5}-\frac{3}{5}e^{-\frac{5}{2}(s_1-s_2)}\right)\left[\frac{\left(k^2+p^2-q^2\right)}{p^2q^2}+\frac{k^2\left(-k^2+p^2+q^2\right)}{p^2q^4}\right]\left(k^2-p^2-q^2\right)+\\
+&\left(\frac{2}{5}-\frac{2}{5}e^{-\frac{5}{2}(\eta-s_1)}\right)\left(\frac{2}{5}+\frac{3}{5}e^{-\frac{5}{2}(s_1-s_2)}\right)\frac{\left(k^2-p^2-q^2\right)\left(-k^2+p^2-q^2\right)}{q^4}\Bigg\}P^0(q)P^0(k).
\end{aligned}
\tag{3.25}
$$

An important difference with the expression for $P11^{(2)}$ is that now the Heaviside function couples the two time integrations modifying their extrema, because while $\Theta(\eta-s_i)=1\ \forall s_i$, now $\Theta(s_1-s_2)=1$ only if $s_1>s_2$; nevertheless, they can be handled in the following way:

$$
\begin{aligned}
\int_{\eta_{in}}^{\eta} ds_1 \int_{\eta_{in}}^{\eta} ds_2\ \Theta(s_1-s_2)\, e^{s_1+s_2}\left(a+b\,e^{-\frac{5}{2}(\eta-s_1)}\right)\left(c+d\,e^{-\frac{5}{2}(s_1-s_2)}\right) =&\\
=\int_{\eta_{in}}^{\eta} ds_1\left(a\,e^{s_1}+b\,e^{-\frac{5}{2}\eta}e^{\frac{7}{2}s_1}\right)\left(c\,e^{s_1}+\frac{2}{7}d\,e^{s_1}\right) =&\\
= e^{2\eta}\left(\frac{1}{2}ac+\frac{1}{7}ad+\frac{2}{9}bc+\frac{4}{63}bd\right).&
\end{aligned}
\tag{3.26}
$$

Henceforth, the time integration in the matter power spectrum contribution (3.25) brings to:

$$P_{11}^{(5)}(k,\eta) = \int \frac{d\mathbf{q}}{(2\pi)^3} \Big[-\frac{k^6}{42p^2q^4} - \frac{k^4}{84p^2q^2} - \frac{31k^4}{252q^4} - \frac{p^6}{18k^2q^4} + \frac{p^4}{12k^2q^2} + \frac{11k^2p^2}{42q^4} + \frac{q^4}{12k^2p^2} + \\ + \frac{5k^2}{28p^2} + \frac{p^2}{12k^2} - \frac{5k^2}{252q^2} - \frac{7q^2}{36k^2} - \frac{5p^4}{84q^4} - \frac{19q^2}{84p^2} - \frac{13p^2}{252q^2} + \frac{85}{252} \Big] P^0(q)P^0(k). \tag{3.27}$$

This time, differently from the other diagram, we can soon evaluate the angular integration, as we see that the initial power spectra don't carry any angular dependence, not contributing to this stage of the integration. Terms with a factor in power of p^2 at the numerator (namely p^0, p^2, p^4 and p^6) are absolutely trivial, while the ones with a factor p^2 at the denominator are solved by means of the following elementary integral:

$$\int_{-1}^{1} dx \, \frac{C(q,k)}{k^2+q^2-2kqx} = \frac{C(q,k)}{q^2} \int_{-1}^{1} dx \, \frac{1}{1+\frac{k^2}{q^2}-2\frac{k}{q}x} = \\ = -\frac{C(q,k)}{2kq} \ln\left(1+\frac{k^2}{q^2}-2\frac{k}{q}x\right)\Bigg|_{-1}^{1} = \frac{C(q,k)}{2kq} \ln\left[\frac{1+\frac{k}{q}}{|1-\frac{k}{q}|}\right], \tag{3.28}$$

where as before x is the cosine of the azimuthal angle between $\mathbf{k}$ and $\mathbf{q}$, while $C(q,k)$ takes into account the remaining dependence with respect to the absolute values of momenta of the different terms in the expression (3.27).
Hence, the angular integration in $P_{11}^{(5)}$ gives, consistently with [49]:

$$P_{11}^{(5)}(k,\eta) = -\frac{e^{2\eta}}{1008k^3\pi^2} \int_0^\infty \frac{dq}{q^3} \Bigg\{ 2kq\left(-6k^6+79k^4q^2-50k^2q^4+21q^6\right) + \\ + 3\left(2k^2+7q^2\right)\left(k^2-q^2\right)^3 \ln\left[\frac{k+q}{|k-q|}\right] \Bigg\} P^0(q)P^0(k). \tag{3.29}$$

The final result for the fully non-linear matter power spectrum evolved at final equal final time η descends, according to Eq.(3.10), summing the tree level result with the terms (3.20) and (3.29), to reach:

$$P_{11}^{1-loop}(k,\eta) = P^0(k) + \int_0^\infty dq \Bigg\{ \frac{k^4e^{2\eta}}{392\pi^2} \int_{-1}^{1} dx \, \frac{\left(7kx+q\left(3-10x^2\right)\right)^2}{\left(k^2-2kqx+q^2\right)^2} P^0\left(k\sqrt{1+\frac{q^2}{k^2}-2\frac{q}{k}x}\right) + \\ - \frac{e^{2\eta}}{1008k^3q^3\pi^2} \Bigg[2kq\left(-6k^6+79k^4q^2-50k^2q^4+21q^6\right) + \\ + 3\left(2k^2+7q^2\right)\left(k^2-q^2\right)^3 \ln\left[\frac{k+q}{|k-q|}\right] \Bigg] P^0(k) \Bigg\} P^0(q). \tag{3.30}$$

3.3.2 The IR limit of the linear kernel.

To deduce the result, the program is to perform the functional derivative of the one loop evolved power spectrum P_{11}^{1-loop} with respect to the primordial one, to compute the linear kernel at tree

level, and then to perform the limit of this object to get the result.
As it is clear that the derivative of the tree level part of P_{11}^{1-loop} hasn't any importance, being disconnected, as we can see in Fig.(3.2), and totally irrelevant in both the IR and UV limits, as it can be understood from Eq.(3.9), actually the evaluation of the limits hides some care, mainly for two reasons.
The first relies on the functional derivative: renaming the loop momentum as $\mathbf{Q}$, the associated cosine between the evolved momentum $\mathbf{k}$ and $\mathbf{Q}$ with X and writing only the needed functional dependences, thanks to the homogeneity and isotropy accorded to our Universe, the expression (3.3) for the connected tree level kernel (or generally when $k \neq q$) is equivalent to:

$$
\begin{aligned}
K_{11}^{tree,conn}(k,q;\eta) &= q\frac{\delta}{\delta P(q)}\int_0^\infty dQ\left\{\int_{-1}^1 dX\,\Big[\cdots\Big]P^0(Q)P^0\big(|\mathbf{k}-\mathbf{Q}|\big)+\Big[\cdots\Big]P^0(Q)P^0(k)\right\}= \\
&= q\int_0^\infty dQ\left\{\int_{-1}^1 dX\,\Big[\cdots\Big]\Big(\delta(q-Q)P^0\big(|\mathbf{k}-\mathbf{Q}|\big)+P^0(Q)\delta(q-|\mathbf{k}-\mathbf{Q}|)\Big)+\right. \\
&\qquad\left.+\Big[\cdots\Big]\delta(q-Q)P^0(k)\right\}= \\
&= q\left\{2\int_{-1}^1 dx\,\Big[\cdots\Big]P^0\big(|\mathbf{k}-\mathbf{q}|\big)+\Big[\cdots\Big]P^0(k)\right\}.
\end{aligned}
\tag{3.31}
$$

The second arises from the presence of the angular dependence in the initial power spectrum in the first constituent of $K_{11}^{tree,conn}$, coming from $P_{11}^{(2)}$; the issue is solved by a Taylor expansion in the small parameter $t=\frac{q}{k}$ around $t_0=0$, consistently with the IR limit, namely:

$$
\begin{aligned}
P^0\left(k\sqrt{1-2tx+t^2}\right) &= P^0(K)\approx P^0(k)+\left[\frac{\partial P^0(K)}{\partial K}\frac{k(t-x)}{\sqrt{1-2tx+t^2}}\right]\Bigg|_{t_0=0}t+ \\
&+\frac{1}{2}\left[\frac{\partial^2P^0(K)}{\partial K^2}\left(\frac{k(t-x)}{\sqrt{1-2tx+t^2}}\right)^2+\frac{\partial P^0(K)}{\partial K}\frac{1-\frac{(x-t)^2}{1-2tx+t^2}}{\sqrt{1-2tx+t^2}}k\right]\Bigg|_{t_0=0}t^2+\mathcal{O}(t^3)= \\
&= P^0(k)-\frac{\partial P^0(k)}{\partial k}kxt+\frac{1}{2}\left[\frac{\partial P^0(k)}{\partial k}k-\frac{\partial P^0(k)}{\partial k}kx^2+\frac{\partial^2P^0(k)}{\partial k^2}k^2x^2\right]t^2+\mathcal{O}(t^3)\equiv \\
&\equiv P^0(k)-xq\dot{P}^0(k)+\frac{1}{2}\left[\frac{q^2}{k}\dot{P}^0(k)-\frac{q^2}{k}x^2\dot{P}^0(k)+q^2x^2\ddot{P}^0(k)\right]+\mathcal{O}\left(\frac{q^3}{k^3}\right),
\end{aligned}
\tag{3.32}
$$

that allows the angular integration also of this constituent of the kernel. Beside the elementary integral written previously in (3.28), looking to the above expansion and (3.20) we see that for this piece other integrals appear, which we report in the following:

$$
\begin{aligned}
&\int_{-1}^1 dx\,\frac{1}{(k^2+q^2-2kqx)^2}=\frac{1}{2kq(k^2+q^2-2kqx)}\Bigg|_{-1}^1=\frac{2}{(k-q)^2(k+q)^2}, \\
&\int_{-1}^1 dx\,\frac{x}{(k^2+q^2-2kqx)}=\int_{-1}^1 dx\left[-\frac{1}{2kq}+\frac{\frac{k^2+q^2}{2kq}}{k^2+q^2-2kq}\right]=-\frac{1}{kq}+\frac{k^2+q^2}{2k^2q^2}\ln\left[\frac{k+q}{|k-q|}\right],
\end{aligned}
\tag{3.33}
$$

$$\int_{-1}^{1} dx \, \frac{x}{(k^2+q^2-2kqx)^2} = \frac{1}{2k^2q^2}\int_{-1}^{1} dx \left[\frac{1}{x-\frac{k^2+q^2}{2kq}} + \frac{\frac{k^2+q^2}{2kq}}{\left(x-\frac{k^2+q^2}{2kq}\right)^2} \right] =$$
$$= \frac{k^2+q^2}{kq(k-q)^2(k+q)^2} - \frac{1}{2k^2q^2}\ln\left[\frac{k+q}{|k-q|}\right],$$
$$\int_{-1}^{1} dx \, \frac{x^2}{(k^2+q^2-2kqx)} = \frac{1}{2kq}\int_{-1}^{1} dx \left[-x - \frac{k^2+q^2}{2kq} + \frac{\left(\frac{k^2+q^2}{2kq}\right)^2}{(k^2+q^2-2kq)} \right] = \tag{3.34}$$
$$= -\frac{k^2+q^2}{2k^2q^2} + \frac{\left(k^2+q^2\right)^2}{4k^3q^3}\ln\left[\frac{k+q}{|k-q|}\right],$$
$$\int_{-1}^{1} dx \, \frac{x^2}{(k^2+q^2-2kqx)^2} = \frac{k^4+q^4}{k^2q^2(k-q)^2(k+q)^2} - \frac{\left(k^2+q^2\right)}{2k^3q^3}\ln\left[\frac{k+q}{|k-q|}\right]$$

which have to be multiplied by a suitable function $C(q,k)$ for each term of the integral, as already said for (3.28).
Recalling that the one loop matter power spectrum is a sum of two constituents, the same happens for the tree level connected kernel function. Adopting a notation analogous to the former (ignoring the superscript for connection), the latter is written as:

$$K_{11}^{tree}(k,q;\eta) = K_{11}^{(2)}(k,q;\eta) + K_{11}^{(5)}(k,q;\eta), \tag{3.35}$$

and according to the result in (3.31), using the above integrals and (3.20) with the expansion (3.32), for $K_{11}^{(2)}$ we get:

$$\begin{aligned} K_{11}^{(2)}(k,q;\eta) =& \frac{e^{2\eta}}{9408\pi^2k^4q^2}\Bigg\{ 8k^3\Bigg[-36k^5q + 10k^3q^3 + 300kq^5 + 3\big(6k^6 + 29k^4q^2 + 15k^2q^4 - 50q^6\big) \times \\ & \times \ln\Big[\frac{k+q}{|k-q|}\Big]\Bigg] P^0(k) + \Bigg[108k^9q + 738k^7q^3 - 890k^5q^5 - 930k^3q^7 - 450kq^9 + \\ & - 3\left(18k^{10} + 117k^8q^2 + 160k^6q^4 - 90k^4q^6 - 130k^2q^8 - 75q^{10}\right)\ln\Big[\frac{k+q}{|k-q|}\Big]\Bigg]\dot{P}^0(k) + \\ & + k\Bigg[-2kq\left(6k^8 + 77k^6q^2 + 25k^4q^4 - 315k^2q^6 - 225q^8\right) + \\ & + 3\left(2k^{10} + 25k^8q^2 + 78k^6q^4 + 50k^4q^6 - 80k^2q^8 - 75q^{10}\right)\ln\Big[\frac{k+q}{|k-q|}\Big]\Bigg]\ddot{P}^0(k)\Bigg\}, \end{aligned} \tag{3.36}$$

while the second is straightforward looking at (3.29):

$$\begin{aligned} K_{11}^{(5)}(k,q;\eta) = -\frac{e^{2\eta}}{1008\pi^2k^3q^2}\Bigg\{ & 2kq\left(-6k^6 + 79k^4q^2 - 50k^2q^4 + 21q^6\right) + \\ & + 3\left(2k^2+7q^2\right)\left(k^2-q^2\right)^3\ln\left[\frac{k+q}{|k-q|}\right]\Bigg\}P^0(k). \end{aligned} \tag{3.37}$$

At last, after having prepared all the ingredients, we are able to afford the last step, namely to take the IR limit of the kernel function. Looking at the above expressions, we can understand that this means taking the IR limit of the logarithms that appear in them and finally to make some considerations on what is suppressed or not. Remembering that for $|z| < 1$:

$$\ln(1-z) = -\sum_{n=1}^{\infty} \frac{z^n}{n} \qquad \text{and} \qquad \ln(1+z) = \sum_{n=1}^{\infty} (-1)^{n+1} \frac{z^n}{n}, \tag{3.38}$$

then:

$$\begin{aligned} \lim_{\frac{q}{k}\to 0} \ln\left[\frac{k+q}{|k-q|}\right] &= \lim_{\frac{q}{k}\to 0} \ln\left[\frac{k+q}{k}\frac{k}{k-q}\right] = \lim_{\frac{q}{k}\to 0} \ln\left[\frac{1+\frac{q}{k}}{1-\frac{q}{k}}\right] = \\ &= \lim_{\frac{q}{k}\to 0} \left(\ln\left[1+\frac{q}{k}\right] - \ln\left[1-\frac{q}{k}\right]\right) \approx 2\frac{q}{k} + \frac{2}{3}\frac{q^3}{k^3} + \frac{2}{5}\frac{q^5}{k^5} + \mathcal{O}\left(\frac{q^7}{k^7}\right). \end{aligned} \tag{3.39}$$

In the following, we are using the truncation to the seventh order, in order to provide stability to the coefficients of the relevant terms. In particular, with the expression (3.32) for $P(p)$, in this limit they are those in $k^2 q$ and q^3, kq^3, k^2q^3, since the remaining are of the type $\frac{q^m}{k^n}$, with $m > n$ and both positive, or q^r, with $r \geq 5$, and therefore strongly suppressed. This is clear if we imagine, as it is often done, to fix a particular value of k and to ask for the behaviour of the kernel at IR q, when it is very small. Ignoring the highly suppressed terms, the IR limit gives:

$$\begin{aligned} K_{11,IR}^{tree}(k,q;\eta) = e^{2\eta}\Bigg[&\frac{k^2 q}{6\pi^2}P^0(k) + \frac{569q^3}{1470\pi^2}P^0(k) - \frac{47kq^3}{210\pi^2}\dot{P}^0(k) + \frac{k^2q^3}{20\pi^2}\ddot{P}^0(k) + \\ &- \frac{k^2q}{6\pi^2}P^0(k) + \frac{58q^3}{315\pi^2}P^0(k)\Bigg], \end{aligned} \tag{3.40}$$

where the contributions at the first line come from $K_{11}^{(2)}$, while those at the second one from $K_{11}^{(5)}$. We now see an important cancellation phenomenon between the two pieces: the term in $k^2 q$ coming from the first exactly cancel with the one coming from the second, eliminating what would otherwise be the dominant term of the limit. At power spectrum level, it is clear that this means that the contributions in $\left(\frac{\mathbf{k}\cdot\mathbf{q}}{q^2}\right)^2$ cancel between each other, as a consequence of the galilean invariance of the dynamics, thus leaving the leading infrared dependence, at the order of q^3, in the LRF.

However, it is possible to extend this crucial result even beyond the one loop order, which we have computed explicitly so far. Indeed, considering for generality different final times η and η', the trispectrum appearing in the connected part of the definition of the LRF (3.7):

$$\langle \phi_a(\mathbf{k},\eta)\phi_b(-\mathbf{k},\eta')\chi_c(-\mathbf{q},\eta_{in})\chi_d(\mathbf{q},\eta_{in})\rangle' \, u_c u_d, \tag{3.41}$$

with the relation:

$$\chi_d(\mathbf{q},\eta_{in})u_d u_c = \frac{i}{P^0(q)}\phi_c(\mathbf{q},\eta_{in}), \tag{3.42}$$

becomes:

$$\frac{1}{P^0(q)^2}\langle \phi_a(\mathbf{k},\eta)\phi_b(-\mathbf{k},\eta')\phi(-\mathbf{q},\eta_{in})\phi(\mathbf{q}.\eta_{in})\rangle' \tag{3.43}$$

In the soft limit ($\frac{q}{k} \to 0$), we can apply two times, one for each soft leg, the relation (2.116), specified at first for the trispectrum and then for the bispectrum, leading the above expression to become:

$$-\left(\frac{\mathbf{q}\cdot\mathbf{k}}{q^2}\right)^2 \left(e^{\eta} - e^{\eta'}\right)^2 P_{ab}(k,\eta,\eta') + \mathcal{O}(q^0). \tag{3.44}$$

Once multiplied for q^3 as according to (3.7), it gives the IR limit of the LFR. With $\mathcal{O}(q^0)$ we indicate terms which do not have the $\left(\frac{k}{q}\right)^2$ enhancement and which, in general, do not vanish for $\eta = \eta'$ and are not proportional to the non-linear power spectrum $P_{ab}(k,\eta,\eta')$: their one loop contributions give the non-vanishing terms of the IR limit of the LRF. On the other hand, the first is the the term that, once multiplied for q^3, gives the $k^2 q$ contribution that, at equal time, vanishes.
We close this section giving the IR limit of the LRF at tree level, from Eq.(3.40):

$$K^{tree}_{11,IR}(k,q;\eta) = e^{2\eta}\left[\frac{2519P^0(k)}{4410\pi^2} - \frac{47k\dot{P}^0(k)}{210\pi^2} + \frac{k^2\ddot{P}^0(k)}{20\pi^2}\right]q^3 = \\ = e^{2\eta}\frac{5038P^0(k) - 1974k\dot{P}^0(k) + 441k^2\ddot{P}^0(k)}{8820\pi^2}q^3, \tag{3.45}$$

meaning that the linear kernel function vanishes as q^3 in the IR limit.

3.3.3 The UV limit of the linear kernel.

The UV limit, namely when $\frac{q}{k} \to \infty$, is somewhat simpler than the previous one.
At first, in this case we need to handle the same logarithm present in (3.36) and (3.37), but expanded in the opposite limit than in (3.46):

$$\lim_{\frac{k}{q}\to 0} \ln\left[\frac{k+q}{|k-q|}\right] = \lim_{\frac{k}{q}\to 0} \ln\left[\frac{k+q}{q}\frac{q}{q-k}\right] = \lim_{\frac{k}{q}\to 0} \ln\left[\frac{1+\frac{k}{q}}{1-\frac{k}{q}}\right] \approx 2\frac{k}{q} + \frac{2}{3}\frac{k^3}{q^3} + \frac{2}{5}\frac{k^5}{q^5} + \mathcal{O}\left(\frac{k^7}{q^7}\right), \tag{3.46}$$

that we use also in this case at the seventh order for stability.
The great difference is that now $K^{(2)}_{11}$ doesn't contribute to the result. Indeed, we bring to the attention that we have to expand $P(p)$ in the context of the present limit, thus here the expansion (3.32) is no more correct and by consequence also the form (3.36) cannot be used there: thus, even taking $P(|\mathbf{k}-\mathbf{q}|) \approx P^0(q)$ and evaluating the angular integral in (3.20), we obtain in place of (3.36) the expression:

$$\tilde{K}^{(2)}_{11}(k,q;\eta) = \frac{e^{2\eta}}{1176\pi^2 kq^2}\left[-36k^5q+10k^3q^3+300kq^5+3\left(6k^6+29k^4q^2+15k^2q^4-50q^6\right)\ln\left[\frac{k+q}{|k-q|}\right]\right]P^0(q), \tag{3.47}$$

which using the above expansion gives the sum between $\frac{9e^{2\eta}}{98\pi^2}\frac{k^4}{q}P^0(q)$ and terms suppressed as $\frac{k^m}{q^n}$, with $m-n>3$ and both positive.
Hence, only the second contribution to the kernel remains, being the same found before in (3.37) and coming from the last two graphs of the one loop perturbative series of the evolved power spectrum in Fig.(3.4). Using the UV Taylor development for the logarithm we get the limit:

$$K^{tree}_{11,UV}(k,q;\eta) = -\frac{61e^{2\eta}}{630\pi^2}P^0(k)k^2q, \tag{3.48}$$

the other terms being suppressed as $\frac{k^m}{q^n}$, with $m>n$ and both positive.

3.3.4 Numerical results.

Without any need for the above analytical approximations in the IR or UV limits, by the direct use of the expressions (3.31) and (3.30) for the linear kernel and the matter power spectrum at one loop, with a software as Wolfram Mathematica we can get numerical results for the linear kernel at tree level at all scales. Calculations are performed for the model that better fits our Universe, that is a flat ΛCDM universe with cosmological parameters fixed according to the Planck Mission results [21], reported in Table (3.1).

Parameter	Value
h	0.6731 ± 0.0096
$\Omega_m h^2$	0.1426 ± 0.0020
$\Omega_b h^2$	0.02222 ± 0.00023
n_s	0.9655 ± 0.0062
σ_8	0.829 ± 0.014
w	$-1.54^{+0.62}_{-0.50}$
$10^9 A_s$	$2.198^{+0.076}_{-0.085}$
τ	0.078 ± 0.019

Table 3.1: The cosmological parameters as constrained by Planck.

These parameters are essentially used to obtain the primordial matter power spectrum, that we generated by means of the CAMB Web Interface[1] choosing as primordial time the redshift $z_{in} = 100$. We assume that the analytic formula used for the linear kernel is intended to be extended and valid for this model by the simple change of the time parameter η, done by means of the calculation of the right growth factor for the case, without changing the momentum dependence of any Feynman rule, as asserted in Section 2.1.

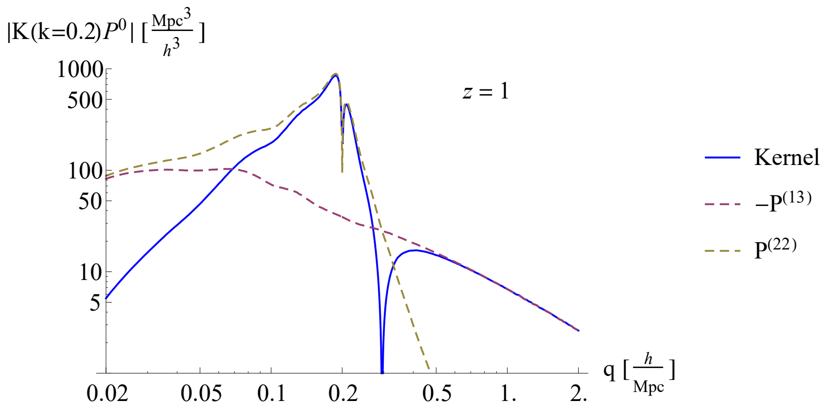

Figure 3.7: Kernel function as predicted at the lowest order of standard perturbation theory at $k = 0.2\,h\text{Mpc}^{-1}$ at $z = 1$. The dashed curves denotate the contributions coming from the graphs without and with the initial power spectrum in the middle, denoted in literature as P^{13} and P^{22}, respectively. Notice also that the first one has been multiplied by (-1)

As we can see from Fig.(3.7), the result is rather compatible with the one from N-body simulations in Fig.(3.1), even if the parameters are slightly different, but two observations are in order

[1]The Code for Anisotropies in the Microwave Background CAMB is an application that computes cosmic microwave background (CMB) spectra given a set of input cosmological parameters, written by A. Lewis and A. Challinor and downloadable from `http://camb.info/`; CAMB Web Interface is a web-based interface to CAMB provided by the LAMBDA (Legacy Archive for Microwave Background Data Analysis) NASA project, available at `http://lambda.gsfc.nasa.gov/`. For further information, see [50, 51, 52, 53].

[14]. The first is that at the IR limit our numerical results agree with that from simulations: we note that the q^3 dependence of the kernel is confirmed by simulations and in particular the complete numerical dependence too, because it is straightforward to show that for redshifts equal or lower than this, the SPT and the simulated non-linear power spectra agree with an error under the one percent; this can be explained by means of the strong galilean invariance that assures such a behaviour, so that even for very different cosmological models, as the Einstein-de Sitter one, this dependence continues to hold. The second is that the situation is very different in the UV region: here, galilean invariance does not provide any clues and moreover standard perturbative approaches are expected to fail at small scales. Indeed, we can see that the LRF measured from simulations is damped compared to the perturbative results, even at higher orders [14]. In particular, our numerical results show that in this region there would be a linearly decreasing behaviour, in the same way we find in the EdS case, and higher orders results suggests an even stronger decay, increasing with time; on the other hand, simulations show that the behaviour is strongly damped, suggesting such an anomaly to be genuinely non-perturbative.
We end the section showing two linear kernels as obtained by the one loop matter power spectrum for two different redshifts.

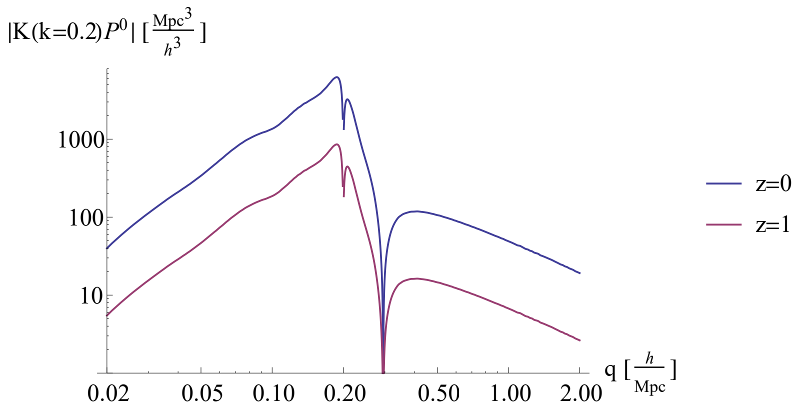

Figure 3.8: Lowest order linear kernel functions at $k = 0.2\, h\mathrm{Mpc}^{-1}$ at $z = 0$ and $z = 1$.

Chapter 4

A numerical analysis for the mildly non-linear regime.

Aim of the present chapter is to analyse the evolved non-linear power spectrum in the range of large scales presenting slight but clear effects of non-linearities, from a non-perturbative point of view. In particular, we will make use of the numerical RegPT code, based on the Γ-expansion approximation scheme, to evolve the primordial power spectrum, that we generate from CAMB, at recent times, pointing out its region of validity. We will then show that the Γ-expansion fails to fulfil the galilean constraint on the IR behaviour of the LRF obtained in the previous chapter and we will show how to correct for it. The need for such a correction will be justified, and its outcome tested, by means of the $\mathrm{FrankenEmu}$ cosmic emulator, a code using nested N-body simulations to generate the non-linear evolved power spectrum.
The chapter consists of two sections: in the first we thought it is right to give a brief insight into the theoretical basis of the RegPT code, the second we will present numerical results without any further delay.

4.1 The Γ-expansion.

In order to explore the theoretical core of the RegPT code, we briefly introduce the Γ-expansion method, following quite closely the literature in [8, 3, 54, 55].
We start recasting the perturbative approach to cosmological dynamics in a more traditional way in Cosmology than the path integral used in the first chapter. In particular, neglecting initial vorticity, the solution in a generic cosmological model for the linearised system of the dynamical equation (2.11) takes the form [38]:

$$\begin{aligned}\delta(\mathbf{x},\tau) &= D^{+}(\tau)A(\mathbf{x}) + D^{-}(\tau)B(\mathbf{x})\\ \theta(\mathbf{x},\tau) &= -H(\tau)[f(\Omega_m,\Omega_\Lambda,\tau)A(\mathbf{x}) + g(\Omega_m,\Omega_\Lambda,\tau)B(\mathbf{x})],\end{aligned} \tag{4.1}$$

where Ω_m, Ω_Λ are the density parameters of matter and the cosmological constant respectively, $A(\mathbf{x}), B(\mathbf{x})$ are spatial functions determined by the initial spatial configuration, $D^{+}(\tau), D^{-}(\tau)$ correspond to the fastest and the slowest growing mode respectively, while f and g are:

$$f(\Omega_m,\Omega_\Lambda,\tau) = \frac{1}{H(\tau)}\frac{\delta D^{+}(\tau)}{\delta\tau} \quad \text{and} \quad g(\Omega_m,\Omega_\Lambda,\tau) = \frac{1}{H(\tau)}\frac{\delta D^{-}(\tau)}{\delta\tau}. \tag{4.2}$$

If we consider a matter dominated universe (characterized by $\Omega_m = 1$ and $\Omega_\Lambda = 0$), so that it simply results:

$$D^+(\tau) = a(\tau) \qquad \text{and} \qquad D^-(\tau) = a^{-\frac{3}{2}}(\tau), \tag{4.3}$$

with the growing mode proportional to the scale factor. We will refer to $D^+(\tau)$ as the linear growth factor.

The assumption of perturbation theory is the possibility to expand the density and the velocity fields about the linear solutions, treating the variance of the linear fluctuations as a small parameter. Looking at the form of the above linear solutions, we understand that these have the nice form of an initial field rescaled by a time variable. In formulas, in Fourier space the perturbative solution to the non-linear dynamical system (2.15) is thus given by:

$$\begin{aligned} \delta(\mathbf{k},\tau) &= \sum_{n=1}^{\infty} \delta^{(n)}(\mathbf{k},\tau) = \sum_{n=1}^{\infty} a^n(\tau)\delta_n(\mathbf{k}) \quad \text{and} \\ \theta(\mathbf{k},\tau) &= \sum_{n=1}^{\infty} \theta^{(n)}(\mathbf{k},\tau) = -H(\tau)\sum_{n=1}^{\infty} a^n(\tau)\theta_n(\mathbf{k}), \end{aligned} \tag{4.4}$$

where we consider only the fastest growing mode, while n indicate the power of the initial fields entering in a given term of the perturbative sum. The linear (growing) solution is recovered when $n = 1$: at this stage indeed $\delta^{(1)}(\mathbf{k},\tau) = a(\tau)\delta_1(\mathbf{k})$ completely characterizes the solution because the linearised continuity equation leads to $\theta_1(\mathbf{k}) = \delta_1(\mathbf{k})$.

According to [3], assumed the most physical initial conditions, given when $\delta_0(\mathbf{k}, \eta = 0)$ and $\theta_0(\mathbf{k}, \eta = 0)$ are proportional random fields, in terms of the initial linear fluctuations $\delta_0(\mathbf{q})$ the equations of motion in (2.15) univocally determine the perturbative modes $\delta_n(\mathbf{k})$ and $\theta_n(\mathbf{k})$ in the form:

$$\begin{aligned} \delta_n(\mathbf{k}) &= \int d\mathbf{q}_1 \cdots \int d\mathbf{q}_n\, \delta(\mathbf{k} - \Sigma_{i=1}^n \mathbf{q}_i) F_n(\mathbf{q}_1, \ldots, \mathbf{q}_n)\, \delta_0(\mathbf{q}_1)\cdots\delta_0(\mathbf{q}_n), \\ \theta_n(\mathbf{k}) &= \int d\mathbf{q}_1 \cdots \int d\mathbf{q}_n\, \delta(\mathbf{k} - \Sigma_{i=1}^n \mathbf{q}_i) G_n(\mathbf{q}_1, \ldots, \mathbf{q}_n)\, \delta_0(\mathbf{q}_1)\cdots\delta_0(\mathbf{q}_n), \end{aligned} \tag{4.5}$$

where F_n and G_n are the kernels of the perturbative development. In the compact form, we organized the two field in the doublet (2.19) and we recast the system (2.15) in the equation (2.20). Analogously to what done until now, by means of the formal expression of ϕ_a given in (2.34) and taken the initial conditions $\phi_a(\mathbf{q}, \eta = 0) = \varphi_a(\mathbf{q}) = u_a\delta_0(\mathbf{q}, \eta = 0)$, we look for a perturbative solution of the form:

$$\phi(\mathbf{k},\eta) = \sum_{n=1}^{\infty} \phi_a^{(n)}(\mathbf{k},\eta), \tag{4.6}$$

with:

$$\begin{aligned} \phi_a^{(n)}(\mathbf{k},\eta) &= \int d\mathbf{q}_1 \cdots \int d\mathbf{q}_n\, \delta(\mathbf{k} - \Sigma_{i=1}^n \mathbf{q}_i)\mathcal{F}^{(n)}_{ac_1\cdots c_n}(\mathbf{q}_1, \ldots, \mathbf{q}_n, \eta)\varphi_{c_1}(\mathbf{q}_1)\cdots\varphi_{c_n}(\mathbf{q}_n) = \\ &= \int d\mathbf{q}_1 \cdots \int d\mathbf{q}_n\, \delta(\mathbf{k} - \Sigma_{i=1}^n \mathbf{q}_i)\mathcal{F}^{(n)}_{ac_1\cdots c_n}(\mathbf{q}_1, \ldots, \mathbf{q}_n, \eta)u_{c_1}\cdots u_{c_n}\delta_0(\mathbf{q}_1)\cdots\delta_0(\mathbf{q}_n) = \\ &= \int d\mathbf{q}_1 \cdots \int d\mathbf{q}_n\, \delta(\mathbf{k} - \Sigma_{i=1}^n \mathbf{q}_i)\mathcal{F}^{(n)}_{a}(\mathbf{q}_1, \ldots, \mathbf{q}_n, \eta)\, \delta_0(\mathbf{q}_1)\cdots\delta_0(\mathbf{q}_n), \end{aligned} \tag{4.7}$$

that, inserted into Eq.(2.20), give the following recursion relation satisfied by the kernels $\mathcal{F}_a^{(n)}$:

$$\mathcal{F}_a^{(n)}(\mathbf{q}_1,\ldots,\mathbf{q}_n,\eta)\delta(\mathbf{k}-\Sigma_{i=1}^n\mathbf{q}_i) =$$
$$= \sum_{m=1}^{n}\int_0^\eta d\eta' g_{ab}(\eta-\eta')e^{\eta'}\gamma_{bcd}(\mathbf{k},\Sigma_{i=1}^m\mathbf{q}_i,\Sigma_{i=m+1}^n\mathbf{q}_i))\mathcal{F}_c^{(m)}(\Sigma_{i=1}^m\mathbf{q}_i,\eta')\mathcal{F}_d^{(n-m)}(\Sigma_{i=m+1}^n\mathbf{q}_i,\eta'), \tag{4.8}$$

that, comparing with the expansion (4.7), should be symmetrised with respect to their arguments. The perturbative term corresponding to $n=1$ coincides with the solution of Eq.(2.20) at lineal level, that is the first term of the full solution for ϕ_a as written in Eq.(2.34), therefore $\mathcal{F}_a^{(1)}(\eta) = g_{ab}(\eta)u_b$. It is worth noting that in this conditions Eq.(4.8) gives the full time dependence of the perturbative solution, while when the initial conditions time is set at the infinite past rather than at zero only the fastest growing mode survives and $\mathcal{F}_a = a^n e^{-\eta}(F_n, G_n) = e^{(n-1)\eta}(F_n,G_n) = e^{(n-1)\eta}F_{a,sym}^{(n)}$. This is the reason for the choice for time we took in the previous chapter.

The solutions for the various kernels give the analytical expressions for the $\phi_a^{(n)}$ fields, but for increasing n they quickly become very difficult to handle; furthermore, they contain much redundant information: as it can be seen from the recursive relation above, they can be all built with the use of two building blocks, the linear propagator and the interaction vertex. Thus, the perturbative expansion for ϕ_a can be obtained by that two objects and the initial field $\varphi_a(\mathbf{q})$, as we have seen when we presented the graphical representation of the perturbative series.

Our first step in introducing the Γ-expansion, is to go back to an object we have already discussed, namely the evolved full non-linear propagator, that is defined in the traditional fashion as:

$$(2\pi)^3 G_{ab}(k,\eta)\delta(\mathbf{k}-\mathbf{k}') = \left\langle \frac{\delta\phi_a(\mathbf{k},\eta)}{\delta\varphi_b(\mathbf{k}')} \right\rangle, \tag{4.9}$$

that, with the help of Eq.(2.34) and Eq.(4.7), can be rewritten as:

$$G_{ab}(k,\eta) = g_{ab}(\eta) + \sum_{n=2}^{\infty}\left\langle \frac{\delta\phi_a^{(n)}(\mathbf{k},\eta)}{\delta\varphi_b(\mathbf{k}')} \right\rangle. \tag{4.10}$$

Deriving with respect to the initial field φ_b each term of the expansion of ϕ_a, that is eliminating from them an initial field in all the possible ways, and taking the ensamble average, that is gluing the remaining initial field lines together with an initial power spectrum (with gaussian initial conditions, only the terms of the perturbative expansion of ϕ_a with an odd number of initial fields play a role, because derived are the only non-vanishing, so that the pairing doesn't leave any initial field line free) gives the same result one gets using our usual Feynman rules, whose first loop diagram is shown in Fig.(3.2).

An alternative to the standard perturbation theory framework is the possibility to reorganise the perturbative expansion by means of non-perturbative quantities able to improve the behaviour of higher-order corrections and the convergence of the resulting series: this new approach is the Γ-expansion, whose building blocks are the multi-point propagators [54]. The $(p+1)$-point propagator, denoted by $\Gamma^{(p)}$, is defined as:

$$\frac{1}{p!}\left\langle \frac{\delta^p\phi_a(\mathbf{k},\eta)}{\delta\varphi_{c_1}(\mathbf{k}_1)\cdots\delta\varphi_{c_p}(\mathbf{k}_p)} \right\rangle = (2\pi)^3\delta(\mathbf{k}-\Sigma_{i=1}^p\mathbf{k}_i)\Gamma_{ac_1\cdots c_p}^{(p)}(\mathbf{k}_1,\ldots,\mathbf{k}_p;\eta). \tag{4.11}$$

It can be seen that the above definition is the generalization of the non-linear propagator as written in (4.9): of course, it is the 2-point propagator $\Gamma_{ab}^{(1)} = G_{ab}$. By this definition and the use of the expansion (4.6) and the expansion in kernels (4.7) we can find in principle all the multi-point propagators. For example the 3-point propagator $\Gamma^{(2)}_{abc}$ is written:

$$\Gamma^{(2)}_{abc}(\mathbf{k}_1,\mathbf{k}_2;\eta)=\sum_{j=0}^{\infty}\binom{2j+2}{j}(2j-1)!!\int d\mathbf{q}_1\cdots d\mathbf{q}_j\,\mathcal{F}^{(2j+2)}_{abc}(\mathbf{k}_1,\mathbf{k}_2,\mathbf{q}_1,-\mathbf{q}_1,\cdots,-\mathbf{q}_j,\eta)P^0(q_1)\cdots P^0(q_j). \tag{4.12}$$

Indeed, inserted (4.6) and (4.7) in the definition, we can rearrange the resulting sum in such a way that each term of it involves the element $\phi^{(2j+2)}_a$, clearly expanded in kernels and functionally derived leaving $2j$ initial fields and the factor, say, $\delta(\mathbf{k}_1-\mathbf{q_z})\delta(\mathbf{k}_2-\mathbf{q_w})$; then, using the $\varphi_a=u_a\delta_0$ initial conditions we are left with j initial power spectra (due to the assumed gaussian initial conditions there isn't any free initial field leg uncoupled, that's why we could limit to the $\phi^{(2j+2)}_a$ terms) and other j Dirac's delta of the kind $\delta(\mathbf{q}_m+\mathbf{q}_n)$: once integrated, the first two deltas introduce in the momentum conservation delta of the integrand the dependence on $\mathbf{k}_{1,2}$, while the other cancel all the other $\mathbf{q}$-dependences in the same delta, that can now be simplified with the one at the right hand side of the definition (4.11), specified for the present case. The indices b and c arises because the derivation eliminated u_b and u_c, fact denoted with a bar, while the factorials terms represents respectively all the possible ways to perform the derivatives and the pairing between initial fields. From all that we have the above result.
We now discuss the relationship between multi-point propagators and non-linear corrections to the power spectrum, showing that the power spectrum P_{ab} can be reconstructed by gluing together $\Gamma^{(p)}$ contributions.
First of all, we can write the power spectrum as:

$$(2\pi)^3\delta(\mathbf{k}_1+\mathbf{k}_2)P_{ab}(k_1)=\langle\phi_a(\mathbf{k}_1,\eta)\phi_b(\mathbf{k}_2,\eta)\rangle=\sum_{n_1n_2}\langle\phi^{(n_1)}_a(\mathbf{k}_1,\eta)\phi^{(n_2)}_b(\mathbf{k}_2,\eta)\rangle\,. \tag{4.13}$$

Following the expansion of ϕ_a in (4.7), for each given choice of n_1 and n_2 we have to calculate a specific ensemble average of n_1+n_2 initial fields φ_a. Assuming gaussian initial conditions, each ensemble average is a sum of various terms, each of them turns to be the product of two-points correlators. Each term constituting a given average can be labelled with three indices r,s,t, where r is the number of connected pairs within the first n_1 fields φ_{c_i} (the two fields both belong to $\phi^{(n_1)}_a$), s is the number of connected pairs within the last n_2 fields (the two fields both belong to $\phi^{(n_1)}_a$) and t is the number of mixed pairs, connecting fields from the first n_1 and the last n_2. Obviously one has $n_1=2r+t$ and $n_2=2s+t$. Among all the ensemble averages appearing for each given choice of n_1 and n_2, written as:

$$\langle\varphi(\mathbf{q}_{c_1})\cdots\varphi(\mathbf{q}_{c_{n_1}});\varphi(\mathbf{q}'_{d_1})\cdots\varphi(\mathbf{q}'_{d_{n_2}})\rangle\,, \tag{4.14}$$

we denote the one corresponding to a given r,s,t triplet with:

$$\langle\varphi(\mathbf{q}_{c_1})\cdots\varphi(\mathbf{q}_{c_{2r+t}});\varphi(\mathbf{q}'_{d_1})\cdots\varphi(\mathbf{q}'_{d_{2s+t}})\rangle_{r,s,t}\,. \tag{4.15}$$

Hence, using the ϕ_a expansion in kernels (4.7) the power spectrum becomes:

$$\begin{aligned}\langle\phi_a(\mathbf{k}_1,\eta)\phi_b(\mathbf{k}_2,\eta)\rangle=&\sum_{r,s,t}\int d\mathbf{q}_1\cdots d\mathbf{q}_{2r+t}\int d\mathbf{q}'_1\cdots d\mathbf{q}'_{2s+t}\Big[\delta(\mathbf{k}_1-\Sigma_{i=1}^{2r+t}\mathbf{q}_i)\delta(\mathbf{k}_2-\Sigma_{i=1}^{2s+t}\mathbf{q}'_i)\times\\&\times\mathcal{F}^{(2r+t)}_{ac_1\cdots c_{2r+t}}(\mathbf{q}_1,\cdots,\mathbf{q}_{2r+t};\eta)\mathcal{F}^{(2s+t)}_{ad_1\cdots d_{2s+t}}(\mathbf{q}'_1,\cdots,\mathbf{q}'_{2s+t};\eta)\times\\&\times\langle\varphi_{c_1}(\mathbf{q}_1)\cdots\varphi_{c_{2r+t}}(\mathbf{q}_{2r+t});\varphi_{d_1}(\mathbf{q}'_1)\cdots\varphi_{d_{2s+t}}(\mathbf{q}'_{2s+t})\rangle_{r,s,t}\Big],\end{aligned} \tag{4.16}$$

that by means of our initial conditions is recast as:

$$\begin{aligned}\langle\phi_a(\mathbf{k}_1,\eta)\phi_b(\mathbf{k}_2,\eta)\rangle = \sum_{r,s,t} t!(2r-1)!!(2s-1)!!\binom{2r+t}{t}\binom{2s+t}{t}\int d\mathbf{q}_1\cdots d\mathbf{q}_r d\mathbf{q}'_1\cdots d\mathbf{q}'_s d\mathbf{q}''_1\cdots d\mathbf{q}'_t \\ \times\,\mathcal{F}_a^{(2r+2)}(\mathbf{q}''_1,\cdots,\mathbf{q}''_t,\mathbf{q}_1,-\mathbf{q}_1,\cdots,-\mathbf{q}'_r,\eta)\mathcal{F}_a^{(2s+2)}(-\mathbf{q}''_1,\cdots,-\mathbf{q}''_t,\mathbf{q}'_1,-\mathbf{q}'_1,\cdots,-\mathbf{q}'_s,\eta) \\ \times\,P^0(q_1)\cdots P^0(q_r)P^0(q_1{}')\cdots P^0(q_s{}')P^0(q_1{}'')\cdots P^0(q_t{}''),\end{aligned} \tag{4.17}$$

that, by generalising the expression for $\Gamma^{(2)}$ in (4.12), gives the final result:

$$P_{ab}(k,\eta) = \sum_{t=1}^{\infty}\int d\mathbf{q}_1\cdots d\mathbf{q}_t\;\delta(\mathbf{k}-\Sigma_{i=1}^t\mathbf{q}_i)\Gamma_a^{(t)}(\mathbf{q}_1,\cdots,\mathbf{q}_t,\eta)\Gamma_b^{(t)}(\mathbf{q}_1,\cdots,\mathbf{q}_t,\eta)P^0(q_1)\cdots P^0(q_t), \tag{4.18}$$

where we denote, analogously to the kernels, $\Gamma_a^{(t)} = \Gamma_{ac_1\cdots,c_t}^{(t)}u_{c_1}\cdots u_{c_t}$.
Now, we want to build a regularized scheme able to describe the multi-point propagators and the quantities built with them in a better way than the standard perturbation theory does: this program requires a advanced analysis of their behaviour at different scales.
Since we are particularly interested in the mildly non-linear scales, we start with the analysis of these quantities in the limit of small scales ($k\to\infty$). It was proved that the multi-point propagators in this limit are exponentially suppressed:

$$\Gamma_a^{(p)}(\mathbf{k}_1,\cdots,\mathbf{k}_p;\eta)\to e^{-\frac{k^2\sigma_d^2e^{2\eta}}{2}}\Gamma_{a,tree}^{(p)}(\mathbf{k}_1,\cdots,\mathbf{k}_p;\eta), \tag{4.19}$$

where $\Gamma_{a,tree}^{(p)}$ is the lowest order non-vanishing expansion of $\Gamma_a^{(p)}$ and the parameter σ_d is the one-dimensional mean-square-root of the displacement field:

$$\sigma_d^2 = \frac{1}{3}\int d\mathbf{q}\frac{P^0(q)}{q^2}. \tag{4.20}$$

Actually, this trend can be easily derived in the Zel'dovich Approximation, in which the density kernels read [8, 3]:

$$F_n(\mathbf{q}_1,\cdots,\mathbf{q}_n) = \frac{1}{n!}\frac{\mathbf{k}\cdot\mathbf{q_1}}{q_1^2}\cdots\frac{\mathbf{k}\cdot\mathbf{q_n}}{q_n^2}, \tag{4.21}$$

where $\mathbf{k}=\mathbf{q}_1+\cdots+\mathbf{q}_n$, hence the matter propagator writes as:

$$\begin{aligned}G_{11}(k,\eta) =&f(\eta)\sum_{n=0}^{\infty}(2n+1)!!\int d\mathbf{q}_1\cdots d\mathbf{q}_n\,F_n(\mathbf{k},\mathbf{q}_1,-\mathbf{q}_1,\cdots,-\mathbf{q}_n)P^0(q_1)\cdots P^0(q_n) = \\ =&f(\eta)\sum_{n=0}^{\infty}\frac{1}{n!}\Big[-\frac{1}{2}\int d\mathbf{q}\Big(\frac{\mathbf{k}\cdot\mathbf{q}}{q^2}\Big)^2P^0(q)\Big]^n = f(\eta)e^{-\frac{k^2\sigma_d^2}{2}}.\end{aligned} \tag{4.22}$$

The problem is that the expression (4.19) doesn't describe correctly the behaviour of the propagators at all the scales. Indeed, at very large ones they are expected to be well described by their standard perturbative expression:

$$\Gamma_a^{(p)}(\mathbf{k}_1,\cdots,\mathbf{k}_p;\eta) = \Gamma_{a,tree}^{(p)}(\mathbf{k}_1,\cdots,\mathbf{k}_p;\eta)+\sum_{n=1}^{\infty}\Gamma_{a,n-loop}^{(p)}(\mathbf{k}_1,\cdots,\mathbf{k}_p;\eta), \tag{4.23}$$

where, for the dominant growing mode, we have:

$$\Gamma_{a,tree}^{(p)}(\mathbf{k}_1,\cdots,\mathbf{k}_p;\eta) = e^{(p-1)\eta}F_{a,sym}^{(p)}(\mathbf{k}_1,\cdots,\mathbf{k}_p), \tag{4.24}$$

for the tree-level contribution term (this can be seen setting $j = 0$ in Eq.(4.12) and generalising at whatever p), and in the same way for the n-th loop order contribution we have:

$$\begin{aligned}\Gamma^{(p)}_{a,n-loop}(\mathbf{k}_1,\cdots,\mathbf{k}_p;\eta) = & e^{(2n+p-1)\eta}\binom{2n+p}{n}(2n-1)!!\int d\mathbf{q}_1\cdots d\mathbf{q}_n\times \\ & \times\mathcal{F}^{(2n+p)}_{abc}(\mathbf{k}_1,\cdots,\mathbf{k}_p,\mathbf{q}_1,-\mathbf{q}_1,\cdots,-\mathbf{q}_n,\eta)P^0(q_1)\cdots P^0(q_n) = \\ = & e^{(2n+p-1)\eta}\bar{\Gamma}^{(p)}_{a,n-loop}(\mathbf{k}_1,\cdots,\mathbf{k}_p).\end{aligned} \tag{4.25}$$

One can verify that the perturbative correction at a given order has the following asymptotic form as $k\to\infty$:

$$\Gamma^{(p)}_{a,n-loop}\to\frac{1}{n!}\Big(-\frac{k^2\sigma_d^2e^{2\eta}}{2}\Big)^n\Gamma^{(p)}_{a,tree}, \tag{4.26}$$

in agreement with (4.19), because summing over all the loops the n-dependent part gives the required exponential. This fact supports the possibility to find a matching scheme which smoothly interpolates between the low-k results, where the standard perturbative approach is reliable, and high-k results, characterized by the exponential suppression, for any multi-point propagator: the approximation derived in such a framework is called the regularized Γ-expansion perturbation theory approach.
It is essentially based on the definition of regularized multi-point propagators, expressed in a straightforward way in terms of the standard perturbative results, used in place of the full ones, difficult to handle, and of the standard perturbative ones, very poor at small scales, for the evaluation of observables like the power spectrum of Eq.(4.16), the bispectrum and so on. Each definition is relative to a given loop, that is it reproduces the right results at the given loop at low-k and the correct high-k behaviour of the propagators. At one loop the definition is:

$$\Gamma^{(p)}_{a,reg}(\mathbf{k}_1,\cdots,\mathbf{k}_p;\eta)=e^{(p-1)\eta}\Big[F^{(p)}_{a,sym}(\mathbf{k}_1,\cdots,\mathbf{k}_p)\Big\{1+\frac{k^2\sigma_d^2e^{2\eta}}{2}\Big\}+e^{2\eta}\bar{\Gamma}^{(p)}_{a,n-loop}(\mathbf{k}_1,\cdots,\mathbf{k}_p)\Big]e^{-\frac{k^2\sigma_d^2e^{2\eta}}{2}}. \tag{4.27}$$

Since the proposed regularized multi-point propagators preserve the expected low and high modes behaviours, the convergence of the Γ-expansion adopting this regularization scheme would be much better than the expansion based on standard perturbation theory tools.
The range of applicability of this regularization scheme is shown to depend on both the momentum k and the power spectrum amplitude [56, 57]. A criterium to define the domain of applicability of the present approach and of the related RegPT code is the following. The upper value of reliability for k, denoted as k_{crit}, is proposed to be obtained from the implicit equation:

$$\frac{k^2_{crit}}{6\pi^2}\int_0^{k_{crit}}dqP_{lin}(q,\eta)=C, \tag{4.28}$$

where C is a fixed constant, $C = 0.3$ for one loop and $C = 0.7$ for two loops, while P_{lin} is the linearly evolved power spectrum defined in (2.69). Below the critical wavenumber, this regularization scheme agrees with results of N-body simulations, while above this value growing discrepancies are found: in particular, at wavenumbers lower than k_{crit} it has been pointed out that the RegPT scheme indeed agrees with N-body simulations mostly within a percent-level precision, for a large number of cosmological models.

4.2 The numerical analysis.

In this section, by using the RegPT code, we analyse the evolved non-linear power spectrum in the IR region and, thanks to the linear kernel function, we propose a way to improve the result

extending its region of validity to smaller scales. The outcome is then compared with what is obtained by N-body simulations. We make aware that all the following power spectra, if not explicitly written as P_{ab}, are referred to the matter-matter component P_{11} and moreover they will be denoted with P and will refer to the $e^{2\eta}\langle\phi\phi\rangle$ version.
We start fixing the cosmological parameters that we always used throughout the whole analysis to generate data from the codes: they are all taken from the final results of the Planck Mission [21] and reported in Table (3.1).
The first step consisted in generating the primordial power spectrum, denoted with $P^0(q)$: we decided to use the $\mathrm{CAMB\ Web\ Interface}$, run with the above parameters for the requested primordial power spectrum at the redshift $z_{in} = 100$. Then we evolved $P^0(q)$ at the two late redshifts $z = 0, 1$ with the RegPT code, selecting the options $-\mathrm{spectrum}$ for the initial configuration and $-\mathrm{direct}$ to ask the application to generate the data following the regularized scheme introduced in the previous section at two loop orders (that is reproducing consistently two loops results at low-k), by evaluating the multi-dimensional integrals that simply generalise at this order Eq.(4.27) and that can be found in [55]. We will denote the full and linear evolved power spectra from this code with $P_z^{\mathrm{RegPT}}(k)$ and $P_{lin,z}^{\mathrm{RegPT}}(k)$ respectively.
As we have said, comparisons are carried on with a cosmic emulator based on N-body simulations, giving the "true" values up to subpercent errors. In particular, we used the $\mathrm{FrankenEmu}$ code[1], giving predictions on the non-linear evolved power spectrum from a chosen set of cosmological parameters, interpolating among a suite of different simulated power spectra. Using the values in Table (3.1), we get the results denoted with $P_z^{\mathrm{emu}}(k)$.
The different power spectra are plotted in Fig.(4.1).

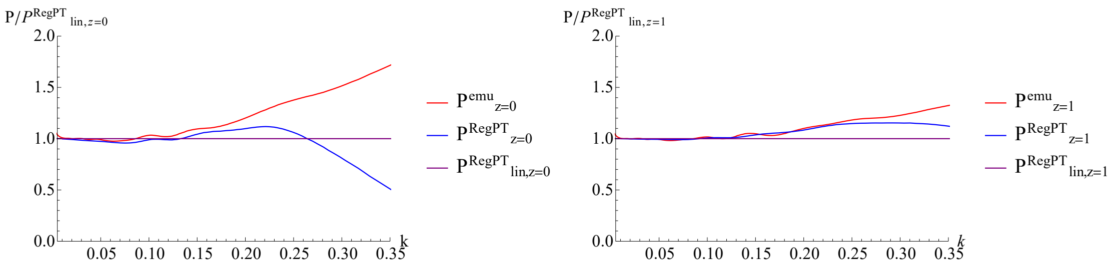

Figure 4.1: Power spectra from the emulator, non-linear and linear RegPT for $z = 0$ (left) and $z = 1$ (right). The unit for the momenta is $h\mathrm{Mpc}^{-1}$.

From the figure it is possible to note that both the $P_z^{\mathrm{RegPT}}(k)$ at $z = 0, 1$ are expected to become non reliable above a critical value of k due to the failure of the regularization scheme at those scales, where in fact they change dramatically their behaviour, and something similar happens, more softly, to the linearly evolved power spectra, because of course they become non predictive at small scales, where non-linear dynamics increases its importance. However, from data it results that the region of reliability of P_z^{RegPT} is larger than the one of $P_{lin,z}^{\mathrm{RegPT}}$ in both the cases: let's see this in a more quantitative way. Remembering the definition of k_{crit} (4.28), we have $k_{crit}^{z=0} \approx 0.16\,h\mathrm{Mpc}^{-1}$ and $k_{crit}^{z=1} \approx 0.25\,h\mathrm{Mpc}^{-1}$: above these values P_z^{RegPT} at $z = 0, 1$ respectively loose their reliability. Defining the discrepancy between the emulator output and one of

[1]The code is available at `http://www.hep.anl.gov/cosmology/CosmicEmu/emu.html`. Further information in [58, 59].

the different outputs (o) of the RegPT code as:

$$\delta_{o,z}(k) = \left| \frac{P_z^{\mathrm{emu}}(k) - P_{o,z}^{\mathrm{RegPT}}(k)}{P_z^{\mathrm{emu}}(k)} \right|, \tag{4.29}$$

numerical data point out that, for these values of k, P_z^{RegPT} have a discrepancy with P_z^{emu} of about 3.5% and 3% respectively for $z = 0, 1$. In order to find the same agreement between $P_{lin,z}^{\mathrm{RegPT}}$ and P_z^{emu} we have to increase the scales, going to $k_{max} \approx 0.09\, h\mathrm{Mpc}^{-1}$ for $z = 0$ and $k_{max} \approx 0.13\, h\mathrm{Mpc}^{-1}$ for $z = 1$. Incidentally, since in the previous chapter we dedicated a lot of space to the analysis of the evolved power spectrum, particularly in its approximation at the one loop perturbative level, it seems nice to compare the linearly evolved power spectrum as given by the RegPT code, according to the definition (2.67), and the one loop expansion as given diagrammatically in Fig.(3.4) and explicitly by the expression (3.30), proving that actually the latter is more precise of the former, but however (hopefully) worse than the one based on the regularized Γ-expansion. The option $-\mathrm{direct1loop}$ of the same code provides this object, $P_{1-loop,z}^{\mathrm{RegPT}}$, and the check confirms what is expected from perturbation theory: with our defined tolerances the highest modes are respectively $k_{max} = 0.13\, h\mathrm{Mpc}^{-1}$ and $k_{max} = 0.19\, h\mathrm{Mpc}^{-1}$ for $z = 0, 1$, higher than in the linear case but lower than the Γ-expansion one. To summarize, in Table (4.1) we report the different values of k_{max}.

	$P_{lin,z}^{\mathrm{RegPT}}$	$P_{1-loop,z}^{\mathrm{RegPT}}$	P_z^{RegPT}
k_{max} at $z = 0$	$0.09\, h\mathrm{Mpc}^{-1}$	$0.13\, h\mathrm{Mpc}^{-1}$	$0.16\, h\mathrm{Mpc}^{-1}$
k_{max} at $z = 1$	$0.13\, h\mathrm{Mpc}^{-1}$	$0.19\, h\mathrm{Mpc}^{-1}$	$0.25\, h\mathrm{Mpc}^{-1}$

Table 4.1: Largest k_{max} accessible by three different models for $P_{11}(k, z)$.

The next step consisted in the computation of the linear kernel function: to this aim, we recast its definition in a handier way than what we used until now, also by means of a slight approximation. Starting from Eq.(3.2), ignoring the initial time dependence and expressing time via the redshift z, we can write:

$$\delta P_{ab}(k, q^\star; z) = \int_0^\infty \frac{dq}{q} K_{ab}(k, q; z) \delta P^0(q, q^\star), \tag{4.30}$$

that is the difference between a non-linear power spectrum evolved from a perturbation of the reference initial power spectrum at a mode $q^\star$, $P^0(q, q^\star)$, and the non-linear power spectrum evolved from the reference one, $\bar{P}^0(q)$, with:

$$P^0(q, q^\star) = \bar{P}^0(q) + \delta P^0(q, q^\star), \tag{4.31}$$

where δP is centered around $q^\star$ and vanishes outside, as we will see below. Introduced the new variable ξ in such a way that:

$$\xi = \ln \frac{q}{q_c} \quad \longleftrightarrow \quad q(\xi) = q_c e^{\xi}, \tag{4.32}$$

where q_c is a scale factor required for dimensional reasons, without any other influence and thus set to $q_c = 1\, h\mathrm{Mpc}^{-1}$, and $\xi^\star = \ln \frac{q^\star}{q_c}$, since $\frac{dq}{q} = d\xi$ the above result is written as:

$$\delta P_{ab}\left(k, q^\star(\xi^\star); z\right) = \int_{-\infty}^{+\infty} d\xi\, K_{ab}\left(k, q(\xi); z\right) \delta P^0\left(q(\xi), q^\star(\xi^\star)\right). \tag{4.33}$$

Now, we suppose to express the modification of the initial power spectrum by a function f as:

$$\delta P^0\left(q(\xi), q^\star(\xi^\star)\right) = \bar{P}^0\left(q(\xi)\right) f\left(\frac{\xi - \xi^\star}{\sigma}\right), \tag{4.34}$$

with f chosen of the form:

$$f\left(\frac{\xi - \xi^\star}{\sigma}\right) = \frac{A}{\sqrt{\pi}} e^{-\frac{(\xi-\xi^\star)^2}{\sigma^2}}, \tag{4.35}$$

were A substantially regulates the magnitude of the perturbation, while σ the interval of scales affected by it.
If we choose the parameters A, σ sufficiently small to make the exponential rapidly suppressed as ξ is out of a very small neighborhood of $\xi^\star$, we can think to approximate the expression (4.33) in:

$$\begin{aligned} \delta P_{ab}\left(k, q^\star(\xi^\star); z\right) = \frac{A}{\sqrt{\pi}} \int_{-\infty}^{+\infty} d\xi \, K_{ab}\left(k, q(\xi); z\right) \bar{P}^0(q(\xi)) e^{-\frac{(\xi-\xi^\star)^2}{\sigma^2}} \approx \\ \approx K_{ab}\left(k, q(\xi^\star); z\right) \bar{P}^0(q(\xi^\star)) I(\sigma), \end{aligned} \tag{4.36}$$

where, by a straightforward gaussian integration:

$$I(\sigma) = \frac{A}{\sqrt{\pi}} \int_{-\infty}^{+\infty} d\xi \, e^{-\frac{(\xi-\xi^\star)^2}{\sigma^2}} = A\sigma, \tag{4.37}$$

thanks to which from the above expression we reach the following form for the linear kernel:

$$K_{ab}(k, q^\star; z) \approx \frac{\delta P_{ab}(k, q^\star, z)}{\bar{P}^0(q^\star) A\sigma}, \tag{4.38}$$

which gives our estimator for the LRF.

To compute (4.38), we used the function (4.35) with both the two parameters and the scales of perturbation chosen trying to accomplish at best three requests: the needed fast suppression of the perturbation, that however had to bring clear consequences at later times, and the central modes of perturbation as smaller as possible, to be able to investigate the IR region using our highest reliable evolved modes: the biggest difficulty concerned the latter issue, as for smaller modes that those we used the evolved objects presented much noise at the scales we were interested in. These observations led us to select the adimensional parameters $A = 0.5$ and $\sigma = 0.05$, while as modes of perturbation $q_i^\star$ we took seven values going from $0.01\, h\mathrm{Mpc}^{-1}$ to $0.07\, h\mathrm{Mpc}^{-1}$ with steps of $0.01\, h\mathrm{Mpc}^{-1}$; this value could not be lowered to avoid an excessive superposition of the perturbed areas. Fig.(4.2) shows a typical modified primordial power spectrum with respect to the unperturbed one. In all the cases, at the peaks, occurring exactly in the above mentioned values $q_i^\star$, the power spectra increase by

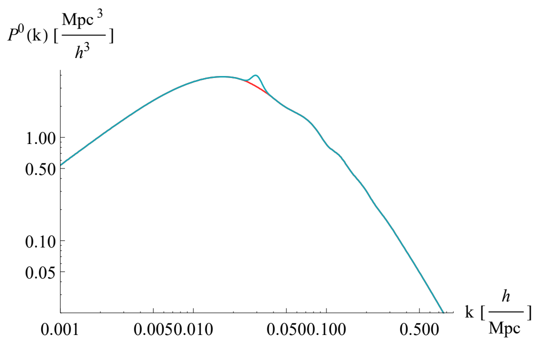

Figure 4.2: Unperturbed (red) and perturbed at $q^\star = 0.03\, h\mathrm{Mpc}^{-1}$ (blue) primordial power spectra.

the 28% with respect to the reference one, while the perturbations stay bigger than the 5% with respect to the reference one in a wavemode range, centered at the maxima, increasing from about $\Delta k \approx 0.003\,h\mathrm{Mpc}^{-1}$ for the lowest mode to $\Delta k \approx 0.021\,h\mathrm{Mpc}^{-1}$ for the highest.
At this point, we were able to evaluate the kernel function according to (4.38), using for the numerator the difference between $P_z^{\mathrm{RegPT}}(k, q^\star)$ perturbed at the mode $q^\star$ and $P_z^{\mathrm{RegPT}}(k)$ unperturbed, for each mode k and redshift $z = 0, 1$: the plots, were we report the ratios between the matter kernel and the central modes of perturbation, are given for $z = 0, 1$ in Fig.(4.3). At

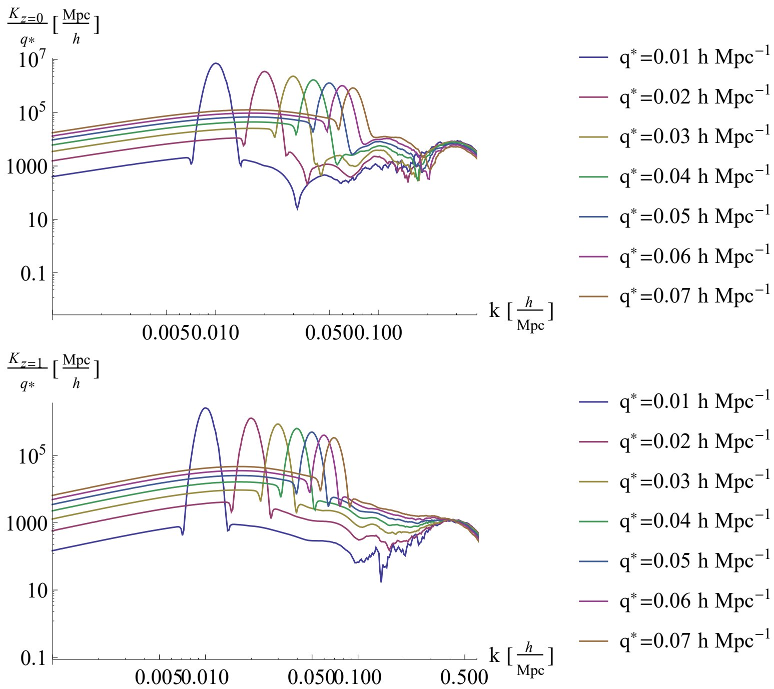

Figure 4.3: Ratios between the linear matter kernel functions and the central perturbation values, for $z = 0$ (up) and $z = 1$ (down).

first, from the figures it is clear what we said above about noise: the lower modes of perturbation, especially $q^\star = 0$, bring an important amount of noise at the scales we are interesting in, namely $k \geq 0.1\,h\mathrm{Mpc}^{-1}$, situation that seems to improve taking higher and higher modes. Secondly, we can check that in the UV region, corresponding to the left side in these plots, the behaviour is consistent with the UV limit at one loop found in the previous chapter, namely it is consistent with a quadratic law in the evolved modes k. On the other hand, a problem arises on the IR region: according to the galileian invariance, in this region the linear kernel should vanish as the cube of the perturbed initial mode $q^\star$, as we verified also in the one loop calculation we made in Chapter 3. Now, in our figure if galileian invariance were respected, we would see that, from $k \approx 0.1\,h\mathrm{Mpc}^{-1}$ on, for each k the ratios between the corresponding values of two ordinates in the plots would behave as the square of the ratios between their related perturbation modes (note that in Fig.(4.3) we plot the LRF divided by $q^\star$): instead, we find that these ratios exhibit a linear dependence and, what's worse, at large wavemodes k, seem even to superpose. This is a clear manifestation of the breaking of galilean invariance in the RegPT scheme. The question is then double, relying in whether it is possible to restore it and, if so, how much would it improve the numerical performance of the new galilean invariant scheme.

Now, we arrive at the heart of this numerical analysis, in which we will use the linear kernel as main tool. The breaking of galilean invariance manifests itself via a linear dependence on $q^\star$ of the linear response function, thereforethe amount of breaking is measured efficiently by the below scale-dependent quantity $C(k)$:

$$C(k) \equiv \lim_{q^\star \to 0} \frac{K_{11}(k, q^\star)}{q^\star}, \tag{4.39}$$

We can therefore correct P_z^{RegPT} introducing an improved power spectrum at mode k and redshift z as follows:

$$P_z^{imp}(k) = P_z^{\mathrm{RegPT}}(k) - C(k) \int_0^\lambda dq\, P^0(q) : \tag{4.40}$$

as can be seen, the above correction, written remembering the relation between the linear kernel and the power spectrum (3.2), removes the wrong contribution to P_z^{RegPT} due to the breaking of galilean invariance and restores this invariance and consequently to improve the behaviour. As we will show below, the improved power spectrum has a better agreement with simulations.

As we can see, the integral restored the correct dimensionality of the power spectrum, while the parameter λ could be seen as a cut-off, reflecting the arbitrariness of the subtraction procedure defined in (4.40). Taking different values for lambda amounts to changing the coefficient of the $\mathcal{O}(q^3)$ terms in the result (3.44), which are left undetermined by galilean invariance. In particular we analysed three values: $\lambda_1 = \frac{k}{2}$, $\lambda_2 = k$ and $\lambda_3 = \infty$. Even if the limits in (4.39) actually arise for each value of k (in the plateau where $k \gtrsim 0.1\, h\mathrm{Mpc}^{-1}$) from the extrapolation at $q^\star = 0$ of the straight line determined by the seven points having as x-coordinates the seven $q_i^\star$ and as y-coordinates the corresponding ratios of Fig(4.3), strong numerical fluctuations led us to compute only a single scale-independent limit (for each redshift) extrapolating the same kind of straight line but with y-coordinates the averages, at each given $q_i^\star$, of the ratios related to all the modes k in the IR interval of reliability, namely starting from $k = 0.1\, h\mathrm{Mpc}^{-1}$ and ending at k_{crit}: it resulted $C_0 \approx 790\, h^{-1}\mathrm{Mpc}$ and $C_1 \approx 50\, h^{-1}\mathrm{Mpc}$.

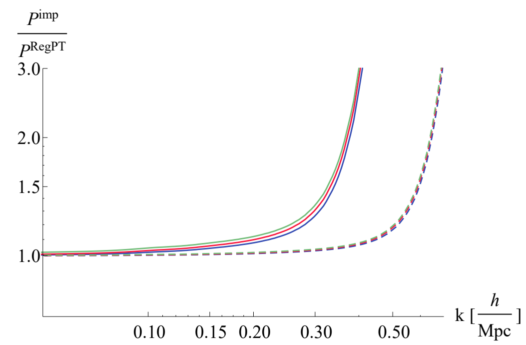

Figure 4.4: Ratios between improved and bare RegPT power spectra with λ_1 (blue), λ_2 (red) and λ_3 (green) at $z = 0$ (continous) and $z = 1$ (dashed).

Actually, in this way at each given redshift the correction in (4.40) depended only on the cut-off and in the case of λ_3 it turned out to be a constant, of course representing a limitation of our analysis. Fig.(4.4) reports a comparison between P_z^{imp} and P_z^{RegPT}.

In Fig.(4.5) we report a comparison between the three improved power spectra obtained with the three different choices for λ, RegPT and the the cosmic emulator. The improvement is evident even at a first glance: for $z = 0$, at the critical mode $k_{crit} = 0.16\, h\mathrm{Mpc}^{-1}$, where with $P_{z=0}^{\mathrm{RegPT}}$ we had a discrepancy, with respect to the emulator power spectrum, of about the 3.5%, now, with the improved version, the discrepancy at this mode is much more lower for λ_1, at about 1.2%, lower for λ_2, at about 2.7%, while greater for the λ_3 case, growing at more than the 4%. Therefore, $P_{z=0}^{imp}$ seems to be able to improve in reproducing the emulator power spectrum, enlarging the interval of reliability: indeed, in the case with λ_1 the 3.5% tolerance is hit only at $k \approx 0.22\, h\mathrm{Mpc}^{-1}$. A quite analogous situation is depicted for $z = 1$: at $k_{crit} = 0.25\, h\mathrm{Mpc}^{-1}$,

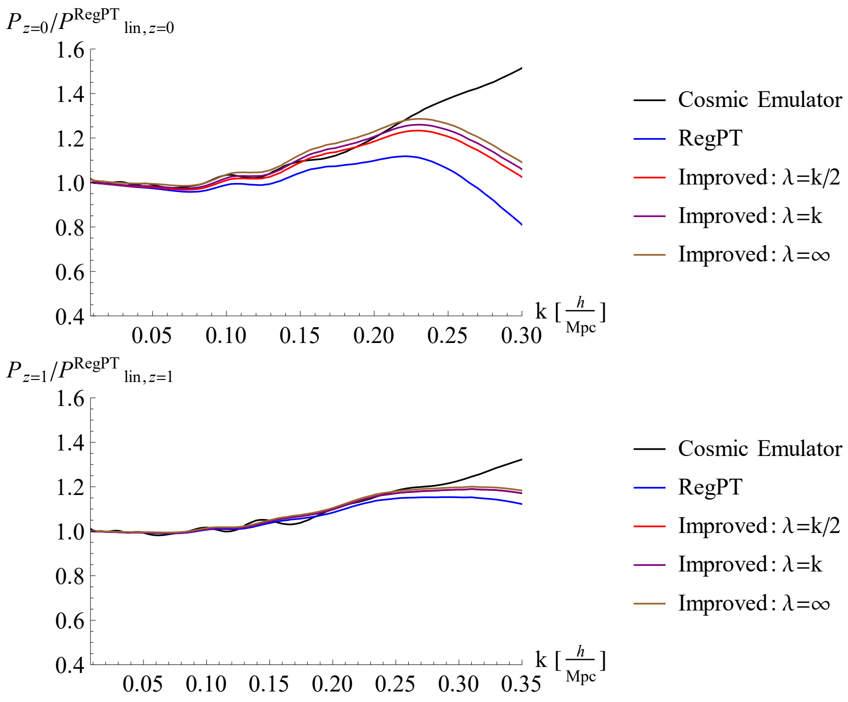

Figure 4.5: P_z^{emu}, $P_z^{\rm RegPT}$ and the three P_z^{imp} with respect to $P_{lin,z}^{\rm RegPT}$, for $z = 0, 1$ (up, down).

$P_{z=1}^{imp}$ has a discrepancy of about the 1%, indifferently to the considered cut-off, due to the great difference in the magnitude of the limits in the $z = 0, 1$ cases, and the reliability interval grows up to $k \approx 0.30\, h\mathrm{Mpc}^{-1}$.

To conclude, we update Table (4.1) with these new results:

	$P_{lin,z}^{\rm RegPT}$	$P_{1-loop,z}^{\rm RegPT}$	$P_z^{\rm RegPT}$	P_z^{imp}
k_{max} at $z = 0$	$0.09\, h\mathrm{Mpc}^{-1}$	$0.13\, h\mathrm{Mpc}^{-1}$	$0.16\, h\mathrm{Mpc}^{-1}$	$0.22\, h\mathrm{Mpc}^{-1}$
k_{max} at $z = 1$	$0.13\, h\mathrm{Mpc}^{-1}$	$0.19\, h\mathrm{Mpc}^{-1}$	$0.25\, h\mathrm{Mpc}^{-1}$	$0.30\, h\mathrm{Mpc}^{-1}$

Table 4.2: Lowest scales accessible by the models analysed so far for the non-linear evolved matter power spectrum.

Chapter 5

A non perturbative interpolating scheme.

5.1 The LRF as an interpolator between modified cosmologies.

In this chapter, we would like to further highlight the power and versatility of the linear response function in handling the properties of the Universe at scales affected by slight non-linearities. In particular, we want to accomplish this aim by implementing something we anticipated at the end of Section 3.1, concerning the possibility of using the LRF to obtain the fully non-linear matter power spectrum for cosmologies with slight modifications with respect to the one taken as reference, that is using the linear kernel as the interpolator of the deviations between the two cosmologies.

As suggested in that passage, such a procedure has all the qualities for allowing a great practical result, namely saving computing time to produce non-linear power spectra for a large landscape of cosmologies. Indeed, an accurate N-body simulation takes in general a very large amount of time and computational memory even to the most advanced calculators. On the contrary, the method we are using actually needs only the simulation for the reference model, since for the "nearby" ones the power spectrum can be obtained from it using the linear response function as an interpolator; clearly, this procedure is reliable within a certain wavemode, because we have cut the power spectrum expansion (3.1) at the linear kernel (3.2), neglecting all the following terms, but we will see that this scale is well beyond the linear regime, making the method very helpful for many situations.

We consider as reference power spectrum the one obtained in a ΛCDM model with parameters fixed by the Planck Mission [21], while the modifications will be done on the parameters A_s, n_s and Ω_m. The analysis presented here can be extended to a more general set of cosmologies, where other parameters are changed. The first two parameters, the amplitude of primordial scalar fluctuations and the spectral index (determining how they change with scale, where $n_s = 1$ means invariance of scale), affect only the primordial power spectrum, while the matter parameter density changes also the growth factor, then the first step consists in determining the extended version of the expressions found in Section 3.1 when also the growth factor is modified.

Analogously with the Taylor expansion of a two-variables function, a functional F of two functions $g(x)$, $h(x)$ can be expanded, around to reference functions $\bar{g}$, $\bar{h}$, as:

$$F[g,h] = F[\bar{g},\,\bar{h}] + \sum_{n_1}^{\infty}\sum_{n_2}^{\infty} \frac{1}{n_1^\star! n_2^\star!} \int dx_1 \cdots dx_{n_1^\star} \int dx'_1 \cdots dx'_{n_2^\star} \times \\ \times \frac{\delta^{(n_1^\star + n_2^\star)} F}{\delta g(x_1)\cdots\delta g(x_{n_1^\star})\,\delta h(x'_1)\cdots\delta h(x'_{n_2^\star})}\Big|_{(\bar{g},\,\bar{h})} \delta g(x_1)\cdots\delta g(x_{n_1^\star})\,\delta h(x'_1)\cdots\delta h(x'_{n_2^\star}), \tag{5.1}$$

where $\delta g(x) = g(x) - \bar{g}(x)$, and the same holds for h. In particular, at the first order in perturbations, that is neglecting all the terms from $\mathcal{O}(\delta^2)$ on, we get:

$$\begin{aligned} F[g,h] =& F[\bar{g},\,\bar{h}] + \int dx \frac{\delta F}{\delta g(x)}\Big|_{(\bar{g},\,\bar{h})} \delta g(x) + \int dx' \frac{\delta F}{\delta h(x')}\Big|_{(\bar{g},\,\bar{h})} \delta h(x') = \\ =& F[\bar{g},\,\bar{h}] + \int dx \left[\frac{\delta F}{\delta g(x)}\Big|_{(\bar{g},\,\bar{h})} \delta g(x) + \frac{\delta F}{\delta h(x)}\Big|_{(\bar{g},\,\bar{h})} \delta h(x) \right]. \end{aligned} \tag{5.2}$$

Now, if the non-linear density-density power spectrum $P_{ab}(\eta, \eta_{in}; \mathbf{k})$ is our functional of $P^0(\eta_{in}; \mathbf{q})$ and $D^+(\eta, \mathbf{k})$, that is $P_{ab}[P^0, D^+](\eta, \eta_{in}; \mathbf{k})$, then at fixed primordial and evolved time, we obtain:

$$P_{ab}[P^0, D^+](\eta, \eta_{in}; \mathbf{k}) = P_{ab}[\bar{P}^0, \bar{D}^+](\eta, \eta_{in}; \mathbf{k}) + \int d\mathbf{q} \left[\frac{\delta P_{ab}[P^0, D^+](\eta, \eta_{in}; \mathbf{k})}{\delta P^0(\mathbf{q})}\Big|_{(\bar{P}^0,\,\bar{D}^+)} \delta P^0(\mathbf{q}) + \right. \\ \left. + \int_{-\infty}^{\eta} d\eta' \, \frac{\delta P_{ab}[P^0, D^+](\eta, \eta_{in}; \mathbf{k})}{\delta D^+(\eta'; \mathbf{q})}\Big|_{(\bar{P}^0,\,\bar{D}^+)} \delta D^+(\eta', \mathbf{q}) \right], \tag{5.3}$$

dove $\delta P^0(\mathbf{q}) = P^0(\mathbf{q}) - \bar{P}^0(\mathbf{q})$ at initial time and $\delta D^+(\eta', \mathbf{q}) = D^+(\eta', \mathbf{q}) - \bar{D}^+(\eta', \mathbf{q})$, noting that the momenta corresponding to the two different quantities, despite of the same label, have different physical meanings: in the first term it is the initial momentum, appearing in P^0, while the second is the momentum at time η'. Introducing spherical coordinates we have, finally:

$$\begin{aligned} P_{ab}[P^0, D^+](\eta, \eta_{in}; \mathbf{k}) = P_{ab}[\bar{P}^0, \bar{D}^+](\eta, \eta_{in}; \mathbf{k}) + \int \frac{dq}{q} \Big[& K^{I}_{ab}(\eta, \eta_{in}; \mathbf{k}) \delta P^0(q, \Omega_q) + \\ & + K^{II}_{ab}(\eta, \eta_{in}; \mathbf{k}) \delta D^+(\eta, q, \Omega_q) \Big], \end{aligned} \tag{5.4}$$

from which, assuming homogeneity and isotropy, we get the following kernels:

$$\begin{aligned} K^{I}_{ab}(\eta, \eta_{in}; k) &= q^3 \int d\Omega_{\mathbf{q}} \frac{\delta P_{ab}[P^0, D^+](\eta, \eta_{in}; k)}{\delta P^0(q)}\Big|_{(\bar{P}^0,\,\bar{D}^+)}, \\ K^{II}_{ab}(\eta, \eta_{in}; k) &= q^3 \int d\Omega_{\mathbf{q}} \int_{-\infty}^{\eta} d\eta' \frac{\delta P_{ab}[P^0, D^+](\eta', \eta_{in}; k)}{\delta D^+(\eta'; q)}\Big|_{(\bar{P}^0,\,\bar{D}^+)}. \end{aligned} \tag{5.5}$$

First of all, we notice that the first kernel above is exactly the one widely studied in Chapter 3. Let's focus briefly on the second kernel, a new term, non-vanishing only when variations of Ω_m are involved: in particular, we can note that if the growth factor is scale independent, which would not be the case in presence of massive neutrinos, we can use a simplified version of the second kernel in (5.5), obtained by the elimination of the time integration, that is fixing the δD^+

at the final time η, with the only formal change, for the expression (5.4), of K^{II}, that differently is written as:

$$K^{II}_{ab}(\eta,\eta_{in};k) = q^3 \int d\Omega_{\mathbf{q}} \frac{\delta P_{ab}[P^0,D^+](\eta,\eta_{in};k)}{\delta D^+(\eta)}\Big|_{(\bar{P}^0,\,\bar{D}^+)}. \tag{5.6}$$

Moreover, since the density matter power spectrum has the leading time dependence given by the factor $e^{2\eta}$, as can be hinted from standard perturbation theory, the above expression can be written by explicit differentiation of the power spectrum as:

$$K^{II}_{ab}(\eta,\eta_{in};k) = 2\,q^3\delta(k-q) \int d\Omega_{\mathbf{q}} \frac{P_{ab}[P^0,D^+](\eta,\eta_{in};k)}{D^+(\eta)}\Big|_{(\bar{P}^0,\,\bar{D}^+)}, \tag{5.7}$$

an expression we will use in the following when considering variations of Ω_m.

5.2 The growth factor.

In this section, we briefly recall well known facts about the behaviour of the growth factor, relevant for our subsequent analysis.
The (linear) growth factor D^+ factors the time dependence of the growing part of the density perturbations:

$$\delta(t,\mathbf{x}) = A(\mathbf{x})D^+(t) + B(\mathbf{x})D^-(t). \tag{5.8}$$

The equation for D^+ can be read from (1.54), which is formally solved by the following expression [20, 18, 60]:

$$D^+(a) = \frac{5\Omega_m}{2}\frac{H(a)}{H_0}\int_0^a da' \left(\frac{H_0}{a'H(a')}\right)^3. \tag{5.9}$$

In the Einstein-de Sitter case the result is, consistently with Section 1.2, $D^+ = a$.

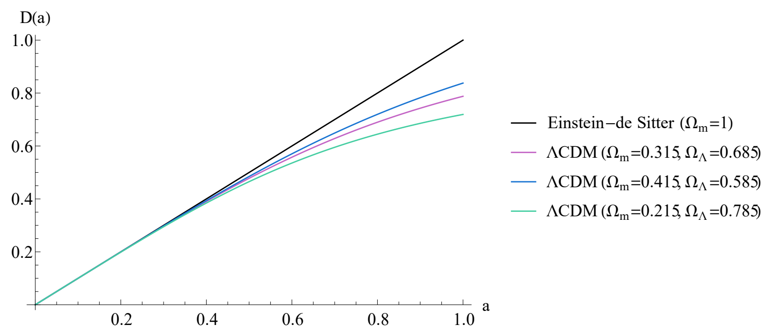

Figure 5.1: Growth factors in four different cases: the second in the legend mostly resembles our Universe, the last two present the situations with more and less matter respectively.

Fig.(5.1) shows the growth factor in four different configurations, all with $\Omega_r = 0$ and $\Omega_K = 1 - \Omega_m - \Omega_r - \Omega_\Lambda = 0$.
To conclude, we introduce the growth rate f_+ as the logarithmic derivative of D^+:

$$f_+(a) = \frac{d\ln D^+}{d\ln a}, \tag{5.10}$$

estimating the deviation of a model with respect to the Einstein-de Sitter one. Fig.(5.2) shows f_+ in the same cosmologies presented in Fig.(5.1). For completeness, we stress that when only matter and cosmological constant are present, through the following relation derived by the Friedman equations:

$$\Omega_m(a) = \frac{\Omega_{m,0}}{a^3 H^2(a)}, \tag{5.11}$$

we can write an excellent approximation for the growth rate [17]:

$$f_+(a) \simeq \Omega_m^{\frac{5}{9}}(a) + \frac{\Omega_\Lambda}{H_0}\left(1 + \frac{1}{2}\Omega_m(a)\right) \approx \Omega_m^{\frac{5}{9}}(a). \tag{5.12}$$

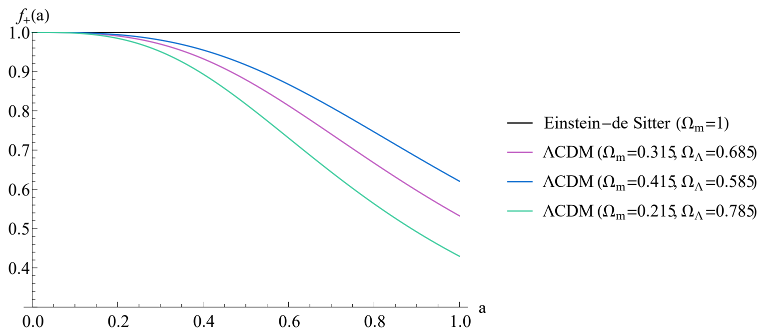

Figure 5.2: Corresponding growth rates to the configuration of Fig.(5.1).

5.3 Numerical results.

In this section we aim to show the results and to describe the way we obtain them in the cases for which there is a change of only a single cosmological parameter at a time.
The procedure we adopted can be summarised in the following steps.

- First of all we choose $\hat{k} = 0.2\,h\mathrm{Mpc}^{-1}$ as the scale at which the evolved matter power spectrum is evaluated for the modified cosmology by means of our interpolation machinery and compared to the one obtained in the modified configuration by the FrankenEmu code, that is considered as our source of "true" values from N-body simulation, without the correction from the tools developed in the previous section, in order to test the validity of the procedure we have developed.

- Secondly, according to the notation fixed for the expansion (5.3), we define a percent discrepancy parameter Δ as:

$$\Delta = 100\left|\frac{P[P^0, D^+](z, z_{in}, \hat{k}) - P_{emu}(z, z_{in}, \hat{k})}{P_{emu}(z, z_{in}, \hat{k})}\right|, \tag{5.13}$$

  estimating the percent difference between the evolved power spectrum computed for the modified cosmology according to (5.3) and the evolved one through the emulator.

- For each of the three parameters to modify, we generate with the CAMB Web Interface a set of primordial (at $z_{in} = 100$) power spectra referred at different slight modifications of the considered parameter with respect to the reference one, defined by Table (3.1), and then we evolve them according to (5.3) in the fashion of (5.4), using the definitions of kernels (5.5) and using for K^I the one loop expression obtained summing (3.36) and (3.37), while for K^{II} the simplified form (5.7) or the full one in (5.5). In particular, referring to the expansion (5.3) as:

$$P_{ab}[P^0, D^+] = P_{ab}[\bar{P}^0, \bar{D}^+] + C^I_{ab} + C^{II}_{ab}, \tag{5.14}$$

we have respectively (considering the matter components and neglecting the subscripts) for C^I the expression:

$$\begin{aligned} C^I(k,\eta) = \int_0^{\Xi} dq \Bigg\{ \int_{-1}^{1} dx \Bigg[\frac{k^4 e^{4\eta}}{196\pi^2} \frac{\big(7kx + q(3-10x^2)\big)^2}{(k^2-2kqx+q^2)^2} \bar{P}^0(\sqrt{k^2-2kqx+q^2}) \Bigg] + \\ - \frac{e^{4\eta}}{1008\pi^2 k^3 q^3} \Bigg[3(2k^2+7q^2)(k^2-q^2)^3 \ln\Big[\frac{k+q}{|k-q|}\Big] + \\ + 2kq\big(-6k^6 + 79k^4q^2 - 50k^2q^4 + 21q^6\big) \Bigg] \bar{P}^0(k) \Bigg\} \delta P^0(q), \end{aligned} \tag{5.15}$$

while, for C^{II} in the complete form, using the one loop power spectrum (3.30):

$$\begin{aligned} C^{II}(k,\eta) = \int_0^{a_f} da' \Bigg\{ \frac{2P^0(k)}{D(a_{in})^2} + \left(\frac{D^+(a')}{D^+(a_{in})^2}\right)^2 \int_0^{\Xi} dq \int_{-1}^{1} dx \times \\ \Bigg[\frac{k^4}{98\pi^2} \frac{\big(7kx + q(3-10x^2)\big)^2}{(k^2-2kqx+q^2)^2} \bar{P}^0(\sqrt{k^2-2kqx+q^2}) P^0(q) \Bigg] + \\ - \frac{1}{252\pi^2 k^3 q^3} \Bigg[3(2k^2+7q^2)(k^2-q^2)^3 \ln\Big[\frac{k+q}{|k-q|}\Big] + \\ + 2kq(-6k^6 + 79k^4q^2 - 50k^2q^4 + 21q^6) \Bigg] P^0(k) P^0(q) \Bigg\} \frac{\partial \bar{D}^+(a')}{\partial a'} \delta D^+(a') \end{aligned} \tag{5.16}$$

or, in the simplified version:

$$C^{II}(k,\eta) = \frac{2\bar{P}(k,\eta)}{D(a_f)} \delta D^+(a_f), \tag{5.17}$$

where a_f is the scale factor at the final time η, determined by the redshift we choose to evolve the statistics, while $\bar{P} = P_{ab}[\bar{P}^0, \bar{D}^+]$. Hence, while for the simplified form above we use directly the fully evolved reference power spectrum, for the complete expression (5.5) we exploited the one loop power spectrum, providing a more precise time dependence than what we used, but meanwhile also a loss on the power spectrum precision.
Since at least for for the first linear kernel we use the one loop expression, knowing it has a bad behaviour in the UV region, that is it diverges oppositely to what simulations show, we performed the momentum integration of the first piece up to a common cut-off $\Xi = 2\,h\mathrm{Mpc}^{-1}$.

- Finally we compare the result with the emulator by determining the relative Δ. If we want to fix a common value $\hat{\Delta}$ for comparison, we can find by trials the two values for each of the three cosmological parameters under consideration corresponding to the maximum enhancement and reduction, with respect to the reference one, that achieve the fixed discrepancy. In such a way it is possible to find the three intervals of the possible values of the three parameters in order to fulfil the condition $\Delta < \hat{\Delta}$.

In the first two tables below, Tables (5.1) and (5.2), we report the results we obtained considering $\hat{\Delta} = 2.2$ with the simplified version of C^{II} (5.17). For comparison, to check the actual improvement, in Table (5.3) we report the values of the discrepancies between the power spectra evolved through the emulator and the corresponding linearly evolved ones, that is the quantity Δ in (5.13) changing the first power spectrum into the linear one: the maxima and minima, for each cosmological parameter, are the same as in Table (5.1) and Table (5.2) for the redshift $z = 0, 1$, respectively. In the same way, in Table (5.4) we report the discrepancies between the the the power spectra evolved through the emulator and the reference ones, without any correction, for the same values of the parameters as before. Finally, Table (5.5) allows a comparison between the previous results and what is obtained by using the complete form for C^{II}, remembering that clearly it affects the result only when there is a variation of the matter density parameter $\Omega_m h^2$.

Parameter	Reference	Min	Max	Min (σ)	Max (σ)	% Min	% Max
n_s	0.9655 ± 0.0062	0.9531	0.9810	$-2.0\,\sigma$	$+2.5\,\sigma$	-1.2	+1.6
$10^9 A_s$	2.198 ± 0.080	2.132	2.292	$-0.9\,\sigma$	$+1.2\,\sigma$	-3.0	+4.3
$\Omega_m h^2$	0.1426 ± 0.0020	0.1356	0.1508	$-3.5\,\sigma$	$+4.1\,\sigma$	-4.9	+5.8

Table 5.1: The lower and upper values satisfying $\Delta < 2.2$ for $z = 0$, their expressions by means of the standard deviations and the higest percent departures from the reference values.

Parameter	Reference	Min	Max	Min (σ)	Max (σ)	% Min	% Max
n_s	0.9655 ± 0.0062	0.9469	0.9841	$-3.0\,\sigma$	$+3.0\,\sigma$	-1.9	+1.9
$10^9 A_s$	2.198 ± 0.080	2.078	2.318	$-1.5\,\sigma$	$+1.5\,\sigma$	-5.5	+5.5
$\Omega_m h^2$	0.1426 ± 0.0020	0.1384	0.1476	$-2.1\,\sigma$	$+2.5\,\sigma$	-2.9	+3.5

Table 5.2: The lower and upper values satisfying $\Delta < 2.2$ for $z = 1$, their expressions by means of the standard deviations and the higest percent departures from the reference values.

Parameter	Δ_L Min	Δ_L Max
n_s	10.6	9.8
$10^9 A_s$	8.2	10.0
$\Omega_m h^2$	7.6	8.6

Parameter	Δ_L Min	Δ_L Max
n_s	7.9	10.6
$10^9 A_s$	6.7	7.1
$\Omega_m h^2$	11.6	7.3

Table 5.3: Discrepancies Δ_L between the linear power spectra and the corresponding evolved ones through the emulator, for $z = 0$ at the left and for $z = 1$ at the right.

We can observe that in almost all cases the discrepancies Δ involving the power spectra evolved by means of the expansion (5.3) are well beyond the three, but in many cases also four times, of that found considering the linearly evolved ones Δ_L and half of that related to the reference ones $\tilde{\Delta}$. In the cases of variations of n_s or A_s the intervals of parameters implementing the bound on discrepancy are smaller at $z = 0$ with respect to $z = 1$, as can be understood intuitively, while for Ω_m the situation is inverted and even considering the full form of C^{II} the

Parameter	$\tilde{\Delta}$ Min	$\tilde{\Delta}$ Max
n_s	3.5	4.7
$10^9 A_s$	3.5	4.1
$\Omega_m h^2$	8.5	7.7

Parameter	$\tilde{\Delta}$ Min	$\tilde{\Delta}$ Max
n_s	5.9	5.7
$10^9 A_s$	5.9	5.6
$\Omega_m h^2$	4.6	4.7

Table 5.4: Discrepancies $\tilde{\Delta}$ between the reference power spectra and the corresponding evolved ones through the emulator, for $z = 0$ at the left and for $z = 1$ at the right.

Bound	Value (σ) at $z = 0$	$\Delta(z = 0)$	Value (σ) at $z = 1$	$\Delta(z = 1)$
Min $\Omega_m h^2$	$-3.5\,\sigma$	0.6	$-2.1\,\sigma$	2.2
Max $\Omega_m h^2$	$+4.1\,\sigma$	0.7	$+2.5\,\sigma$	2.2

Table 5.5: Results using the full time-dependent form for C^{II} in (5.5).

configuration is more improved at $z = 0$ than at $z = 1$, leading to think this is really caused by the second correction: this is probably due to the fact that the change in this parameter modifies the growth principally at very low redshifts, as by the way appears by Fig.(5.1), retarding or anticipating the time when the cosmological constant dominates and hence modifying substantially the correction at $z \sim 0$.

However, it is clear that such a non-standard perturbative approach, that actually uses statistical objects coming from standard perturbation theory, the linear kernel at lowest order and the power spectrum at one loop, even if it can of course be improved using higher loops statistics or going beyond the linear kernel, appears a good candidate for the need we expressed at the beginning of the chapter, an object acting as a general interpolator encoding small modifications of a reference cosmology at large scales.

Conclusions.

In this conclusions, we will summarise the main ideas having inspired this work, highlight the original results we have obtained and point out further possible improvements and outlooks. Throughout the thesis, motivated by the need for new methods for the study of the Large Scale Structure of the Universe at mildly non-linear scales, we investigated the potentialities of the linear response function.

After a general introduction on both theoretical and observative approaches to the study of the LSS, we presented standard perturbation theory in a field theory fashion, resulting in the formulation of the Feynman diagrams of the theory. Then, we defined and motivated the linear response function, the functional derivative of the non-linear evolved power spectrum at a scale k with respect to the (linear) power spectrum at initial time at a scale q, which proves to be a good probe of the coupling between different modes; moreover, we evaluated this object at the lowest order in standard perturbation theory, pointing out, through comparison with N-body simulations, the breakdown of this approach for scales $q \gg k$ and, oppositely, the proof of its validity at scales $q \ll k$, whose behaviour is strongly constrained by galilean invariance.

Then, we developed two applications aiming at showing the power and the versatility of the linear response function. First we used it as a tracer of galilean invariance: in particular, we provided a way to improve the non-linear matter power spectrum as computed by means of the Γ-expansion analytical method at slightly non-linear scales $k \approx 0.10 - 0.25\, h\mathrm{Mpc}^{-1}$, where the approach, as commonly happens to the majority of the semi-analytical methods, breaks the invariance under galilean transformations. As a result, we were able to increase the reliability scale from $k = 0.16\, h\mathrm{Mpc}^{-1}$ to $k = 0.22\, h\mathrm{Mpc}^{-1}$ at redshift $z = 0$, where the discrepancy with simulations is under the 3.5%, while at $z = 1$ a discrepancy of the 1% is shifted from $k = 0.25\, h\mathrm{Mpc}^{-1}$ to $k = 0.30\, h\mathrm{Mpc}^{-1}$. In the second application we used the linear kernel as a tool to interpolate between different cosmologies: in particular, by means of a Taylor expansion of the non-linear matter power spectrum in the deviations between the initial reference power spectrum and the modified one, we could obtain the evolved power spectra in cosmologies with slightly modifications in the cosmological parameters with respect to the reference. We obtained that the evolved modified power spectra generally differ from the corresponding simulated ones within about the 2% by changing the parameters within an enhancement or reduction of about 3σ around the present experimental values. This method can of course be improved, for example by including the quadratic kernel function or by going beyond the one loop expression for the power spectrum used to evaluate the kernels. This result actually opens the doors to a limitation of the number of the needed N-body simulations and can surely be extended to more general cosmologies, such as in the case of a non-negligible amount of massive neutrinos in the Universe.

Bibliography

[1] H.-J. Seo and D. J. Eisenstein. Probing dark energy with baryonic acoustic oscillations from future large galaxy redshift surveys. *The Astrophysical Journal*, 598(2):720, 2003.

[2] J. Lesgourgues and S. Pastor. Massive neutrinos and cosmology. *Physics Reports*, 429(6):307–379, 2006.

[3] M. Crocce and R. Scoccimarro. Renormalized cosmological perturbation theory. *Physical Review D*, 73(6):063519, 2006.

[4] A. S. Szalay, T. Matsubara, and S. D. Landy. Redshift-space distortions of the correlation function in wide-angle galaxy surveys. *The Astrophysical Journal Letters*, 498(1):L1, 1998.

[5] R. Watkins and H. A. Feldman. Large-scale bulk flows from the Cosmicflows-2 catalogue. *Monthly Notices of the Royal Astronomical Society*, 447(1):132–139, 2015.

[6] R. E. Smith, R. Scoccimarro, and R. K. Sheth. Scale dependence of halo and galaxy bias: Effects in real space. *Physical Review D*, 75(6):063512, 2007.

[7] L. Hui, E. Gaztanaga, and M. LoVerde. Anisotropic magnification distortion of the 3D galaxy correlation. I. Real space. *Physical Review D*, 76(10):103502, 2007.

[8] M. Crocce and R. Scoccimarro. Memory of initial conditions in gravitational clustering. *Physical Review D*, 73(6):063520, 2006.

[9] J. J. M. Carrasco, M. P. Hertzberg, and L. Senatore. The effective field theory of cosmological large scale structures. *Journal of High Energy Physics*, 2012(9):1–40, 2012.

[10] D. Baumann, A. Nicolis, L. Senatore, and M. Zaldarriaga. Cosmological non-linearities as an effective fluid. *Journal of Cosmology and Astroparticle Physics*, 2012(07):051, 2012.

[11] A. Manzotti, M. Peloso, M. Pietroni, M. Viel, and F. Villaescusa-Navarro. A coarse grained perturbation theory for the Large Scale Structure, with cosmology and time independence in the UV. *Journal of Cosmology and Astroparticle Physics*, 2014(09):047, 2014.

[12] D. Blas, M. Garny, M. M. Ivanov, and S. Sibiryakov. Time-Sliced Perturbation Theory for Large Scale Structure I: General Formalism. *arXiv preprint arXiv:1512.05807*, 2015.

[13] S. Matarrese and M. Pietroni. Resumming cosmic perturbations. *Journal of Cosmology and Astroparticle Physics*, 2007(06):026, 2007.

[14] T. Nishimichi, F. Bernardeau, and A. Taruya. Anomalous coupling of the small-scale structures to the large-scale gravitational growth. *arXiv preprint arXiv:1411.2970*, 2014.

[15] M. Pietroni. Response function (Cosmology indipendence of the UV).

[16] E. Bertschinger. Cosmological Dynamics. *arXiv preprint astro-ph/9503125*, 1995.

[17] P. Coles and F. Lucchin. *Cosmology: The Origin and Evolution of Cosmic Structure*. John Wiley & Sons, 2003.

[18] P. J. E. Peebles. *The large-scale structure of the Universe*. Princeton university press, 1980.

[19] S. Matarrese. Notes on gravitation instability. *Lectures given at Scuola Normale Superiore di Pisa*, 2002-2005.

[20] S. Dodelson. *Modern cosmology*. Academic press, 2003.

[21] Planck Collaboration. XIII. *arXiv preprint arXiv:1502.01589*, 2015.

[22] E. Vanmarcke. *Random fields: analysis and synthesis*. World Scientific, 2010.

[23] J. A. Peacock. *Cosmological physics*. Cambridge university press, 1999.

[24] M. M. Rao. *Stochastic processes: inference theory*. Springer, 2014.

[25] D. J. Eisenstein, I. Zehavi, D. W. Hogg, R. Scoccimarro, M. R. Blanton, R. C. Nichol, R. Scranton, H.-J. Seo, M. Tegmark, Z. Zheng, et al. Detection of the baryon acoustic peak in the large-scale correlation function of SDSS luminous red galaxies. *The Astrophysical Journal*, 633(2):560, 2005.

[26] Martin White. Baryon Acoustic Oscillations: A standard ruler method for determining the expansion rate of the Universe. *Lectures given at the IUCCA School*, 2008.

[27] Ya. B. Zel'Dovich. Gravitational instability: An approximate theory for large density perturbations. *Astronomy and astrophysics*, 5:84–89, 1970.

[28] S. N. Gurbatov, A. I. Saichev, and S. F. Shandarin. A model for describing the development of the large-scale structure of the universe. *Soviet Physics Doklady*, 30:921, 1985.

[29] V. Springel, S. D. M. White, A. Jenkins, C. S. Frenk, N. Yoshida, L. Gao, J. Navarro, R. Thacker, D. Croton, J. Helly, et al. Simulating the joint evolution of quasars, galaxies and their large-scale distribution. *arXiv preprint astro-ph/0504097*, 2005.

[30] J. M. Bardeen, J. R. Bond, N. Kaiser, and A. S. Szalay. The statistics of peaks of Gaussian random fields. *The Astrophysical Journal*, 304:15–61, 1986.

[31] D. Baumann. Cosmology: Part III Mathematical Tripos. *Lectures at DAMTP, University of Cambridge*.

[32] J. N. Fry. The Galaxy correlation hierarchy in perturbation theory. *The Astrophysical Journal*, 279:499–510, 1984.

[33] M. H. Goroff, B. Grinstein, S.-J. Rey, and M. B. Wise. Coupling of modes of cosmological mass density fluctuations. *The Astrophysical Journal*, 311:6–14, 1986.

[34] B. Jain and E. Bertschinger. Second order power spectrum and nonlinear evolution at high redshift. *arXiv preprint astro-ph/9311070*, 1993.

[35] R. Scoccimarro. Transients from initial conditions: a perturbative analysis. *Monthly Notices of the Royal Astronomical Society*, 299(4):1097–1118, 1998.

[36] R. Scoccimarro. A new angle on gravitational clustering. *Annals of the New York Academy of Sciences*, 927(1):13–23, 2001.

[37] C. Rossetti. *Metodi matematici della Fisica*. Levrotto & Bella, 2000.

[38] H. M. Crocce. Renormalized Cosmological Perturbation Theory. *Dissertation for the degree of PhD, New York University*, 2007.

[39] M. Pietroni. Flowing with time: a new approach to non-linear cosmological perturbations. *Journal of Cosmology and Astroparticle Physics*, 2008(10):036, 2008.

[40] R. Penco and D. Mauro. Perturbation theory via Feynman diagrams in classical mechanics. *European journal of physics*, 27(5):1241, 2006.

[41] E. Gozzi, M. Reuter, and W. D. Thacker. Hidden BRS invariance in classical mechanics, II. *Physical Review D*, 40(10):3363, 1989.

[42] S. Matarrese. An introduction to path-integrals and their cosmological applications. *Based on lectures given at the University of Perugia in late eighties*.

[43] E. Calzetta and B.-L. Hu. Nonequilibrium quantum fields: Closed-time-path effective action, Wigner function, and Boltzmann equation. *Physical Review D*, 37(10):2878, 1988.

[44] A. Heavens. Statistics of clustering. *Lectures given in Padova*, 2002.

[45] C. Itzykson and J.-B. Zuber. *Quantum field theory*. Dover Books on Physics, 1980.

[46] M. Peloso and M. Pietroni. Galilean invariance and the consistency relation for the non-linear squeezed bispectrum of large scale structure. *Journal of Cosmology and Astroparticle Physics*, 2013(05):031, 2013.

[47] A. Kehagias and A. Riotto. Symmetries and Consistency Relations in the Large Scale Structure of the Universe. *Nuclear Physics B*, 873(3):514–529, 2013.

[48] M. Peloso and M. Pietroni. Ward identities and consistency relations for the large scale structure with multiple species. *Journal of Cosmology and Astroparticle Physics*, 2014(04):011, 2014.

[49] P. McDonald. Dark matter clustering: a simple renormalization group approach. *Physical Review D*, 75(4):043514, 2007.

[50] A. Lewis, A. Challinor, and A. Lasenby. Efficient computation of cosmic microwave background anisotropies in closed Friedmann-Robertson-Walker models. *The Astrophysical Journal*, 538(2):473, 2000.

[51] U. Seljak and M. Zaldarriaga. Apj, 469, 437 crossref. *Web of Science*, 1996.

[52] M. Zaldarriaga, U. Seljak, and E. Bertschinger. Integral solution for the microwave background anisotropies in nonflat universes. *The Astrophysical Journal*, 494(2):491, 1998.

[53] M. Zaldarriaga and U. Seljak. CMBFAST for Spatially Closed Universes. *arXiv preprint astro-ph/9911219*, 2000.

[54] F. Bernardeau, M. Crocce, and R. Scoccimarro. Multipoint propagators in cosmological gravitational instability. *Physical Review D*, 78(10):103521, 2008.

[55] A. Taruya, F. Bernardeau, T. Nishimichi, and S. Codis. Direct and fast calculation of regularized cosmological power spectrum at two-loop order. *Physical Review D*, 86(10):103528, 2012.

[56] A. Taruya, T. Nishimichi, S. Saito, and T. Hiramatsu. Nonlinear evolution of baryon acoustic oscillations from improved perturbation theory in real and redshift spaces. *Physical Review D*, 80(12):123503, 2009.

[57] T. Nishimichi, A. Shirata, A. Taruya, K. Yahata, S. Saito, Y. Suto, R. Takahashi, N. Yoshida, T. Matsubara, N. Sugiyama, et al. Modeling Nonlinear Evolution of Baryon Acoustic Oscillations: Convergence Regime of N-body Simulations and Analytic Models. *Publications of the Astronomical Society of Japan*, 61(2):321–332, 2009.

[58] E. Lawrence, K. Heitmann, M. White, D. Higdon, C. Wagner, S. Habib, and B. Williams. The coyote universe. III. simulation suite and precision emulator for the nonlinear matter power spectrum. *The Astrophysical Journal*, 713(2):1322, 2010.

[59] K. Heitmann, E. Lawrence, J. Kwan, S. Habib, and D. Higdon. The coyote universe extended: precision emulation of the matter power spectrum. *The Astrophysical Journal*, 780(1):111, 2013.

[60] A. J. S. Hamilton. Formulae for growth factors in expanding universes containing matter and a cosmological constant. *Monthly Notices of the Royal Astronomical Society*, 322(2):419–425, 2001.